NUMERICAL SIMULATIONS OF EUTROPHICATION PROCESSES IN İZMİR BAY WITH A COUPLED THREE DIMENSIONAL ECO-HYDRODYNAMIC MODEL

A THESIS SUBMITTED TO
GRADUATE SCHOOL OF MARINE SCIENCES
OF
MIDDLE EAST TECHNICAL UNIVERSITY

BY

ÖZGE YELEKÇİ

IN PARTIAL FULFILLMENT OF THE REQUIREMENTS
FOR
THE DEGREE OF MASTRER OF SCIENCE
IN
PHYSICAL OCEANOGRAPHY

JANUARY 2013

Approval of the thesis:

NUMERICAL SIMULATIONS OF EUTROPHICATION PROCESSES IN İZMİR BAY WITH A COUPLED THREE DIMENSIONAL ECO-HYDRODYNAMIC MODEL

submitted by **ÖZGE YELEKÇİ** in partial fulfillment of the requirements for the degree of **Mastrer of Science in Physical Oceanography Department, Middle East Technical University** by,

Prof. Dr. Ahmet E. Kıdeyş _____
Director, Graduate School of **Marine Sciences**

Prof. Dr. Emin Özsoy _____
Head of Department, **Physical Oceanography**

Assistant Prof. Dr. Bettina Fach Salihoğlu _____
Supervisor, **Physical Oceanography**

Dr. Valeria Ibello _____
Co-supervisor, **Physical Oceanography**

Examining Committee Members:

Prof. Dr. Zahit Uysal
Marine Biology and Fisheries _____

Prof. Dr. Semal Yemenicioğlu
Marine Geology and Geophysics _____

Assistant Prof. Dr. Barış Salihoğlu
Physical Oceanography _____

Assistant Prof. Dr. Bettina Fach Salihoğlu
Physical Oceanography _____

Dr. Valeria Ibello
Physical Oceanography _____

Date: _____

I hereby declare that all information in this document has been obtained and presented in accordance with academic rules and ethical conduct. I also declare that, as required by these rules and conduct, I have fully cited and referenced all material and results that are not original to this work.

Name, Last Name: ÖZGE YELEKÇİ

Signature :

ABSTRACT

NUMERICAL SIMULATIONS OF EUTROPHICATION PROCESSES IN İZMİR BAY WITH A COUPLED THREE DIMENSIONAL ECO-HYDRODYNAMIC MODEL

Yelekçi, Özge

M.S., Department of Physical Oceanography

Supervisor : Assistant Prof. Dr. Bettina Fach Salihoğlu

Co-Supervisor : Dr. Valeria Ibello

January 2013, 111 pages

A three dimensional time-dependent coupled ecosystem model is applied to İzmir Bay for the first time. Delft3D modelling suite's FLOW and ECO modules are adapted and tuned for the region. A reference model with a time frame of three years is produced that represents the current physical and biogeochemical status of the bay. Model skill assessment methods are used as a measure of model performance and to address the shortcomings of it. The hydrodynamics model is able to produce physical features in terms of seasonality and spatial distribution within reasonable ranges, whereas the ecosystem model has certain discrepancies which can be reduced with improved quality of model inputs, such as open boundary conditions, and fresh water and nutrient fluxes. The reference model is used as a tool with predictive capacity to assess the ecosystem response of the bay to possible changes it may undergo in the future. Five nutrient enrichment/reduction scenarios are constructed to predict the reactions of the bay to changing external inputs of DIN and PO_4. Results suggest that both physical and biogeochemical properties of the bay show strong horizontal gradients between outer and inner regions in which both natural and anthropogenic influences are effective. It is revealed that Outer bays are mostly occupied by waters originating from the oligotrophic

Aegean Sea, while eutrophicated inner regions are mainly controlled by local influences such as increased fresh water inputs and excessive wastewater discharges. Results of the nutrient enrichment/reduction scenarios suggest that the N-limited Inner and Middle bays and the P-limited Outer bays, give contrasting reactions to changes in inputs of DIN and PO_4 such that the former is more sensitive to DIN input whereas the latter is more sensitive to PO_4 input. Due to the existence of these two contrasting environments in the bay, availability of one nutrient is dependent on the availability of the other, therefore treatment of both should be considered in parallel. Among the scenarios tested in this study, the best possible option to reduce eutrophication in İzmir Bay is to prevent the increase of PO_4 input and to reduce the DIN input simultaneously. These outcomes are aimed to provide a scientific insight for coastal policy makers and environmental managers on how changes in anthropogenic influences can impact the marine ecosystem of the bay.

Keywords: İzmir Bay, eutrophication, coupled ecosystem modelling, hydrodynamics, Delft3D

ÖZ

ÜÇ BOYUTLU BÜTÜNLEŞİK EKO-HİDRODİNAMİK MODEL İLE İZMİR KÖRFEZİNDE ÖTROFİKASYON SÜRECİNİN SAYISAL BENZEŞİMLERİ

Yelekçi, Özge
Yüksek Lisans, Fiziksel Oşinografi Bölümü
Tez Yöneticisi : Yar. Doç. Dr. Bettina Fach Salihoğlu
Ortak Tez Yöneticisi : Dr. Valeria Ibello

Ocak 2013, 111 sayfa

Üç boyutlu zamana bağlı bir bütünleşik ekosistem modeli İzmir Körfezine ilk kez uygulanmıştır. Delft3D modelleme süitinin FLOW ve ECO modülleri bölge için uyarlanmış ve modifiye edilmiştir. Körfezin mevcut fiziksel ve biyojeokimyasal durumunu temsil eden üç yıllık bir referans modeli üretilmiştir. Modelin performans ölçütü olarak ve eksikliklerini tespit etmek için model beceri değerlendirme yöntemleri uygulanmıştır. Hidrodinamik modeli, mevsimsellik ve mekansal dağılımı açısından fiziksel özellikleri makul sınırlar içerisinde üretebilmektedir, ancak ekosistem modeli, açık sınır kuşulları, tatlu su ve nutrient akısı gibi model girdilerinin kalitesinin arttırılmasıyla giderilebilecek bazı tutarsızlıklar içermektedir. Referans modeli gelecekte gerçekleşmesi muhtemel değişikliklere körfezin ekosistem yanıtını değerlendirmek için öngörü kapasiteli bir araç olarak kullanılmıştır. Değişen karasal ÇİN ve PO_4 girdilerine körfezin tepkilerini tahmin etmek üzere beş nutrient zenginleştirme/azaltma senaryosu oluşturulmuştur. Sonuçlar, körfezin fiziksel ve biojeokimyasal özelliklerinin hem doğal hem de insan etkisindeki sebepler nedeniyle dış ve iç bölgeler arasında yatayda keskin değişkenlikler gösterdiğini önermektedir. Dıs körfezin çoğunlukla Ege Denizin'den gelen oligotrofik sulara sahip olduğu, ötrofik İç körfezin ise daha çok artan tatlı su akısı ve aşırı

atıksu girdisi gibi yerel etkilerin altında olduğu ortaya koyulmuştur. Nutrient zenginleştirme / azaltma senaryolarının sonuçları N-sınırlı İç ve Orta körfezin ÇİP girdisine karşı daha hassas, P-sınırlı Dış körfezin PO_4 girdisine karşı daha hassas olup ÇİP ve PO_4 girdilerine karşıt tepkiler verdiğini göstermiştir. Körfezde bu iki zıt ortamın bir arada bulunması bir nutrientin bulunabilirliğinin diğer nutrientin bulunabilirliğine bağlı olmasına sebep olmaktadır, bu sebeple nutrientlerin ikisinin de arıtımının paralel olarak değerlendirilmesi gerekmektedir. Bu çalışmada test edilenler içerisinde körfezdeki ötrofikasyonun azaltılması için olası en iyi senaryonun PO_4 girdilerinin artmasının önlenmesiyle birlikte ÇİP girdilerinin azaltılması yönünde olduğu ortaya koyulmuştur. Bu neticelerin kıyı bölgelerle ilgili karar vericilere ve çevre yöneticilerine insan kaynaklı etmenlerin körfezin denizel ekosistemini nasıl etkilediği hususunda bilimsel bir görüş bildireceği amaçlanmaktadır.

Anahtar Kelimeler: İzmir Körfezi, ötrofikasyon, bütünleşik ekosistem modelleme, hidrodinamik, Delft3D

Ailem, Ülkü, Kemal ve Erman'a

ACKNOWLEDGMENTS

I would like to thank my supervisors Asst. Prof. Dr. Bettina Fach Salihoğlu and Dr. Valeria Ibello for guiding me throughout the preparation of this thesis. Also, I am thankful to Asst. Prof. Dr. Barış Salihoğlu and Prof. Dr. Süleyman Tuğrul for supporting me during my study. I also would like to thank Assc. Prof. Dr. Erdem Sayın and Prof. Dr. Filiz Küçüksezgin from Dokuz Eylül University, Institute of Marine Sciences and Technology for sharing their knowledge on İzmir Bay and providing me with data needed for this study. This study was conducted within the project SINHA (Project No: 107G066), funded by TÜBİTAK.

The members of the examining committee, Prof. Dr. Zahit Uysal, and Prof. Dr. Semal Yemenicioğlu have shared their valuable comments during the defense and revisions of this thesis.

I want to mention all the staff of technicians and RV Bilim 2 for doing the hardest part of the work, and Erkal Yurtsever, Atölye, İdare, and Muhasebe for there can be no academics without them.

Muhteşem Akif Korkmaz and Esin Yalçın, I just love you. Çaglar Yumruktepe has given me the best advice and insight a colleague can ask for. I had the privillage of sharing a room with Ceren Güraslan, Panter, Vincent, Sala, and Şırdan. Anıl Akpınar, Ersin Tutsak, Adil Sözer, and Özgür Gürses have made life bearable for the last three and a half years I spent in METU-IMS. I thank all of you for being my friends. And Mişa, thank you for just being yourself.

I can not thank enough to Nuray Çelik and Mertkan Tüer for sharing their home with me, and for being the most amazing room mates.

I am so grateful to know Ali Aydoğdu, and very thankful for the support and encouragement he gave, when I needed it the most.

I couldn't have achieved anything without my family, I am so lucky to have you.

TABLE OF CONTENTS

LIST OF TABLES

TABLES

LIST OF FIGURES

FIGURES

CHAPTER 1

INTRODUCTION

1.1 STUDY AREA

Figure 1.1: Western Turkey and location of İzmir Bay along the Aegean Sea coast.

İzmir Bay is a small "L" shaped bay at the Aegean Sea coast of Turkey (Figure 1.1). In the north, it opens to the Aegean Sea and in the southeast inner coast, densely populated city of İzmir, which is the third largest city of Turkey, is located. According to its geographical properties, the bay is divided into three regions; Inner, Middle, and Outer bays, and Outer bay is further divided into three subregions; Outer I, Outer II, and Outer III bays (Figure 1.2) (Sayın, 2003).

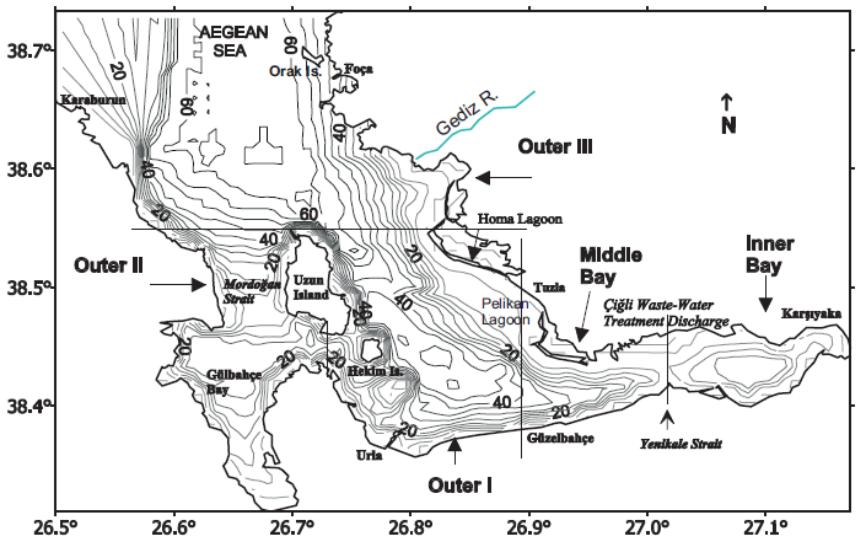

Figure 1.2: Geography of İzmir Bay (From Sayın et al. (2006))

Outer Bay is the north-south extending section which is 20 km wide and 40 km long, and Middle and Inner Bays are the east-west extending section which is 5-7 km wide and 24 km long (Sayın, 2003). Outer III is the northernmost part of the bay where it is connected to the Aegean Sea. It is the deepest region of the bay with a maximum depth of around 70 m. In this region Aegean Sea water inflows around Karaburun and İzmir Bay water outflows around Foça (Sayın et al., 2006). Outer III also receives the largest fresh water input to the bay, Gediz River. Outer II is the southwest corner of the bay covering Gülbahçe Bay in the south and Mordoğan strait in the north. Aegean Sea waters occupying Outer III region flow into Outer II through Mordoğan strait which has a sill depth of $\sim$ 14m (Sayın et al., 2006). Outer I is the region south of Outer III and east of Outer II and it is the transitionary region between the Outer and Inner bays. Inner Bay is the rather shallow southeast part of the bay and it is separated by the rest of the bay by the very shallow ($\leq$ 10 m) Yenikale sill (Sayın, 2003). Middle Bay is the part between the Outer and Inner Bays.

1.1.1 PHYSICAL PROPERTIES OF İZMİR BAY

Sayın et al. (2006) investigates the physical properties of characteristic water masses observed in İzmir Bay by analyzing the data collected during 37 cruises between January 1993 and March 2004. In their study, seasonal variation of the thermohaline structure in the bay is described as follows. In winter, strong horizontal gradients of temperature and salinity are

formed between the Outer and Inner Bay regions. These differences are due to relatively warmer and more saline (15-16 °C, ~ 39 psu) Aegean Sea water entering the bay from the north and colder and fresher (13-14 °C, ~ 38.2 psu) water occurring in Inner Bay due to rapid cooling of the sallow regions and fresh water inputs. In this season the bay is well mixed and temperature and salinity are vertically homogeneous. In spring, surface warming initiates the vertical stratification. At the surface, horizontal temperature gradient reverses with respect to winter, this time due to rapid warming of the Inner Bay region, whereas, near bottom waters preserve winter properties. In summer, water column is strongly stratified, with temperatures ranging from 26 °C at the surface to 16 °C at the bottom. A sharp pycnocline is observed at around 25-30 m depth. Salinity ranges between 39-39.45 psu. In fall, water column starts to mix. Thermocline deepens to around 40 m and surface temperature and salinity are ~ 22 °C and ~ 38.4 psu.

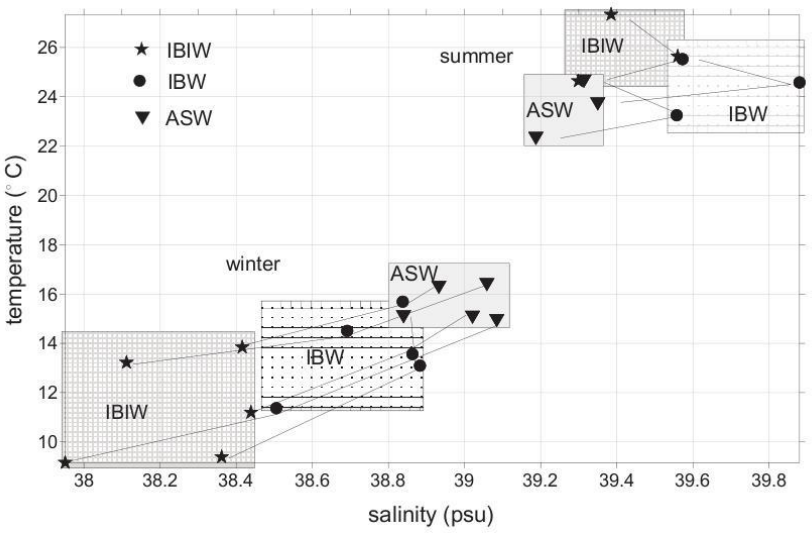

Figure 1.3: T-S diagram showing different water masses present in İzmir Bay (From Sayın et al. (2006))

Sayın et al. (2006) also investigates different water masses with distinct temperature - salinity characteristics occurring in the bay (Figure 1.3). It is seen that İzmir Bay Inner water (IBIW) is the coldest in winter and the warmest in summer, and it is under the influence of fresh water input. Whereas, Aegean Sea water (ASW) carries in the properties of the Aegean Sea with waters relatively warmer and more saline in winter, and cooler and fresher in summer, thus causing horizontal gradients along the bay. İzmir Bay water (IBW) is the transitional water mass between these two ends of the bay and its properties are also affected by local influences

like Gediz River and shallow salt producing regions.

Literature on observations of current velocity in İzmir Bay is non-existent, however, modelling studies by Ivanov et al. (1997, 1998), Sayın (2003), and Sayın et al. (2006) provide information on general circulation patterns. In Sayın (2003), it is shown that, in the case of northerly winds, inflowing Aegean Sea water enters the bay off the north eastern coast, Foça, and follows the eastern coast line. This inflowing water forms an anticyclonic gyre in Outer I region, called the Middle Gyre. Sayın et al. (2006), however, states that inflow occurs off the northwestern coast, Karaburun, passes the Mordoğan strait, and then turns to east forming the Middle Gyre, and outflow occurs off the northeastern coast, Foça. In both studies it is shown that the circulation in the bay is driven by wind and thermohaline forces. Ivanov et al. (1997) states that, independent of the direction of wind forcing, compensation flows occur below a certain depth in opposite directions to the surface flows.

1.1.2 CHEMICAL AND BIOLOGICAL PROPERTIES OF İZMİR BAY

İzmir Bay is the receiver of substantial amounts of material both from natural and anthropogenic sources. Starting from 1930's, İzmir bay is subject to eutrophication and pollution due to increased population and domestic waste (Özkan et al., 2008). As early as 1950's researchers reported red-tide events and fish mortalities occurring in the bay (Numann, 1955; Acara and Nalbantoglu, 1960). In 1990's with rapid development in industries and urbanization, eutrophication started to become a major problem with more frequent and severe red-tides and anoxic conditions in bottom waters (Gençay and Büyükışık, 2004; Bizsel et al., 2001).

Pollutants the bay receives can be listed under nine major groups as follows: *i*) domestic waste water of inhabitants of the city of İzmir, *ii*) industrial waste water from sources located around İzmir, *iii*) loads carried by Gediz River and other small creeks that discharge into the bay, *iv*) loads carried by rainfall onto urban areas and the catchment area of the bay, *v*) pesticides and fertilizers carried by rainfall onto or drainage from agricultural areas around the bay, *vi*) loads due to harbor and maritime activities in the bay, *vii*) loads deposited from the atmosphere, *viii*) loads carried from bottom sediments into the water column and *ix*)material exchange with open ocean (SINHA, 2010). Major pollutants originate from industrial waste water by 50%, from rainfall by 15%, from agricultural activity by 10% and from other sources by 15%

(UNEP, 1994). Before 2000, 308,000 m^3 of domestic and 105,000 m^3 of industrial waste water per day (UNEP, 1993) and 911 tons of ortho-PO_4, 1621 tons of NO_x-N and 23,500 tons of NH_4-N per year (UNEP, 1994) was discharged into the bay without treatment. Because of this situation, the bay is considered an effective pollution source even for the Aegean Sea (Bizsel and Bizsel, 2001).

Dissolved Inorganic Phosphorus (DIP), a pollutant of domestic origin, in the bay showed a rapid increase in the last decades such that it ranged between 0.00-0.02 μM in 1974-75 (Geldiay et al., 1975), between 0.05-1.9 μM in 1977-79 (Kocataş and Geldiay, 1980), between 0.76-1.96 μM in 1983-85 (Büyükışık, 1986) and between 0.36-49 μM in 1993-94 (Bizsel et al., 2001). This increase was a direct indicator of eutrophication caused by domestic pollutants (Bizsel et al., 2001). Also during 1990's anoxic conditions in the sediment and bottom waters with oxygen concentrations lower than 0.7 ml/l was observed (Bizsel et al., 2001). In contrast to the phosphorus limited nature of the Mediterranean and Aegean Seas (Krom et al., 1991, 1992; Tselepides et al., 2000), anthropogenic phosphorus loading into İzmir Bay caused nitrogen limitation (Büyükışık and Erbil, 1987; Büyükışık, 1986; Bizsel and Uslu, 2000).

Çiğli Waste Water Treatment Plant (WWTP) was installed in early 2000 within the Great Channel Project of İzmir (Küçüksezgin et al., 2006), which aimed at collecting all domestic and industrial waste water outlets and small creeks in a single subterranean channel surrounding the entire inner bay coast and preventing any untreated water discharge into the bay (http://www.izsu.gov.tr). The WWTP treats phosphorus and nitrogen with activated sludge processes (Kontas et al., 2004). After the installation of the WWTP, a decrease was observed in Nitrogen to Phosphorus (N:P) ratios in Inner and Middle bays which indicated that phosphorus was not removed efficiently during treatment (Küçüksezgin et al., 2004). Küçüksezgin et al. (2006) reported a marked decrease in maximum Chlorophyll-*a* (Chl-*a*) concentrations in Inner and Middle bays from 26 μg/l in 1996-98 to 2.6 μg/l in 2003 but no observation of improvement in water quality and Kontas et al. (2004) recorded even an increasing trend in phosphate concentrations. Sunlu et al. (2008) stated that the response of the sediment might not be as fast as the water column and might delay the effects of the treatment.

In the Outer bay, in autumn and winter seasons, NO_x-N and PO_4 concentrations are highest due to decreased uptake by phytoplankton but in the same periods Chl-*a* concentrations increased in vicinity of the Gediz River input (Küçüksezgin et al., 2006; Kontas et al., 2004),

in spring season, concentrations decrease during the bloom of phytoplankton (Küçüksezgin et al., 2005). In Inner and Middle bays, nutrient and Chl-*a* concentrations are higher than the Outer bay (Figure 1.4) (Küçüksezgin et al., 2006). Maximum concentrations of NO_x-N and PO_4 are observed in autumn and summer seasons respectively due to increased bacterial activity and Chl-*a* concentrations are higher in spring and autumn seasons (Küçüksezgin et al., 2006). Phytoplankton abundance and particulate organic concentrations in the bay showed a clear maximum in spring season (Küçüksezgin et al., 2005).

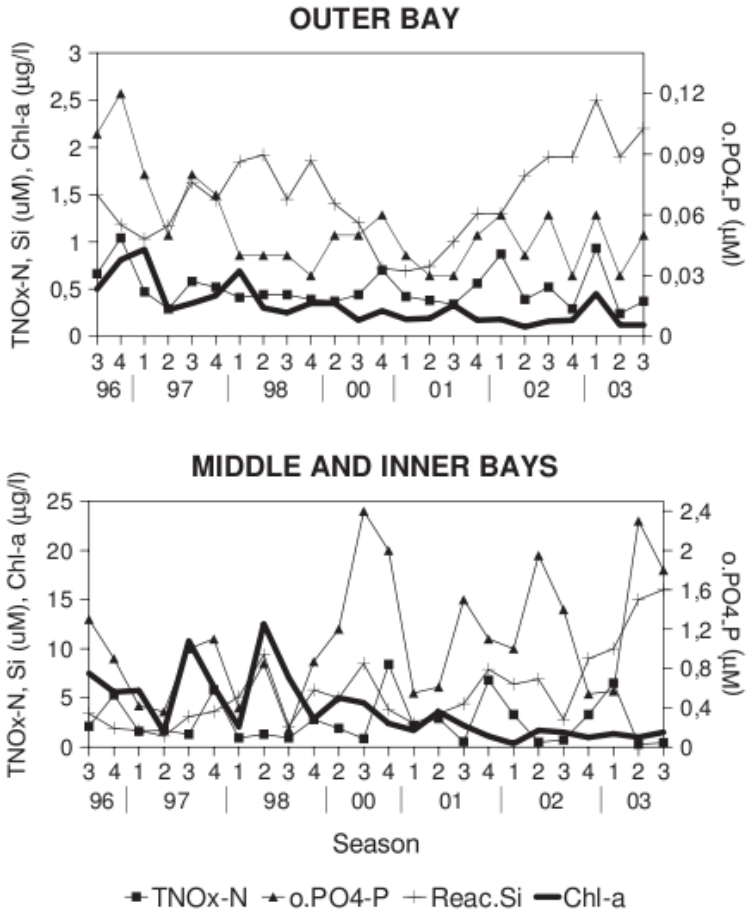

Figure 1.4: Seasonal variations of nutrient and chlorophyll-a concentrations in İzmir Bay (1: winter, 2: spring, 3: summer, 4: autumn) (From Küçüksezgin et al. (2006))

In the current state of the bay, generally, Outer bay region shows Aegean Sea characteristics and towards the inner parts an eutrophicated state is observed (Küçüksezgin et al., 2006; Kontas et al., 2004). In 2002-2003, in the Outer bay, PO_4 ranged between 0.01-0.19 μM, NO_x-N between 0.1-1.4 μM, NH_4-N between 0.1-0.69 μM, Si between 0.48-4.8 μM and

Chl-*a* between 0.01-0.94 μg/l, with N:P ratio ranging between 3-18 and in Inner and Middle bays, PO_4 ranged between 0.14-4.5 μM, NO_x-N between 0.12-8.6 μM, NH_4-N between 0.1-6.7 μM, Si between 1-32 μM and Chl-*a* between 0.13-3.7 μg/l, with N:P ratio ranging between 0.06-17 (Küçüksezgin et al., 2006). NO_x-N and PO_4 concentrations showed a slight increase with depth, accompanied by a decrease in dissolved oxygen and NH_4-N concentrations (Küçüksezgin et al., 2005).

1.2 AIMS AND OBJECTIVES

Because İzmir Bay is home to many still undisturbed natural sites and at the same time one of the largest cities of Turkey, it is of great importance both ecologically and economically. Eutrophication caused rapid and uncontrolled development around the region has deteriorated the environmental status of the inner parts and has threatened a larger region of the bay over the last decades. Today, with the help of treatment facilities, the bay is undergoing a healing process. However, although many researchers have been interested in it, scientifically there are still many unknowns about the processes and dynamics in the bay, such as the inflow/outflow at the Aegean Sea boundary, or the nutrient feedback from the sediments. Thus, it is essential that a proper understanding of physical and biogeochemical properties of the bay and descriptions of major characteristics are investigated more profoundly.

Driven by the above described circumstances, this study on İzmir Bay is conducted within the context of the project "SINHA: URBAN WASTEWATER MANAGEMENT ALONG COASTAL AREAS OF TURKEY: RE-IDENTIFICATION OF HOT SPOTS & SENSITIVE AREAS, DETERMINATION OF ASSIMILATION CAPACITIES BY MONITORING AND MODELLING AND DEVELOPMENT OF SUSTAINABLE URBAN WASTEWATER INVESTMENT PLANS" funded by TÜBİTAK (The Scientific and Technological Research Council of Turkey).

First and foremost, the purpose of this study is to help understand the current physical and biogeochemical state of İzmir Bay and the processes contributing to its eutrophication by making use of a three-dimensional coupled eco-hdyrodynamic model. The outputs of the modelling study, together with observations, provide a detailed description of the physical and biogeochemical dynamics of the area, its seasonal cycle and spatial variability. Secondly,

the purpose is to use this model as a predictive tool to investigate the possible response of the bay to changes in nutrient loads it receives by conducting a series of modelling experiments. It is aimed that the outcome of this study as a whole serves as a useful tool for coastal policy makers and environmental managers to understand and forecast how changes in boundary conditions (increase/decrease of urbanization, agricultural, or industrial activities) can impact the marine ecosystem of the bay.

The specific objectives of this study are:

- Adapting and tuning Delft3D modelling suite's FLOW and ECO modules to İzmir Bay and validating the model to serve as a predictive tool,
- Obtaining three-dimensional representations of physical-biogeochemical processes and time-dependent distributions of related parameters, as well as analyzing them together with observations,
- Investigating the response of the bay to possible changes it may undergo in terms of nutrient loads.

In light of these objectives, in Chapter 1 of this thesis, a description of İzmir Bay is given, in Chapter 2, general information on Delft3D modelling suite, FLOW and ECO modules, inputs and forcings used in the reference model set-ups, and methods of model skill assessment are presented, in Chapter 3, results of the hydrodynamics and ecosystem reference model with assessment of model skill, and analysis of nutrient enrichment/reduction scenarios are given, in Chapter 4, outcomes of the study are discussed, and in Chapter 5 a conclusion is given.

CHAPTER 2

MATERIALS AND METHODS

The Delft3D Modelling Suite

Delft3D, a fully integrated modelling suite, has been developed for 3D computations of coastal, river, lake, and estuarine regions, with a multi-disciplinary approach by WL | Delft Hydraulics in Netherlands. The framework (Figure 2.1) consists of several modules that can interact with each other.

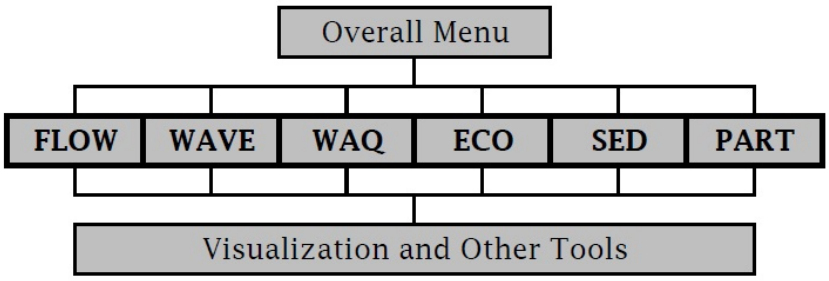

Figure 2.1: Delft3D modelling framework.

Simulations that each module is capable of carrying out can be listed as:

FLOW, 2D and 3D hydrodynamic, temperature, salinity, transport, on-line sediment transport and morphology.
WAVE, short wave propagation.
WAQ, general field water quality.
ECO, complex eutrophication and ecological.
SED, cohesive and non-cohesive sediment transport.
PART, particle tracking and oil spill.

The 3D coupled eco-hydrodynamic model presented in this study is constructed using Delft3D-FLOW and Delft3D-ECO modules. Description of these two modules are given in the following subsections. All in information given in this chapter is referred to the corresponding user manuals of these modules prepared by WL | Delft Hydraulics (WL | Delft Hydraulics, 2009c,a). Detailed information regarding the rest of the model suite can be found in the user manuals of each module or tool or on www.wldelft.nl .

2.1 DESCRIPTION OF DELFT3D-FLOW MODULE

Delft3D-FLOW is a multi-dimensional hydrodynamic simulation program that computes non-steady flow and transport phenomena resulting from tidal and meteorological forcings. It is based on the full Navier-Stokes equations with the shallow water approximation applied. Delft3D-FLOW can be applied to simulations of salt intrusion in estuaries, fresh water river discharges in bays, thermal stratification in lakes and seas, cooling water intakes and waste water outlets, sediment transport including feedback on the flow, transport of dissolved material and pollutants, and etc. The results of the hydrodynamic module can be used in (i.e. coupled to) all other modules of Delft3D through the use of a communication file.

Delft3D-FLOW solves the 2D (depth averaged) or 3D non-linear shallow water equations, derived from the 3D Navier Stokes equations for incompressible free surface flow, under the Boussinesq approximation. The system of equations consists of the horizontal equations of motion, the continuity equation, and the transport equations for conservative constituents. In 3D, vertical velocities are computed from the continuity equation.

Table 2.1: List of symbols used in Delft3D-FLOW

Symbol	Unit	Definition
ξ, η	–	Horizontal, curvilinear co-ordinates (x, y)
$\sqrt{G_{\xi\xi}}$, $\sqrt{G_{\eta\eta}}$	m	Coefficients used to transform curvilinear to rectangular co-ordinates
ζ	m	Water level above some horizontal plane of reference (datum)
d	m	Depth below some horizontal plane of reference (datum)
H	m	Total water depth ($H = d + \zeta$)

Table 2.1 – List of symbols used in Delft3D-FLOW (continued)

Symbol	Unit	Definition
σ	$-$	Scaled vertical co-ordinate, $\sigma = \frac{z-\zeta}{d+\zeta}$, (surface, $\sigma = 0$; bed level, $\sigma = -1$)
u	ms^{-1}	Flow velocity in the x- or ξ-direction
v	ms^{-1}	Flow velocity in the y- or η-direction
ω	ms^{-1}	Fluid velocity in the z-direction
u_b	ms^{-1}	Near-bed fluid velocity vector
U	ms^{-1}	Depth averaged velocity in the ξ-direction
V	ms^{-1}	Depth averaged velocity in the η-direction
f	s^{-1}	Coriolis parameter (inertial frequency)
g	ms^{-2}	Acceleration due to gravity
P_ξ	$kgm^{-2}s^{-2}$	Gradient hydrostatic pressure in ξ-direction
P_η	$kgm^{-2}s^{-2}$	Gradient hydrostatic pressure in η-direction
F_ξ	ms^{-2}	Turbulent momentum flux in ξ-direction
F_η	ms^{-2}	Turbulent momentum flux in η-direction
M_ξ	ms^{-2}	Source or sink of momentum in ξ-direction
M_η	ms^{-2}	Source or sink of momentum in η-direction
$\vec{\tau}_b$	Nm^{-2}	Bed shear stress due to current and waves
$\tau_{b\xi}$	$kgms^{-2}$	Bed shear stress in ξ-direction
$\tau_{b\eta}$	$kgms^{-2}$	Bed shear stress in η-direction
$\vec{\tau}_s$	Nm^{-2}	Shear stress at surface
ν_{3D}	m^2s^{-1}	Part of eddy viscosity due to turbulence model in vertical direction
ν_V	m^2s^{-1}	Vertical eddy viscosity
ν_{mol}	m^2s^{-1}	Kinematic viscosity (molecular) coefficient
ν_V^{back}	m^2s^{-1}	Background vertical eddy viscosity for momentum equations
ν_H	m^2s^{-1}	Horizontal eddy viscosity
ν_{SGS}	m^2s^{-1}	Sub-grid scale (SGS) horizontal eddy viscosity
ν_H^{back}	m^2s^{-1}	Background horizontal eddy viscosity
D_V^{back}	m^2s^{-1}	Background vertical eddy diffusivity for transport equation

Table 2.1 – List of symbols used in Delft3D-FLOW (continued)

Symbol	Unit	Definition
D_V	$m^2 s^{-1}$	Vertical eddy viscosity
D_H	$m^2 s^{-1}$	Horizontal eddy viscosity
σ_{c_0}	$-$	Prandtl-Schmidt number for constituent (0.7 for salinity and temperature)
σ_c	$-$	Prandtl-Schmidt number
σ_{mol}	$-$	Prandtl-Schmidt number for molecular mixing
ρ	kgm^{-3}	Density of water
ρ_0	kgm^{-3}	Reference density of water
ρ_a	kgm^{-3}	Density of air
ρ_w	$-$	Specific density of water
λ_d	s^{-1}	First order decay coefficient
C_d	$-$	Wind drag coefficient
U_{10}	ms^{-1}	Averaged wind speed at 10 m above free surface
q_{in}	s^{-1}	Local source per unit volume
q_{out}	s^{-1}	Local sink per unit volume
P	ms^{-1}	Precipitation
E	ms^{-1}	Evaporation
c	kgm^{-3}	Mass concentration
Q	ms^{-1}	lobal source or sink per unit area
Q_{tot}	$Jm^{-2}s^{-1}$	Heat flux through free surface
Q_{sn}	$Jm^{-2}s^{-1}$	Net solar insolation
Q_{an}	$Jm^{-2}s^{-1}$	Net atmospheric radiation
Q_{br}	$Jm^{-2}s^{-1}$	Back radiation (long wave radiation)
Q_{ev}	$Jm^{-2}s^{-1}$	Heat loss due to evaporation
Q_{co}	$Jm^{-2}s^{-1}$	Heat loss due to convection
T_s	$^\circ C$	Water temperature at free surface
c_p	$Jkg^{-1}{}^\circ C^{-1}$	Specific heat of sea water
Δz_s	m	Thickness of the surface layer

Hydrodynamic and Transport Equations

Continuity Equation:

The depth averaged continuity equation is given by

$$\frac{\partial \zeta}{\partial t} + \frac{1}{\sqrt{G_{\xi\xi}}\sqrt{G_{\eta\eta}}}\frac{\partial\left[(d+\zeta)U\sqrt{G_{\eta\eta}}\right]}{\partial \xi} + \frac{1}{\sqrt{G_{\xi\xi}}\sqrt{G_{\eta\eta}}}\frac{\partial\left[(d+\zeta)V\sqrt{G_{\xi\xi}}\right]}{\partial \eta} = Q, \tag{2.1}$$

where,

$$Q = H\int_{-1}^{0}(q_{in} - q_{out})\,\mathrm{d}\sigma + P - E. \tag{2.2}$$

q_{in} and q_{out} are the local sources and sinks of water, and P and E are, respectively, the non-local source term due to precipitation and the non-local sink term due to evaporation.

Momentum Equations in the Horizontal Direction:

Momentum equations in ξ- and η-directions are given by

$$\frac{\partial u}{\partial t} + \frac{u}{\sqrt{G_{\xi\xi}}}\frac{\partial u}{\partial \xi} + \frac{v}{\sqrt{G_{\eta\eta}}}\frac{\partial u}{\partial \eta} + \frac{\omega}{d+\zeta}\frac{\partial u}{\partial \sigma} - \frac{v^2}{\sqrt{G_{\xi\xi}}\sqrt{G_{\eta\eta}}}\frac{\partial \sqrt{G_{\eta\eta}}}{\partial \xi}$$

$$+\frac{uv}{\sqrt{G_{\xi\xi}}\sqrt{G_{\eta\eta}}}\frac{\partial \sqrt{G_{\xi\xi}}}{\partial \eta} - fv = -\frac{1}{\rho_0\sqrt{G_{\xi\xi}}}P_\xi + F_\xi + \frac{1}{(d+\zeta)^2}\frac{\partial}{\partial \sigma}\left(\nu_V\frac{\partial u}{\partial \sigma}\right) + M_\xi, \tag{2.3}$$

and

$$\frac{\partial v}{\partial t} + \frac{u}{\sqrt{G_{\eta\eta}}}\frac{\partial v}{\partial \xi} + \frac{v}{\sqrt{G_{\eta\eta}}}\frac{\partial v}{\partial \eta} + \frac{\omega}{d+\zeta}\frac{\partial v}{\partial \sigma} + \frac{uv}{\sqrt{G_{\xi\xi}}\sqrt{G_{\eta\eta}}}\frac{\partial \sqrt{G_{\eta\eta}}}{\partial \xi}$$

$$-\frac{u^2}{\sqrt{G_{\xi\xi}}\sqrt{G_{\eta\eta}}}\frac{\partial \sqrt{G_{\xi\xi}}}{\partial \eta} + fu = -\frac{1}{\rho_0\sqrt{G_{\eta\eta}}}P_\eta + F_\eta + \frac{1}{(d+\zeta)^2}\frac{\partial}{\partial \sigma}\left(\nu_V\frac{\partial v}{\partial \sigma}\right) + M_\eta. \tag{2.4}$$

P_ξ and P_η represent the pressure gradient in the baroclinic pressure terms, and density variations are neglected elsewhere. F_ξ and F_η forces represent the unbalance of horizontal Reynold's stresses. M_ξ and M_η represent the external sources and sinks of momentum.

Vertical Velocities:

The physical vertical velocity w is not involved in the model equations and the vertical velocity ω is the velocity relative to the moving σ-plane and it is computed from the continuity equation by

$$\frac{\partial \zeta}{t} + \frac{1}{\sqrt{G_{\xi\xi}}\sqrt{G_{\eta\eta}}}\frac{\partial\left[(d+\zeta)u\sqrt{G_{\eta\eta}}\right]}{\partial \xi} + \frac{1}{\sqrt{G_{\xi\xi}}\sqrt{G_{\eta\eta}}}\frac{\partial\left[(d+\zeta)v\sqrt{G_{\xi\xi}}\right]}{\partial \eta} + \frac{\partial \omega}{\partial \sigma} = H\left(q_{in} - q_{out}\right). \tag{2.5}$$

Hydrostatic Pressure Assumption:

For water with non-uniform density, and with atmospheric pressure taken into account, the horizontal pressure gradients are given as

$$\frac{1}{\rho_0\sqrt{G_{\xi\xi}}}P_\xi = \frac{g}{\sqrt{G_{\xi\xi}}}\frac{\partial \zeta}{\partial \xi} + g\frac{d+\zeta}{\rho_0\sqrt{G_{\xi\xi}}}\int_\sigma^0\left(\frac{\partial \rho}{\partial \xi} + \frac{\partial \rho}{\partial \sigma}\frac{\partial \sigma}{\partial \xi}\right)\mathrm{d}\sigma', \tag{2.6}$$

and

$$\frac{1}{\rho_0\sqrt{G_{\eta\eta}}}P_\eta = \frac{g}{\sqrt{G_{\eta\eta}}}\frac{\partial \zeta}{\partial \eta} + g\frac{d+\zeta}{\rho_0\sqrt{G_{\eta\eta}}}\int_\sigma^0\left(\frac{\partial \rho}{\partial \eta} + \frac{\partial \rho}{\partial \sigma}\frac{\partial \sigma}{\partial \eta}\right)\mathrm{d}\sigma'. \tag{2.7}$$

Transport Equation:

The transport of matter and heat is modelled by an advection-diffusion equation in three dimensions and is given as follows

$$\frac{\partial (d+\zeta)\,c}{\partial t} + \frac{1}{\sqrt{G_{\xi\xi}}\sqrt{G_{\eta\eta}}}\left\{\frac{\partial\left[\sqrt{G_{\eta\eta}}\,(d+\zeta)\,uc\right]}{\partial \xi} + \frac{\partial\left[\sqrt{G_{\xi\xi}}\,(d+\zeta)\,vc\right]}{\partial \eta}\right\} + \frac{\partial \omega c}{\partial \sigma} = \frac{d+\zeta}{\sqrt{G_{\xi\xi}}\sqrt{G_{\eta\eta}}}\left\{\frac{\partial}{\partial \xi}\left[\frac{D_H}{\sigma_{c_0}}\frac{\sqrt{G_{\eta\eta}}}{\sqrt{G_{\xi\xi}}}\frac{\partial c}{\partial \xi}\right] + \frac{\partial}{\partial \eta}\left[\frac{D_H}{\sigma_{c_0}}\frac{\sqrt{G_{\xi\xi}}}{\sqrt{G_{\eta\eta}}}\frac{\partial c}{\partial \eta}\right]\right\} + \frac{1}{d+\zeta}\frac{\partial}{\partial \sigma}\left[\frac{\nu_{mol}}{\sigma_{mol}} + max\left(\frac{\nu_{3D}}{\sigma_c}, D_V^{back}\right)\frac{\partial c}{\partial \sigma}\right] - \lambda_d(d+\zeta)c + S, \tag{2.8}$$

where λ_d is the first order decay process, and S is the source and sink terms per unit area due to discharge q_{in} or withdrawal q_{out} of water, heat exchange through the free surface Q_{tot}, such that

$$S = (d + \zeta)(q_{in}c_{in} - q_{out}c) + Q_{tot}. \tag{2.9}$$

Boundary Conditions

Flow Boundary Conditions:

Vertical boundary conditions for flow at the bottom ($\sigma = -1$) are given as

$$\omega|_{\sigma=-1} = 0 \ , \ \frac{\nu_V}{H}\frac{\partial u}{\partial \sigma}\bigg|_{\sigma=-1} = \frac{1}{\rho_0}\tau_{b\xi} \ \text{ and } \ \frac{\nu_V}{H}\frac{\partial v}{\partial \sigma}\bigg|_{\sigma=-1} = \frac{1}{\rho_0}\tau_{b\eta}, \tag{2.10}$$

where, $\tau_{b\xi}$ and $\tau_{b\eta}$ are the ξ and η components of the bed shear-stress, respectively. The bed shear-stress is defined as $\vec{\tau}_b = \frac{g\rho_0\vec{u}_b|\vec{u}_b|}{C_{3D}^2}$, where, u_b is the velocity just above the bed. Vertical boundary conditions for flow at the free surface ($\sigma = 0$) are given as

$$\omega|_{\sigma=0} = 0 \ , \ \frac{\nu_V}{H}\frac{\partial u}{\partial \sigma}\bigg|_{\sigma=0} = \frac{1}{\rho_0}|\vec{\tau}_s|\cos(\theta) \ \text{ and } \ \frac{\nu_V}{H}\frac{\partial v}{\partial \sigma}\bigg|_{\sigma=-1} = \frac{1}{\rho_0}|\vec{\tau}_s|\sin(\theta), \tag{2.11}$$

where θ is the angle between the wind stress and the direction of the grid-line η. The magnitude of the wind shear-stress, $|\vec{\tau}_s|$, is defined as $|\vec{\tau}_s| = \rho_a C_d U_{10}^2$, where, ρ_a is the density of air, C_d is the wind drag coefficient, and U_{10} is the wind speed at 10 meters.

For the open boundaries, Delft3D-FLOW offers water level, velocity, discharge, Neumann, or Riemann type of boundary conditions. For the model used in this study, Riemann type of boundary condition is set. The user defined forcing at the open boundary, $F_R(t)$, namely the Riemann invariant (in U-direction) is given by the expression, $U \pm \zeta\sqrt{\frac{g}{d}} = F_R(t)$. If measured elevation data is not available, the barotropic forcing is approximated by the superposition of free surface gradient for long term circulation, tidal fluctuations, meteorological forcing, and waves.

At closed (land-water) boundaries, flow normal to the boundary is set to *zero*, whereas for flow along the closed boundary, either the free slip condition (zero tangential shear-stress)

for large scale simulations, where influence of the walls can be neglected, or the partial slip condition for small scale flow, where the tangential shear-stress is computed from frictional velocities, can be specified. For the model used in this study, the partial slip condition is set

Transport Boundary Conditions:

Transport boundary conditions at the free surface and bed, except the heat exchange through the free surface, are given as

$$\frac{D_V}{H}\left.\frac{\partial c}{\partial \sigma}\right|_{\sigma=-1} = 0 \text{ and } \frac{D_V}{H}\left.\frac{\partial c}{\partial \sigma}\right|_{\sigma=0} = 0. \tag{2.12}$$

At the open boundaries, transport is described by the advection-diffusion equation. At outflow no boundary condition is allowed and at inflow one boundary condition is needed. To avoid the discontinuity in the concentration at the turn of the flow, when the concentration of the outflow differs from the concentration at the inflow, Thatcher-Harleman boundary condition is applied. This condition is described by the expression

$$C(t) = C^{out} + \frac{1}{2}\left(C^{bnd} - C^{out}\right)\left[\cos\left\{\pi\frac{T_{ret} - t_{out}}{T_{ret}}\right\} + 1\right] \ , \ 0 \leq t_{out} \leq T_{ret}, \tag{2.13}$$

where, C^{out} is the computed concentration at the last time of the outflow, C^{bnd} is the used defined background concentration, t_{out} is the time elapsed since the last outflow, and T_{ret} is the transition time of the concentration at the boundary from the outflow value to the inflow value.

Turbulence

The horizontal eddy viscosity coefficient, ν_H, is a superposition of three parts and is described via the relation:

$$\nu_H = \nu_{SGS} + \nu_{3D} + \nu_H^{back}, \tag{2.14}$$

where, ν_{SGS} is the part associated with the sub-grid scale turbulence and it is computed by a dedicated SGS-turbulence model, ν_{3D} is the part associated with the three-dimensional tur-

bulence and is computed through a turbulence closure model, and ν_H^{back} is the user defined background value. Similarly the vertical eddy viscosity coefficient, ν_V, is described as

$$\nu_V = \nu_{mol} + max\left(\nu_{3D}, \nu_V^{back}\right), \tag{2.15}$$

where ν_{mol} is the kinematic viscosity of water. In this study, ν_V is determined by the $k-\varepsilon$ turbulence closure model implemented in Delft3D-FLOW, in which both the turbulent energy k and dissipation rate of turbulent kinetic energy ε are calculated and ν_V is computed from k, ε, and mixing length L.

Heat Flux Equations

The heat exchange at the sea bed is set to *zero*, which may lead to over prediction of the water temperature in shallow regions. Through the free surface heat exchange is computed via a heat flux model implemented in Delft3D-FLOW by separate fluxes due to incoming radiation, back radiation, evaporation and convection. The heat balance equation at the free surface is

$$Q_{tot} = Q_{sn} + Q_{an} - Q_{br} - Q_{ev} - Q_{co}, \tag{2.16}$$

where, Q_{tot} is the total heat flux through the air-water interface, Q_{sn} is the net incident solar radiation, Q_{an} is the net incident atmospheric radiation, Q_{br} is the back radiation, Q_{ev} is the evaporative heat flux, and Q_{co} is the convective heat flux. The change in temperature in the top layer, T_s, is given by

$$\frac{\partial T_s}{\partial t} = \frac{Q_{tot}}{\rho_w c_p \Delta z_s}, \tag{2.17}$$

where, c_p is the specific heat capacity of sea water, ρ_w is the specific density of water, and Δz_s is the thickness of the top layer.

2.2 SET-UP OF THE HYDRODYNAMIC MODEL

For this study, it is very important to construct a physical setting that realistically represents the thermohaline structure and dynamics in such a small domain where even minor influences have considerable effects. The spatial resolution of the model is set to 0.5 km in the horizontal (Figure 2.2) and 20 σ-layers in the vertical direction to resolve these small scale processes. The model has a time step of 5 minutes. To initialize the model, spatially uniform temperature and salinity averaged from *in situ* measurements of corresponding season are used. It initially starts at March 2007 with uniform 15°C temperature, 39.1 psu salinity, and 0 m water level. It spins up for 10 months until January 2008 and then runs for three years until January 2011.

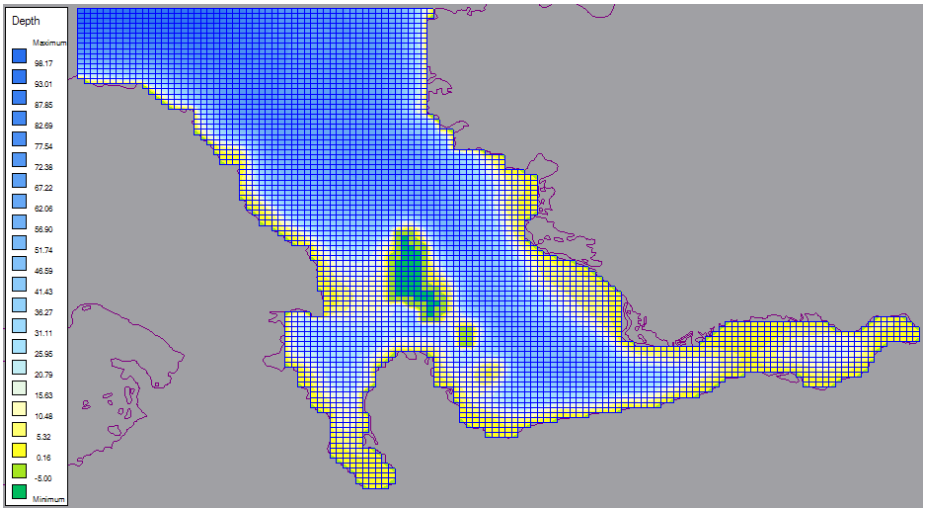

Figure 2.2: Numerical grid and bathymetry used in this study.

At the open boundaries, for flow boundary conditions the Riemann type boundary condition is set with Riemann invariant equal to 0 m s^{-1}. Thus, inflow and outflow at the boundary is not forced but rather with this kind of absorbing boundary condition the error at the boundary is minimized while keeping the boundary open. Heat and salt transport through the open boundaries also have an important role in determining resulting modelled fields of these parameters. For the boundary conditions of the entire time span, *in situ* measurements are prescribed time and space dependent and vertically integrated to sigma layers.

Another important forcing used in this model is the wind stress, since it is stated by Sayın (2003) and Sayın et al. (2006) that the general circulation is mainly wind driven. Direct measurements of wind velocity available at State Meteorological Institute do not adequately

resolve the spatial distribution over the surface area of the domain and is temporally discontinuous at times. Therefore, SeaWINDS remotely sensed wind stress fields are used to construct wind forcing inputs. This data set is temporally high resolution (6 h.) but spatially coarse (0.25 deg.), considering the small area of the bay, so it is applied on a larger grid containing the model domain within to allow for the proper spatial variation (Figure 2.3).

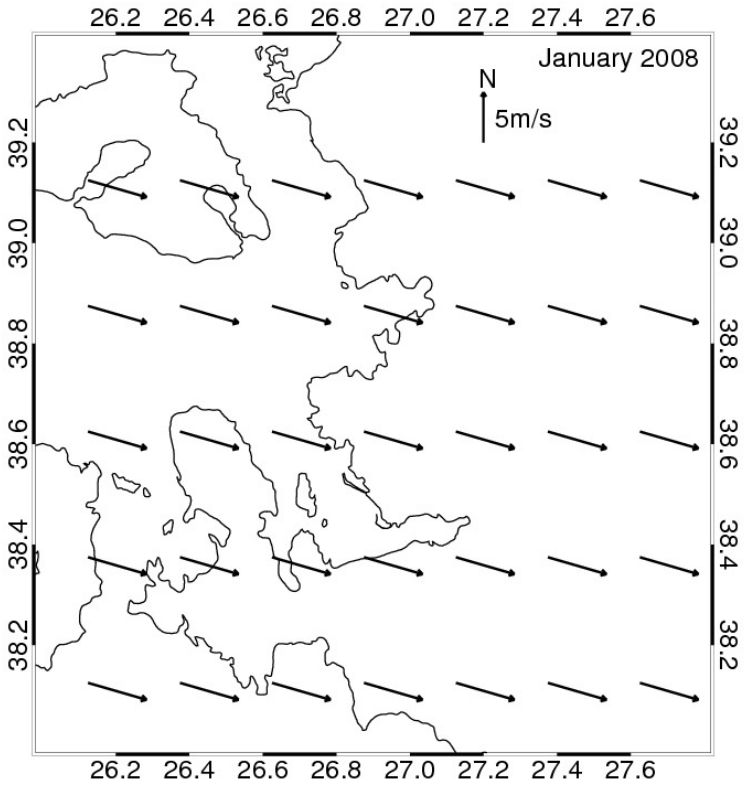

Figure 2.3: A sample from January 2008 of time and space varying wind stress fields.

Heat flux through the free surface is one of the main factors determining the thermohaline structure in the bay, since the majority of the bay is very shallow and reacts strongly to warming and cooling. The built-in heat flux model in Delft3D-FLOW computes the incoming solar radiation at the latitude of the model domain and calculates the heat flux through the free surface by taking into account the air temperature, relative humidity, and cloudiness. Meteorological input required for calculations is obtained from the ECMWF ERA-Interim data set (Figure 2.4). Temporal resolution of this input is very high (3 h.) but the spatial resolution is quite low (1.5 deg.) for the study area, however, the latter is not taken into consideration because meteorological forcing is applied spatially uniform since variation over this small

domain can be ignored.

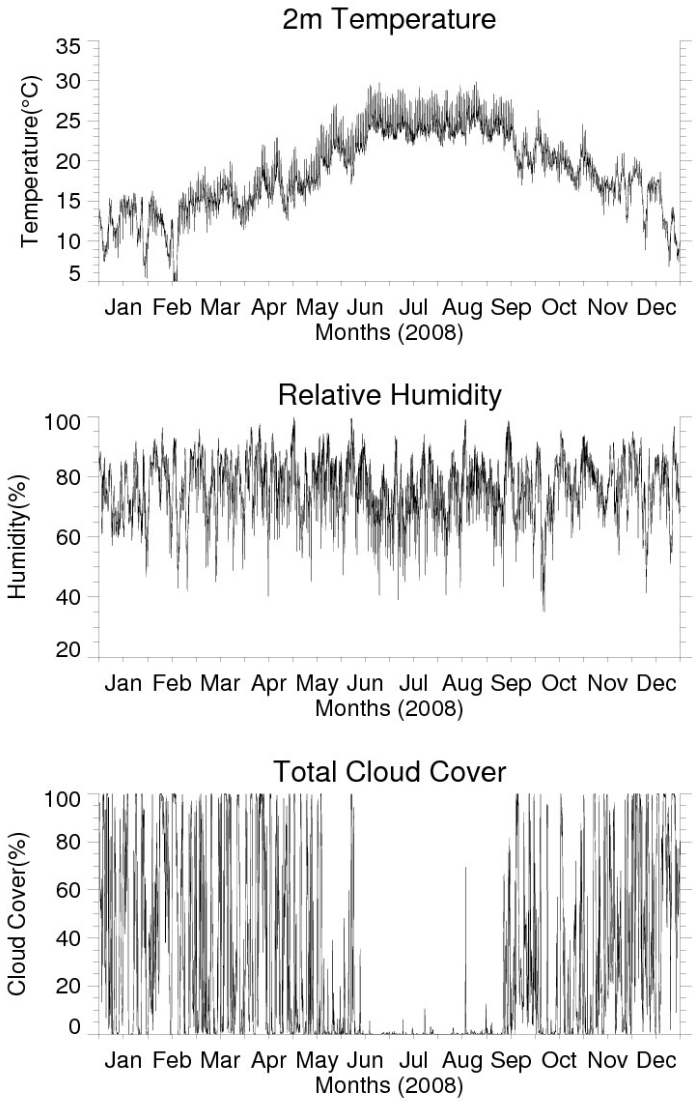

Figure 2.4: A sample from 2008 of time-series meteorogical inputs.

Fresh water fluxes to the bay are another important influence on the thermohaline structure and because they are the major sources of loads discharged into the bay, it is of great concern to properly include them in the hydrodynamics model that is to be coupled to the ecosystem model. The main fresh water input to İzmir Bay is the Gediz River. For Gediz River, monthly flux averaged over more than 50 years of observations are available, but has been considered not applicable for this study for it did not represent the actual flux during the time covered by the model. Instead, the actual annual flux is obtained from the MED POL reports (METU-IMS and DEU-IMST, 2007, 2008, 2009) for the years of interest and distributed monthly

by using precipitation data retrieved from ECMWF ERA-Interim data set (Figure 2.5). To represent the contribution of Çigli Waste Water Treatment Plant and also rain drainage on the shallow inshore regions, point sources of fresh water are added to Inner and Outer II bays and, a fraction of calculated Gediz River flux is prescribed. To eliminate discrepancies between modelled and observed salinity, these fluxes are tuned on the basis of observed salinity in each respective region. No measurement or literature is available on the temperature of the fresh water inputs and *in situ* measurements performed at the closest point to the sources are prescribed as input. It may be considered *biased* to tune external forcings based on the properties of the water body that is to be modelled, but in this study it was the only reasonable option to properly cover for the unavailable input mandatory for this modeling study.

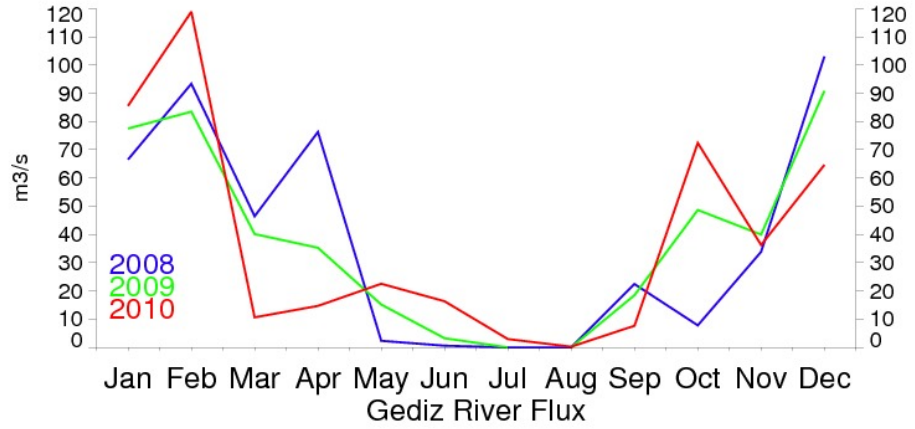

Figure 2.5: The time-series flux data of Gediz River.

2.3 DESCRIPTION OF DELFT3D-ECO MODULE

Delft3D-ECO is the ecological module in the Delft3D modelling suite and it contains the sophisticated algae model BLOOM. Delft3D-ECO can be used for simulations of eutrophication featuring the competition between several groups of algae species, adaptation of algae to environmental changes in terms of stoichiometry and growth characteristics, limiting factors for algae growth, oxygen kinetics including daily cycles.

Ecological processes involved in the ecosystem model in this study can be grouped under tree main sets: general water quality processes (such as, advection-diffusion of nutrients, sinking and remineralization of particulate organic matter, and etc.), processes of interactions be-

tween the sediment and the overlying water (such as, resuspension), and processes of primary production. In the following paragraphs, descriptions of these three groups of processes are given. (Note: Biological and chemical processes that are used in Delft3D-ECO, as well as in other modules of Delft3D are stored in a single process library called DELWAQ. A number of models developed by WL | Delft Hydraulics serving different purposes and having different names (for example, GEM (Blauw et al., 2009)) are all constructed by selection of necessary processes from the same library. Thus, while giving the description of Delft3D-ECO, literature regarding other models and modules by WL | Delft Hydraulics is referred to as well.)

General Water Quality Processes

The advection-diffusion equation is given by

$$\frac{\partial C}{\partial t} = -u\frac{\partial C}{\partial x} - v\frac{\partial C}{\partial y} - w\frac{\partial C}{\partial z} + \frac{\partial}{\partial x}\left(D_x\frac{\partial C}{\partial x}\right) + \frac{\partial}{\partial y}\left(D_y\frac{\partial C}{\partial y}\right) + \frac{\partial}{\partial z}\left(D_z\frac{\partial C}{\partial z}\right) + S + P, \quad (2.18)$$

and balance equations of state variables (Blauw et al., 2009) are given by

$$\frac{dNO_3}{dt} = nit - den - upt_N * (1 - f_{am}) \quad (2.19)$$

$$\frac{dNH_4}{dt} = dec_{PON} + dec_{PON_S} - nit + rsp_{N,G} + f_{aut} * mor_N - upt_N * f_{am} \quad (2.20)$$

$$\frac{dPO_4}{dt} = dec_{POP} + dec_{POP_S} + rsp_{P,G} + f_{aut} * mor_P - upt_P \quad (2.21)$$

$$\frac{dSi}{dt} = dec_{POSi} + dec_{POSi_S} + f_{aut} * mor_{Si} - upt_{Si} \quad (2.22)$$

$$\frac{dO_2}{dt} = rea + (gro_C - dec_{POC} - dec_{POC_S}) * s_O - nit * s_{NO} \quad (2.23)$$

$$\frac{dPOX}{dt} = mor_X * (1 - f_{aut}) - sed_{POX} - dec_{POX} - grz_{POX} - exc_{POX} \quad (2.24)$$

$$\frac{dPOX_S}{dt} = (sed_{POX} - dec_{POX_S} - bur_{POX_S} + exc_{POX_S}) * Z. \quad (2.25)$$

Table 2.2: List of symbols used in advection-diffusion and balance equations

Symbol	Unit	Definition
C	gm^{-3}	Concentration
u, v, w	ms^{-1}	Components of the velocity vector
$D_{x,y,z}$	m^2s^{-1}	Components of the dispersion tensor
S	$gm^{-3}s^{-1}$	Source and sink of mass due to loads and boundaries
P	$gm^{-3}s^{-1}$	Source and sink of mass due to processes
NO_3	gNm^{-3}	Nitrate
NH_4	gm^{-3}	Ammonium
PO_4	gPm^{-3}	Ortho-phosphate
Si	$gSim^{-3}$	Dissolved silicate
POX	gXm^{-3}	Particulate organic matter
POX_S	gXm^{-3}	Particulate organic matter in the sediment
nit	$gNm^{-3}d^{-1}$	Nitrification
den	$gNm^{-3}d^{-1}$	Denitrification
rea	$gO_2m^{-3}d^{-1}$	Reaeration
gro	$gCm^{-3}d^{-1}$	Net phytoplankton growth
sed	$gXm^{-3}d^{-1}$	Settling
upt_X	$gXm^{-3}d^{-1}$	Uptake of nutrients by phytoplankton growth
dec_X	$gXm^{-3}d^{-1}$	Decomposition of dead particulate organic matter
$rsp_{X,G}$	$gXm^{-3}d^{-1}$	Respiration by filterfeeders
grx_X	$gXm^{-3}d^{-1}$	Grazing by filterfeeders
exc_X	$gXm^{-3}d^{-1}$	Excretion of organic matter by filterfeeders
mor_X	$gXm^{-3}d^{-1}$	Formation of dead organic matter by phytoplankton mortality
bur_X	$gXm^{-3}d^{-1}$	Burial
f_{am}	–	Fraction of ammonium in nitrogen uptake
f_{aut}	–	Autolysis fraction of mortality
s_O	gO_2gC^{-1}	Oxygen carbon ratio in detritus
s_{NO}	gO_2gN^{-1}	Oxygen nitrogen ratio in NO_3
Z	m	Water depth

Sediment-Water Interaction Processes

A sub-model called SWITCH (Sediment Water Interaction by Transport and Chemistry) predicts the nutrient fluxes across the sediment-water interface. Concentrations of detritus, oxygen, NH_4, NO_3, PO_4 and Si in the sediment and in the pore water are simulated dynamically using mass-balance equations (WL | Delft Hydraulics, 2009b). SWITCH is applied as any other process in the DELWAQ library.

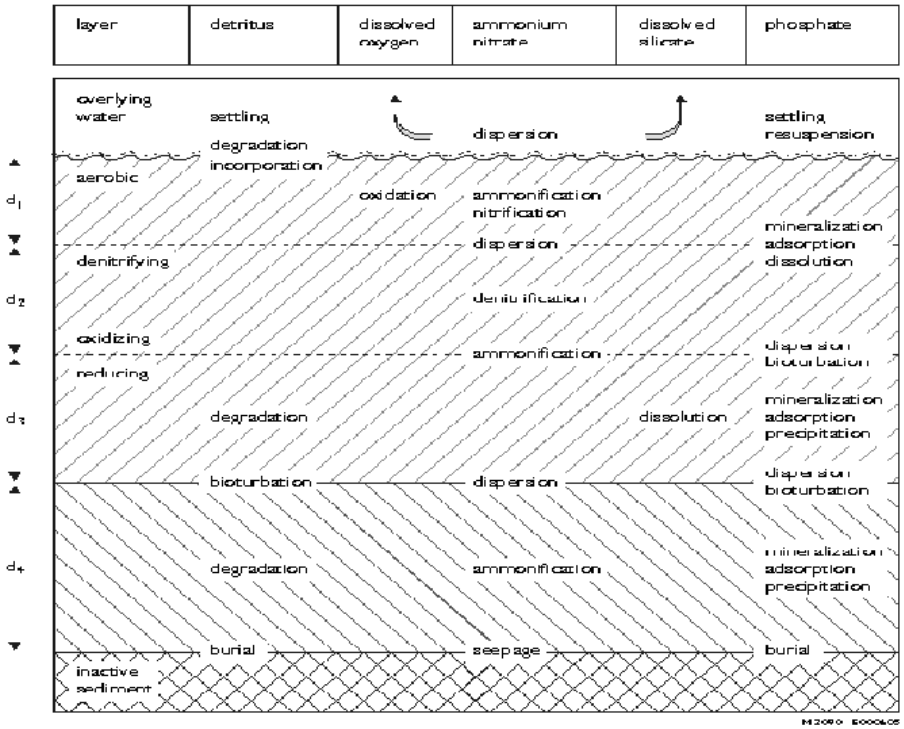

Figure 2.6: Overview of the processes included in SWITCH from (WL | Delft Hydraulics, 2009b).

In Figure 2.6, a schematic representation of all the processes that SWITCH is capable of carrying out and the vertical layering are presented. In the following part, brief descriptions processes that are related to this study are given in terms of substances. For further information the Technical Reference Manual for SWITCH, prepared by WL | Delft Hydraulics, can be referred to.

Oxygen is consumed in degradation of detritus in the boundary layer and in nitrification and chemical oxidation in the the aerobic layer. The amount of **detritus** settling to sediment is

computed by Delft3D-ECO and used by SWITCH as input. Detritus is subject to settling, resuspension, incorporation from the boundary layer into the sediment, degradation, and burial. **NH_4**, produced during degradation of detritus can be transported vertically and through nitrification it is converted to NO_3 under aerobic conditions. **NO_3**, produced through nitrification can be transported vertically and below the aerobic layer it is subject to denitrification. **PO_4** is similarly produced during the degradation of detritus and can be transported vertically.

Primary Production Processes

At the heart of the Delft3D-ECO module is the phytoplankton model BLOOM (Los, 2009). The model distributes the available resources in an optimal way among the different types of algae. In other words, the purpose of the BLOOM model is "*selecting the best adopted combination of phytoplankton types at a certain moment and at a certain location consistent with the available resources, the existing biomass levels at the beginning of a time interval, and the potential rates of change of each type*" (Los, 2009, chap. 1). BLOOM model has been applied to Southern North Sea and has been validated for 25 years' of data in the Dutch coastal zone. In the following paragraphs distinctive features of the BLOOM model is explained and in the rest of this subsection all information is referred to Los (2009, chap. 1).

One of the main processes in the model is the competition between phytoplankton species. Requirement (defined as the amount of a resource per unit biomass of the phytoplankton necessary to survive), as well as, growth rates are essential according to the general theory on *K*- and *r*-strategies. BLOOM operates according to a two-parameter principle, taking into account both the potential growth rate and requirement as its selection criterion. The model considers P_{n_k}/n_{ik} to determine which species will be dominant, where P_{n_k} is the potential net growth rate of species k under the prevailing light conditions, and n_{ik} is its requirement for resource i such as a nutrient or light. In practice this means that in model simulations opportunistic, *r*-selected, species with high maximum growth rates dominate, when the average light intensity is high, for instance, during the spring bloom, whereas, efficient *K*-selected species with lower maximum growth rates and lower resource requirements dominate, when the average light intensity is low and external forcings are relatively stable.

The idea of 'conditional steady states' is another feature of the BLOOM model. In reality, not every theoretically possible (i.e. unconditional) steady state can be achieved in a short time in eutrophic waters, where growth rates are lower than maximum due to turbidity and are

not sufficient for a complete shift in species dominance. BLOOM adopted the idea that the number of acceptable solutions can be limited to those that might be achieved given the growth and mortality rates of the prevailing conditions, allowing for the combination of species which cannot reasonably be achieved within a time-step of the model to be left out. In practice, BLOOM delimits the biomass of a species to its potential net growth rate if at the beginning of a time-step its biomass is small compared to its equilibrium value, whereas, if its biomass is sufficiently close to its steady state, then its biomass is determined by the availability of the resources.

Another important characteristic of the BLOOM model is its approach to the concept of adaptation to varying conditions. The functional groups of the model are 'species' representing a taxonomic species, or a broader group of species that are ecologically similar. To account for the variations in the internal stoichiometry of a species, there are subunits called 'types' under each model species. A type represents the physiological state of a species under different conditions of limitation. Basically there are three types under each species representing the condition of the species under N (N-type), P (P-type), and light (E-type) limitation. Each type has different fixed characteristics of nutrient content, and rates of specific extinction, growth, mortality, and sedimentation. At any time-step, distribution of these three types are selected at any ratio given the environmental conditions, so the average characteristics of a species vary continuously in time and space. Thus, in BLOOM, by appropriate selection of the parameters of types of each species, dependence between limiting factors and inter-specific variations is modelled.

Nutrient Balance:

The total concentration, C_i, of a nutrient i in the water column is defined as

$$C_i = \sum_k (n_{ik} B_k) + d_i + w_i, \tag{2.26}$$

where, n_{ik} is the requirement of species k for nutrient i, d_i and w_i are the amount of nutrient i in dead algae and the amount dissolved in the water column, respectively.

Nutrient Recycling:

The rate of change of d_i is given by

$$\frac{d}{dt}d_i = \sum_k \left(f_p M_k n_{ik} B_k\right) - m_i d_i - s d_i \tag{2.27}$$

where, f_p is the fraction of dead phytoplankton cells that are not immediately taken out of the live pool, M_k is the mortality rate of species k, m_i is the remineralization constant of nutrient i, and s is the settling constant of dead cells. M_k and m_i are both temperature dependent.

Energy Limitation:

The response of phytoplankton to light shows much stronger variations compared to other resources. This variation is due to 1) change of level of irradiance in very short time scales (such as within a day), 2) the depth at which phytoplankton is exposed to light, and 3) differences in the reaction to light of different species. In BLOOM, instead of a functional relationship between the light intensities and the corresponding growth rates, a look-up table for each species, which is constructed using experimental data sets, consisting of the correct efficiency factor, E_k, for any light condition is used. The overall energy budget is then

$$\frac{d}{dt}B_k = \left(Pg_k^{max} E_k - M_k - R_k\right) B_k. \tag{2.28}$$

where Pg_k^{max} is the maximum gross growth rate, and M_k and R_k are mortality and respiration rates respectively.

Specific light extinction coefficient for living algae of type k is denoted by K_k, and total extinction due to total living material is

$$KL = \sum_k \left(K_k B_k\right). \tag{2.29}$$

Similarly, assuming the extinction due to dead algae is a fraction, e_d, of the extinction due to living algae, the total extinction due to dead material is

$$KD = e_d \sum_k \left(K_k f_p M_k B_k\right). \tag{2.30}$$

For a species k at a certain value of the average extinction, K_k^{max}, the net growth of this species is exactly zero. On the other hand, when the extinction is at a minimum value, K_k^{min},

light intensity becomes too high and photo inhibition results in low growth rates. Hence,

$$K_k^{min} \leq KL + KD + KW \leq K_k^{max}, \tag{2.31}$$

where, KW is the extinction due to all other materials in water. If the total extinction is outside this range, then B_k will be zero.

Growth and Mortality Limits:

When environmental conditions (such as nutrient concentrations) improve at a rate larger than the potential growth rate of a species k, the species may not reach the level at which light or a nutrient becomes limited in a single time-step of the model. To account for this, during the optimization process constraints are set to delimit the maximum biomass increase within the time interval. It is assumed that losses are low during the exponential growth and mortality can be ignored in the computation of this constraint. For an algae type k, maximum possible biomass concentration, B_k^{max} is

$$B_k^{max} = B_k^0 \exp\left(p_{nk}\Delta t\right), \tag{2.32}$$

where, B_k^0 is the initial concentration at the beginning of the time interval, $p_{nk}(= Pg_k^{max}E_k - R_k)$ is the net production rate constant, and Δt is the time interval. B_k^0 is taken as the net result of the previous time-step of the BLOOM computation.

When the environmental conditions decline rapidly, decrease in biomass concentration is constrained to avoid the complete removal of a species within a time-step. The minimum biomass of species k, B_k^{min}, is obtained assuming there is no production but only mortality, such that

$$B_k^{min} = B_k^0 \exp\left(-M_{nk}\Delta t\right). \tag{2.33}$$

This minimum value is computed for each type of a species k, hence the maximum possible mortality cannot be exceeded, but shifts from one type to another remain possible. When a conflict occurs between the constraints on mortality and energy, such that light availability drops suddenly, demanding the biomass to be small, but according to equation (2.33), a large

amount of biomass needs to be maintained, constraint on mortality overrules. In other words, types disappear according to equation (2.33) in unfavorable conditions.

Grazing:

In this study, grazing as a forcing function approach is applied. The biomass levels are prescribed as a function of time and space for one or more grazers. Also their filtration and digestion rates, food preference, and nutrient stoichiometry can be specified in advance. As much phytoplankton biomass is taken as to sustain the prescribed grazer biomass and when there is no sufficient phytoplankton, the grazer biomass is reduced.

2.4 SET-UP OF THE REFERENCE ECOSYSTEM MODEL

Ecosystem model is off-line coupled to the hydrodynamics model. It is run on the same computational grid and flow velocity, temperature, and salinity fields are taken from the hydrodynamic model output with the required temporal resolution. It has a time step of 12 hours. It initially starts at March 2007 with uniform values obtained from the measurements. It spins up for ten months and then runs from January 2008 until January 2011 covering a total of three years.

The sources of nutrient loads prescribed in the model are fresh water discharges, atmospheric input, and input through the open boundary. For the open boundaries inputs are taken from the measured nutrient concentration at the Outer III bay. Atmospheric deposition fluxes are taken from estimations for the northern Levantine by Koçak et al. (2010). Gediz river nutrient and dissolved oxygen concentrations are taken from the the MED POL reports (METU-IMS and DEU-IMST, 2007, 2008, 2009). Since no measurement is available for rain drainage points, data measured in similar regions are adapted. For Gulbahce bay region, PO_4 values measured within the MED POL project at the Lamas river (Mersin, Turkey) are used, and for the Inner bay region, PO_4 values measured within the SINHA project (SINHA, 2010) at the Çigli WWTP are used. NO_3 and NH_4 input is then tuned with respect to distribution of N/P ratio in these regions, computed from the available nutrient measurements. Organic material carried by Gediz river and rain drainage, and Cigli WWTP is computed from the BOD_5 measured at the Gediz river and Çigli WWTP respectively, using the empirical relations given by

$$DOC = BOD_5 \div 3 \text{ for rivers, } DOC = BOD_5 \div 2.5 \text{ for waste waters,} \quad (2.34)$$
$$\frac{DOC}{DON} = 10 \ , \ \frac{DOC}{DOP} = 200 \ , \ \frac{DOC}{DOSi} = 200 \ , \text{ and } DOM : POM = 1 : 1 \ .$$

2.5 SET-UPS OF THE NUTRIENT ENRICHMENT/REDUCTION SCENARIOS

Table 2.3: List of scenario runs.

Run	PO_4	DIN
Reference	-	-
A	-	+10%
B	-	-10%
C	+10%	-
D	+10%	+10%
E	+10%	-10%

As one of the main objectives of this study is evaluating the ecosystem response of the bay to possible changes that may occur in the future in terms of nutrient loads, a set of experimental ecosystem model scenarios are designed (Table 2.3). Main assumptions at the basis of these scenarios are *i*) treatment of PO_4 is not improved, so it either stays in today's level (runs A, and B) or increases (runs C, D, and E), *ii*) treatment of DIN is improved, so a reduction occurs in DIN loads (runs B, and E), and *iii*) treatment of DIN is not improved, so it either stays in today's level (run C) or increases (runs A, and D). As the urbanization increases, the load of PO_4, a pollutant of domestic origin, increases, and it have been stated by Küçüksezgin et al. (2004), Küçüksezgin et al. (2006), and Kontas et al. (2004) that even after treatment facilities had been installed, PO_4 level have continued to increase, therefore to keep the scenarios as realistic as possible it is not assumed that a reduction occurs in PO_4. The purpose of separately increasing/decreasing PO_4 and DIN loads is to enable the evaluation of the different responses of the contrasting N-limited and P-limited environments existing in the bay. Overall analysis of the scenario results will provide a comprehension of relative effect of these two nutrients on the eutrophication process of the bay, and furthermore the outcome of this study will provide a valuable insight for policy makers on improvement of wastewater treatment facilities.

2.6 MODEL SKILL ASSESSMENT METHODS

Stow et al. (2009) lists a series of measures to assess model skill of coupled marine ecosystem models. Among these, three statistical measures are used in this study for the skill assessment of reference hydrodynamics and ecosystem runs. The definition of chosen parameters are given by

r, the correlation coefficient of model results and observations:

$$r = \frac{\sum_{i=1}^{n}(O_i - \bar{O})(P_i - \bar{P})}{\sqrt{\sum_{i=1}^{n}(O_i - \bar{O})^2 \sum_{i=1}^{n}(P_i - \bar{P})^2}} \tag{2.35}$$

RMSE, root mean squared error:

$$RMSE = \sqrt{\frac{\sum_{i=1}^{n}(P_i - O_i)^2}{n}} \tag{2.36}$$

AAE, average absolute error:

$$AAE = \frac{\sum_{i=1}^{n}|P_i - O_i|}{n} \tag{2.37}$$

where P is the model results and O is the observations.

The correlation coefficient, r, varies between -1 and 1, negative values indicating negative correlation. This parameter is a measure of how model results vary with varying observations, such that if model results increase/decrease in correlation to increasing/decreasing values of observations r is closer to 1, but if model results fail to vary with increasing/decreasing observations or vice-versa, r is closer to 0. Although r gives a sense of how a model performs when compared to a observation data set, it does not measure the actual difference between the model and observation. RMSE and AAE, on the other hand, are direct measures of error between these two. AAE is the simple average of the absolute difference between model results and observations, and RMSE is a weighted average of the the same error such that larger

errors have a greater contribution. Thus, together with RMSE and AAE, r is used in this study to evaluate the performance of the reference models.

Model misfit versus observation analyses are also used to address the shortcomings of the reference models. Model error is plotted against the observations and plots are color-coded with respect to time and space. These plots reveal when and where the model fails or achieves to produce the observed values and give profound insight on model performance such that the models incapability or success in capturing certain features is revealed in terms of the density of error points in certain ranges of observation values.

CHAPTER 3

RESULTS

In this chapter, results of the hydrodynamics and ecosystem reference model, and analysis of nutrient enrichment tests are given. Reference model results are presented with comparisons to available measurements. Model skill assessment analyses are given separately for hydrodynamics and ecosystem reference models at the end of each respective section. Results of the nutrient enrichment/reduction scenarios are given in terms of percent differences with respect to the ecosystem reference run in selected parameters.

3.1 HYDRODYNAMIC MODEL RESULTS AND SKILL ASSESSMENT

Most important outcome of the hydrodynamic modelling effort is that the time-dependent representation of the physical setting present in İzmir Bay is obtained for the first time in this region. In this section, surface current velocity, temperature, and salinity fields, time-depth distributions of temperature and salinity from two points, and model skill assessment analyses in terms of temperature and salinity are given.

Yearly averaged surface current velocity fields (Figure 3.1) show the flow patterns that are present in the bay independent of the season. It can be seen that Aegean Sea waters enter the bay from the north and mainly follow the eastern and western coast lines. In Outer III bay a cyclonic gyre is observed in all three yearly averages. Along the eastern coast Gediz River plume can be prominently seen. Along the western coast line the branch of inflowing water passes Mordoğan Strait, turns to east, and reaches Outer I bay. In Inner bay a weak anti-cyclonic pattern is seen.

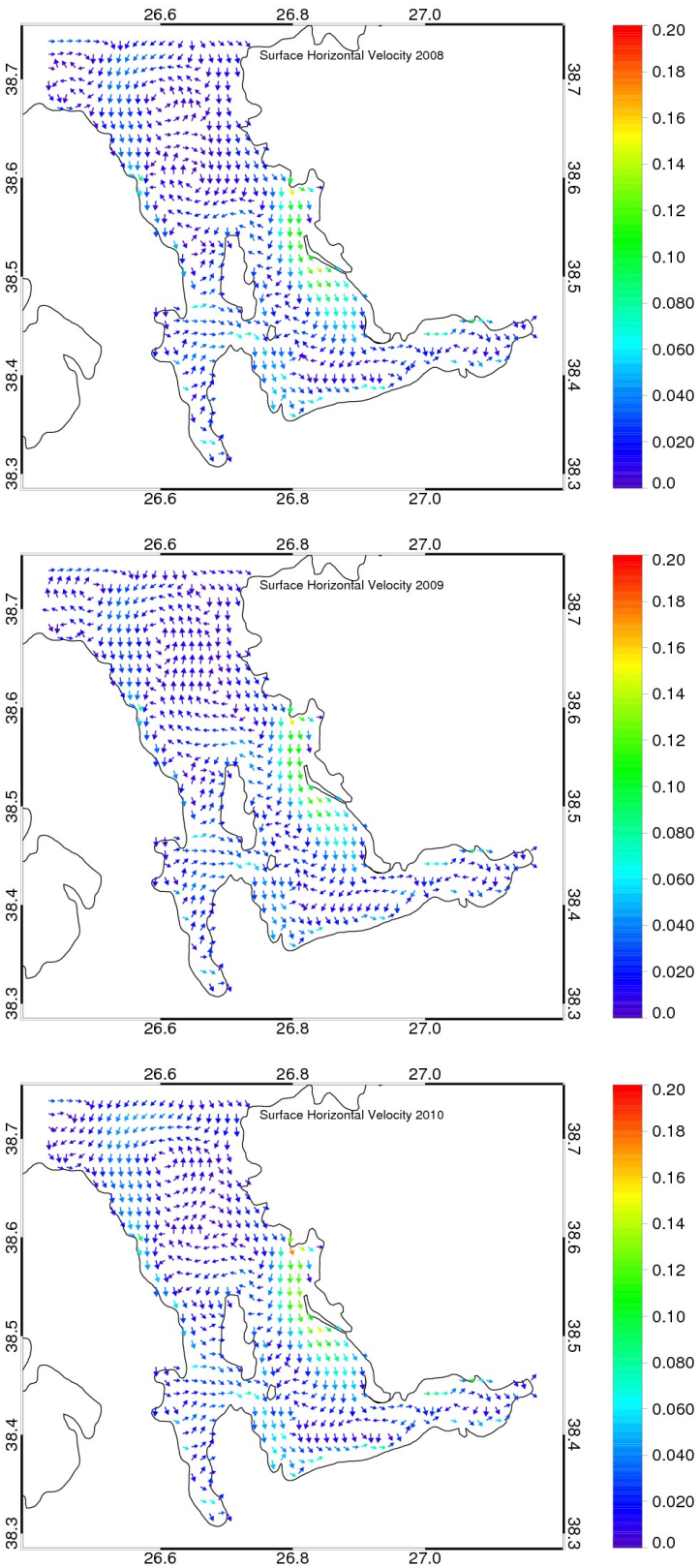

Figure 3.1: Yearly averaged surface horizontal current velocity model results from 2008 (top), 2009 (middle), and 2010 (bottom).

In November 2008 (Figure 3.2), it is seen that the bay is under the influence of mixing and surface temperature model results show a horizontally uniform distribution of around 18 °C. Surface salinity model results range between 39.2 - 39.5 psu. In the surface flow field Gediz River plume is observed to be prominent along the eastern coast. Model results are slightly lower, around 39.2 psu, compared to measurements in vicinity of this plume and also in Outer II and Inner bays, influenced by fresh water inputs.

In February 2009 (Figure 3.3), model results show that temperature ranges between 11-14 °C. As seen in the monthly averaged surface velocities, warmer Aegean Sea waters enter the bay from the north and occupy the Outer III region. Towards the inner parts temperature gradually drops forming a horizontal gradient. Minimum temperatures are seen in the shallow inner regions due to rapid cooling. A similar horizontal gradient is seen in the salinity fields due to increased fresh water flux in this season. Salinity is around 39.0 psu in the Outer III region reflecting Aegean Sea characteristics. It drops to around 38.0 psu in inner parts and Gediz River mouth, as well.

In April 2009 (Figure 3.4), surface temperature model results range between 14 -17 °C. Inflowing Aegean Sea waters are seen in the northwestern parts of the bay with warmer temperatures. Shallow regions react more rapidly to the onset of warming and show higher temperatures. In this season, horizontal salinity gradient is more pronounced. Aegean Sea waters with salinities around 39.2 psu occupy the northeast and towards the inner regions salinity drops down to 35.0 psu. The influence of the Gediz river lowers the salinity in the whole of the Outer I bay. An outflow, also seen in the surface velocities, along the western coast carries fresh waters towards the north, decreasing salinity in the western parts of the Outer III bay. It can be seen that this salinity pattern is in agreement with *in-situ* observations.

In July 2009 (Figure 3.5), horizontal temperature gradient seen in February is reversed such that, Aegean Sea waters with temperatures around 21 °C enter the bay from the north and temperatures increase to about 28 °C towards the shallow regions due to rapid warming. Model results show that inflowing cooler waters follow the eastern coast line of the Outer III and Outer I bays, lowering temperatures in these parts, causing an discrepancy with the measurements. Surface salinity model results are mostly uniform around 39.5 psu. Gediz River is dry during most of the summer and no fresh water influence is seen in Outer III Outer I bays.

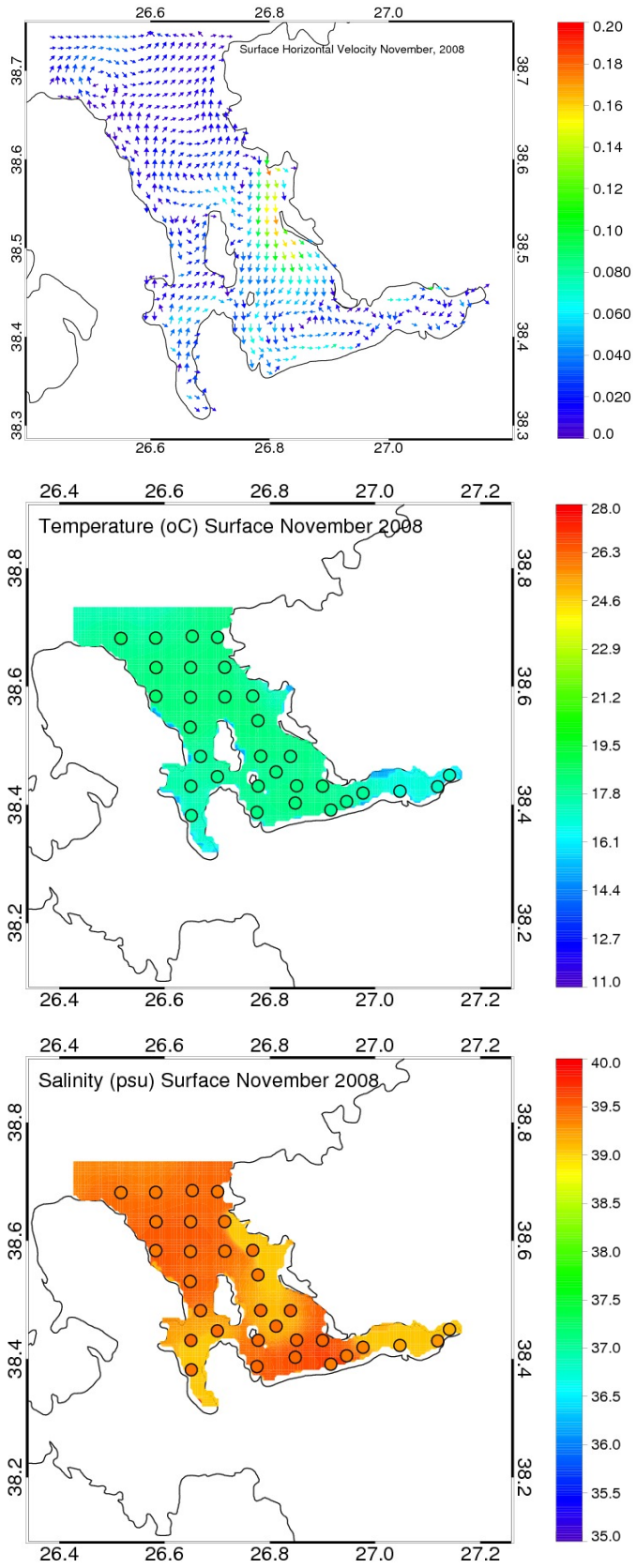

Figure 3.2: Surface current velocity (top), temperature (middle), and salinity (bottom) model results (background) in comparison to measurements (colored dots) from November 2008.

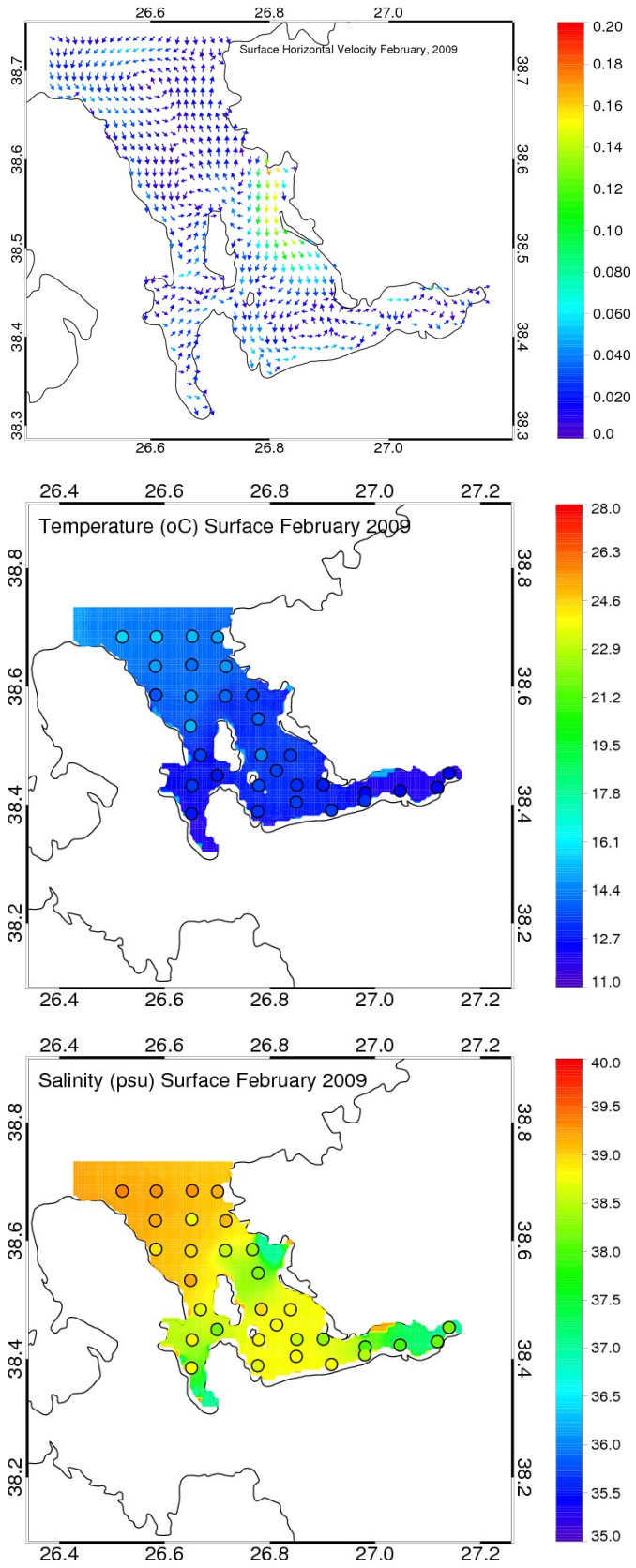

Figure 3.3: Surface current velocity (top), temperature (middle), and salinity (bottom) model results (background) in comparison to measurements (colored dots) from February 2009.

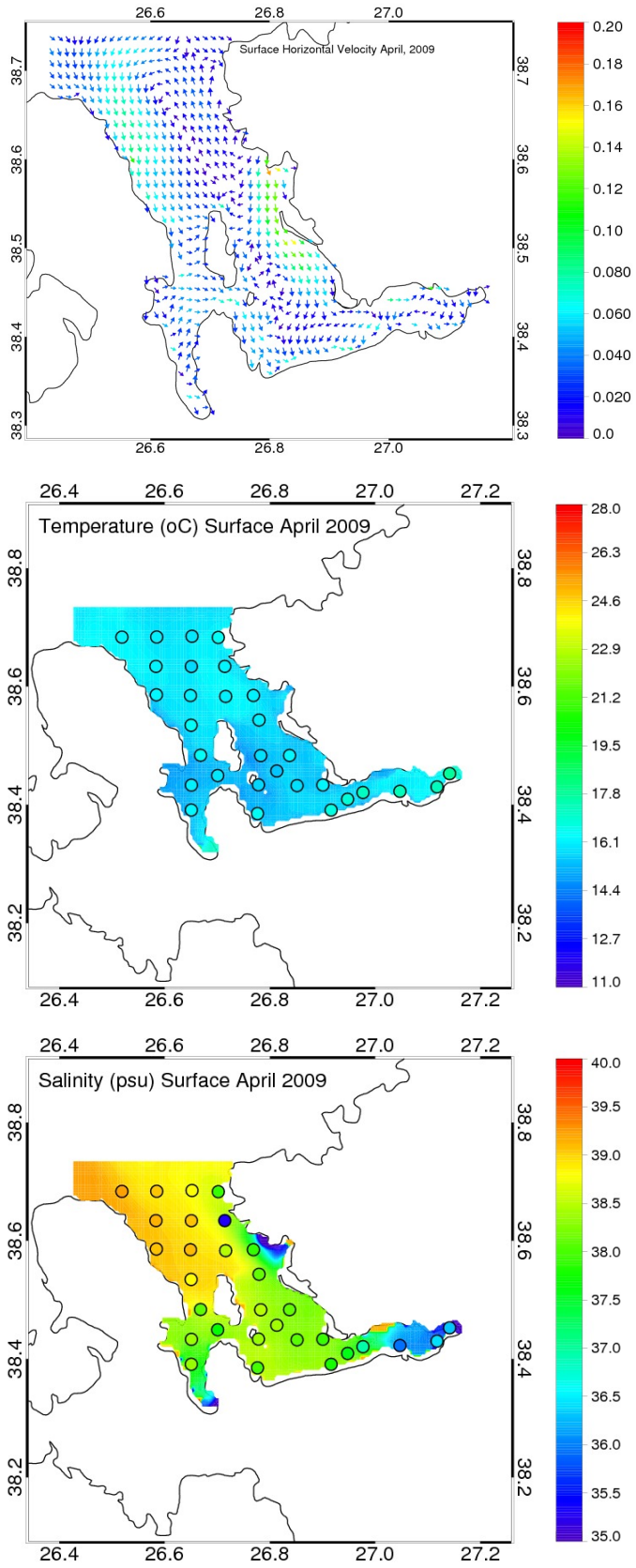

Figure 3.4: Surface current velocity (top), temperature (middle), and salinity (bottom) model results (background) in comparison to measurements (colored dots) from April 2009.

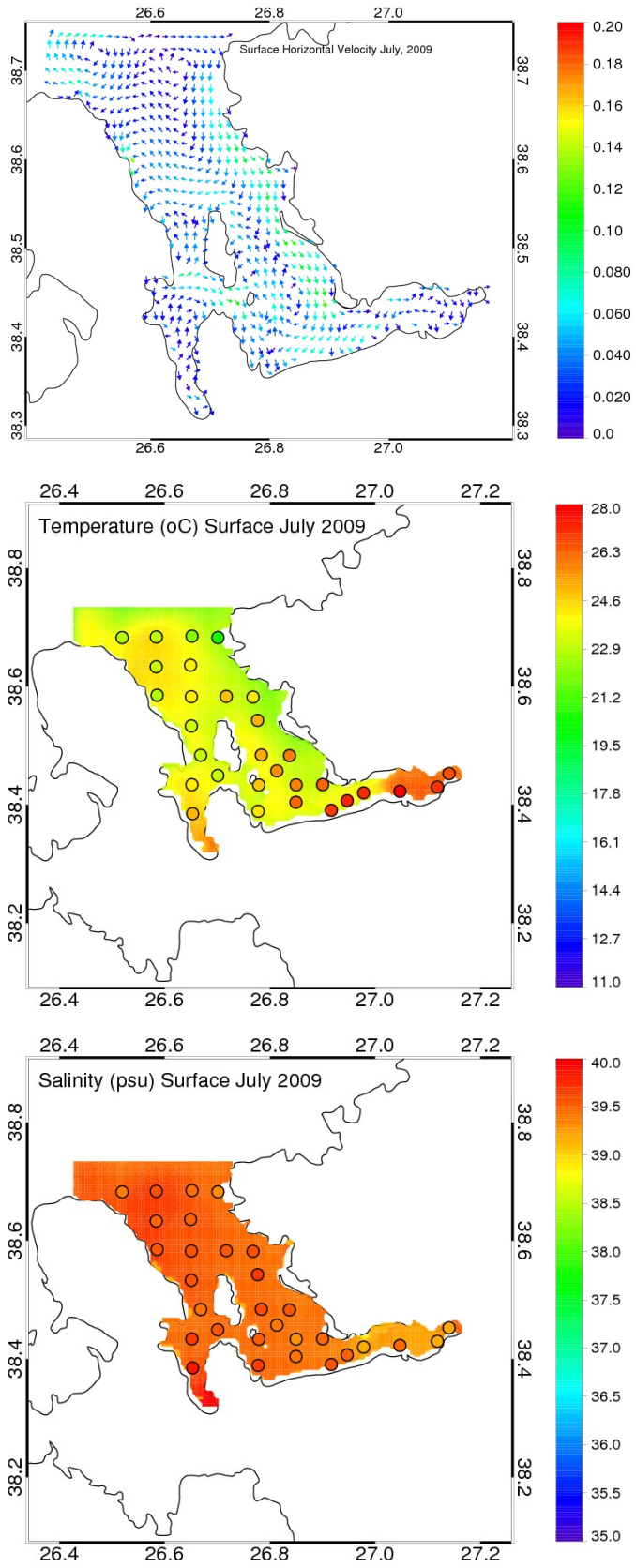

Figure 3.5: Surface current velocity (top), temperature (middle), and salinity (bottom) model results (background) in comparison to measurements (colored dots) from July 2009.

In November 2009 (Figure 3.6), due to mixing and onset of winter cooling, surface temperature model results are uniform around 19 °C, which is about 1 °C warmer than the previous November. This difference between the two consecutive years is confirmed with the observations. Also, fresh water inputs have a slightly more pronounced influence on modelled salinity compared to the previous year dropping it to 37.5 psu around Gediz River mouth, and in Outer II and Inner bays. In the Outer III bay, with the influence of the inflow seen in the velocity fields, salinity model results are around 39.2 psu showing Aegean Sea characteristics. Towards Outer I bay it increases to 39.4 psu.

In February 2010 (Figure 3.7), surface temperature model results range between 12 - 16 °C and show the horizontal gradient same as the previous year. Compared to the previous winter, as in autumn, the bay is observed to be warmer. Incoming Aegean Sea water occupying the western parts of the Outer III bay is warmer with temperatures of around 16 °C. Towards the shallower regions it drops to around 12 °C. Similarly modelled salinity shows the strong horizontal gradient seen in winter. As seen in the flow field, inflow along the northeastern coast brings the saline Aegean Sea water with 39.2 psu salinity. Effect of Gediz River is carried northward along the eastern coast by the outflow seen in the velocity field which is seen both in model results and measurements. Shallow Outer II and Inner bays are also heavily influenced by fresh water inputs with salinities as low as 35.0 psu.

In April 2010 (Figure 3.8), model results of surface temperature show the onset of warming with temperatures ranging between 14- 17 °C. Aegean Sea inflow along the northwestern coast with warmer waters and inner regions with cooler waters maintain the horizontal gradient. In modelled salinity, Aegean Sea influence in Outer III bay is more emphasized compared to the previous spring with slightly higher values of around 39.4 psu along the northwestern coast. In Inner and Outer II bays fresh water inputs drop the salinity to around 38.0 psu. Outer I region and the vicinity of the Gediz River plume also have slightly fresher waters of around 38.5 - 38.7 psu. Observations show the northward outflow of less saline waters along the east coast as in the previous season, but this feature does not exist in the model results, hence there occurs a discrepancy in salinity around this region.

In July 2010 (Figure 3.9), horizontal gradient in surface temperature reverses with respect to winter. Cooler Aegean Sea waters enter the bay from the north with temperatures around 24 °C and towards the inner parts surface temperature reaches to around 28 °C. It can be seen in

the surface velocity fields that inflow enters the bay off the northeastern coast and continues as far south as Outer I bay. This slightly stronger flow causes surface temperature model results to be lower than measurements. A horizontal gradient quite stronger than the previous summer is observed in modelled salinity. In Outer III bay Aegean Sea water with salinities around 39.6 psu is present and in Inner bay, heavily under the influence of fresh water inputs, salinity drops to 37.5 psu. A similar fresh water influence around the Gediz River mouth is observed in model results but not in measurements.

The time-depth distributions of modelled temperature and salinity in the Inner bay (Figure 3.10), show that this shallow part is vertically homogeneous in all seasons and the properties of the water column have a pronounced seasonal cycle. In winter, lower temperatures and lower salinities compared to the rest of the bay are seen in this region with around 11 - 12 °C and 36.5 - 37.0 psu. Towards late summer both parameters peak such that temperatures are around 28 °C and salinities are around 40.0 psu. Between the years, no significant difference in seasonal cycle is observed in terms of temperature but the year 2009 is slightly warmer in all seasons than the rest. In terms of salinity in years 2008 and 2009 seasonal variation is typical of the region but in year 2010 an exceptionally low salinity is seen in both model results and in measurements.

In Outer III bay, time-depth distributions (Figure 3.11) show the seasonal variation of thermocline and halocline in this deepest part of the bay. In winter, the water column in entirely mixed and modelled temperature and salinity are homogeneous around 14 - 15 °C and 39.0 - 39.2 psu, except for the short periods when fresh water originating from Gediz River reaches this part of the bay in upper layers and decreasing the salinity down to around 38.5 psu. With the onset of warming in late spring, a thermo/halocline starts to appear around 30 meters deep. Surface layers heat up to around 20 - 21 °C and salinity is around 39.2 - 39.4 psu, with occasional fresh water intrusions similar to winter. Water column is strongly stratified during summer with a thermo/halocline depth of around 20 meters. Upper layers reach around to 28 °C and 40.0 psu, whereas deeper parts are around 17 - 18 °C and 39.2 psu. Starting from early autumn thermo/halocline deepens and in early December it completely disappears with the start of winter mixing.

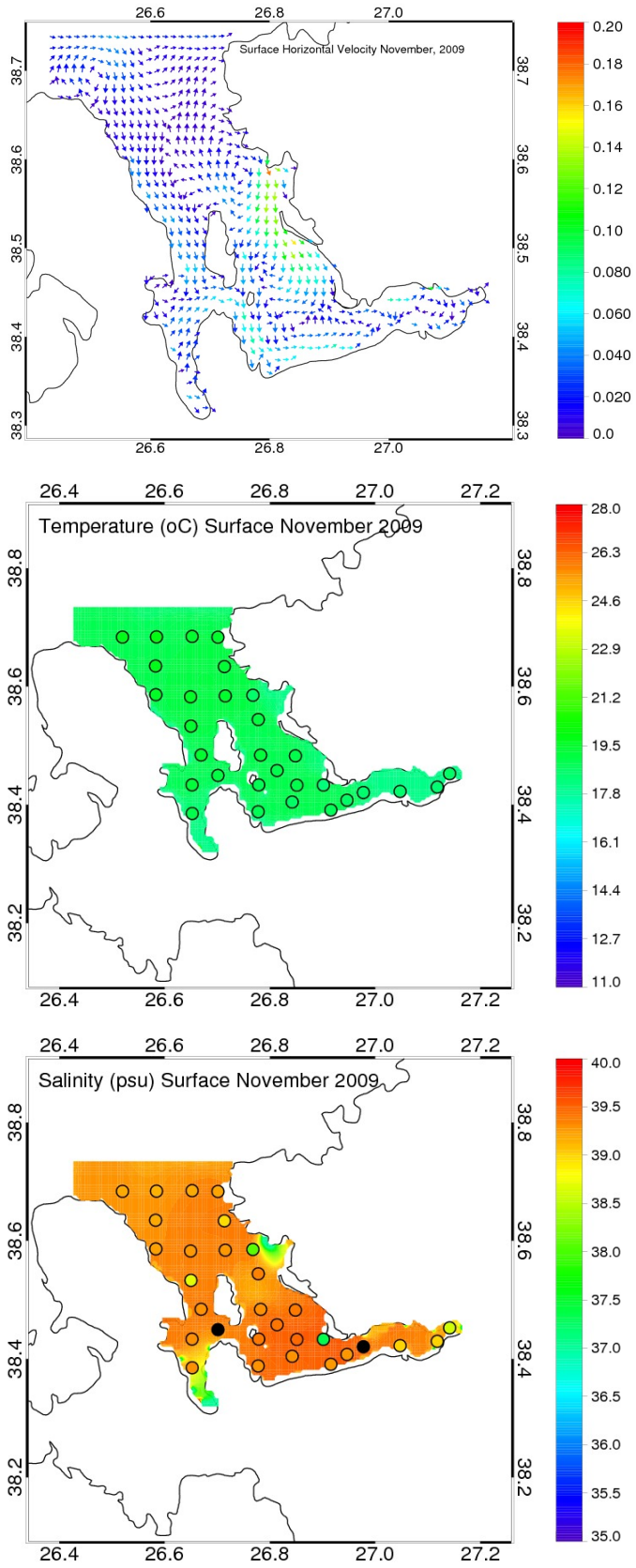

Figure 3.6: Surface current velocity (top), temperature (middle), and salinity (bottom) model results (background) in comparison to measurements (colored dots) from November 2009.

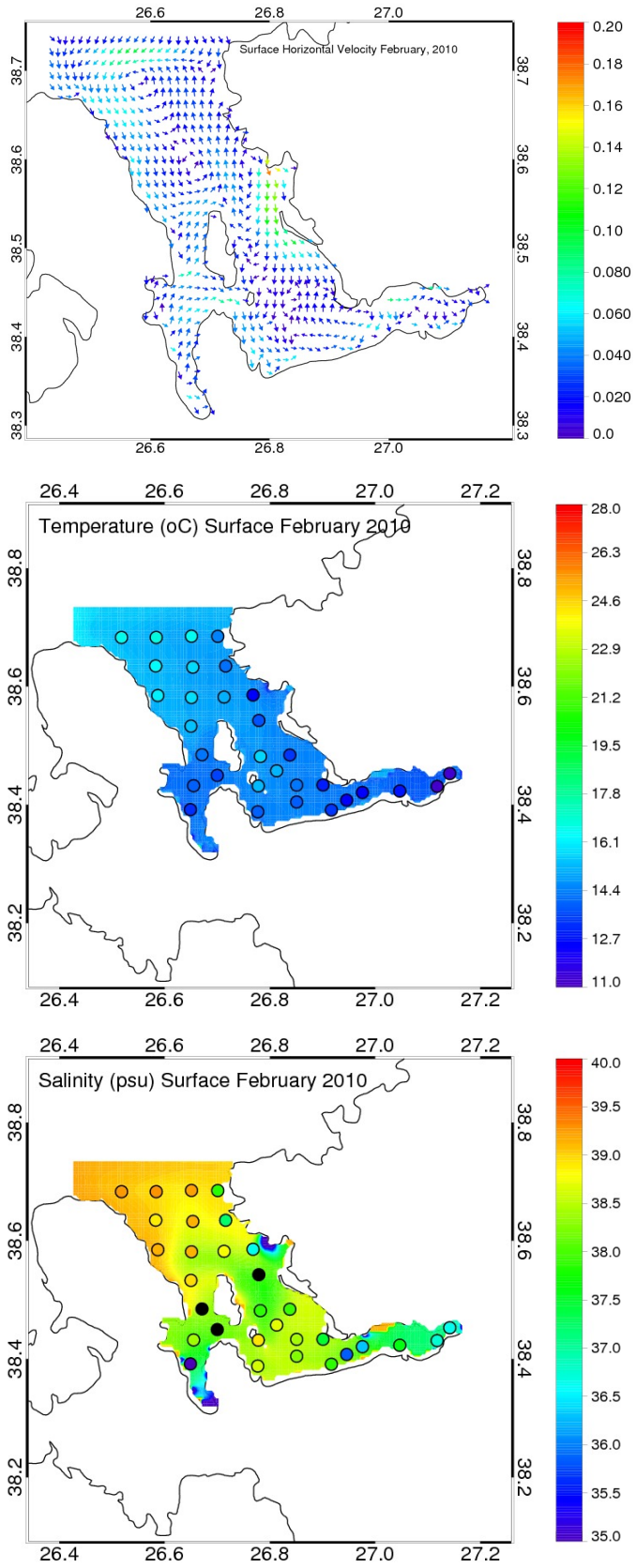

Figure 3.7: Surface current velocity (top), temperature (middle), and salinity (bottom) model results (background) in comparison to measurements (colored dots) from February 2010.

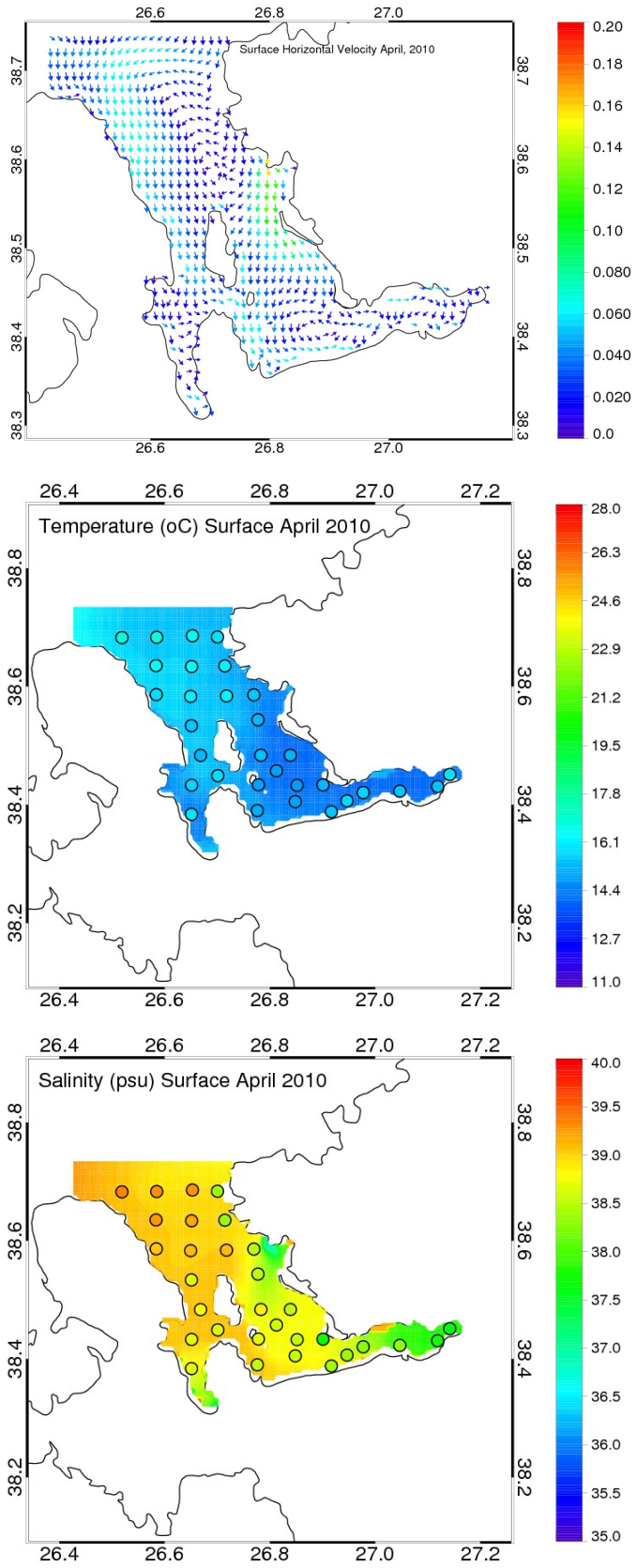

Figure 3.8: Surface current velocity (top), temperature (middle), and salinity (bottom) model results (background) in comparison to measurements (colored dots) from April 2010.

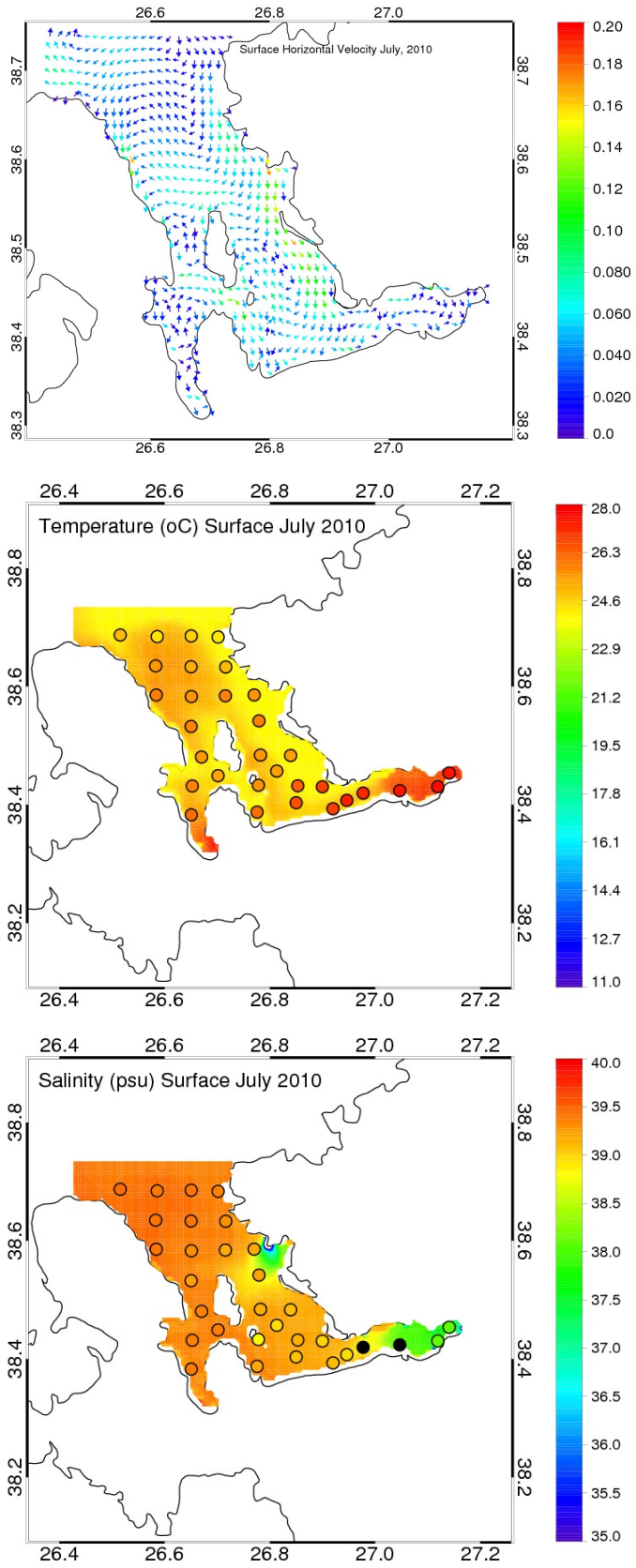

Figure 3.9: Surface current velocity (top), temperature (middle), and salinity (bottom) model results (background) in comparison to measurements (colored dots) from July 2010.

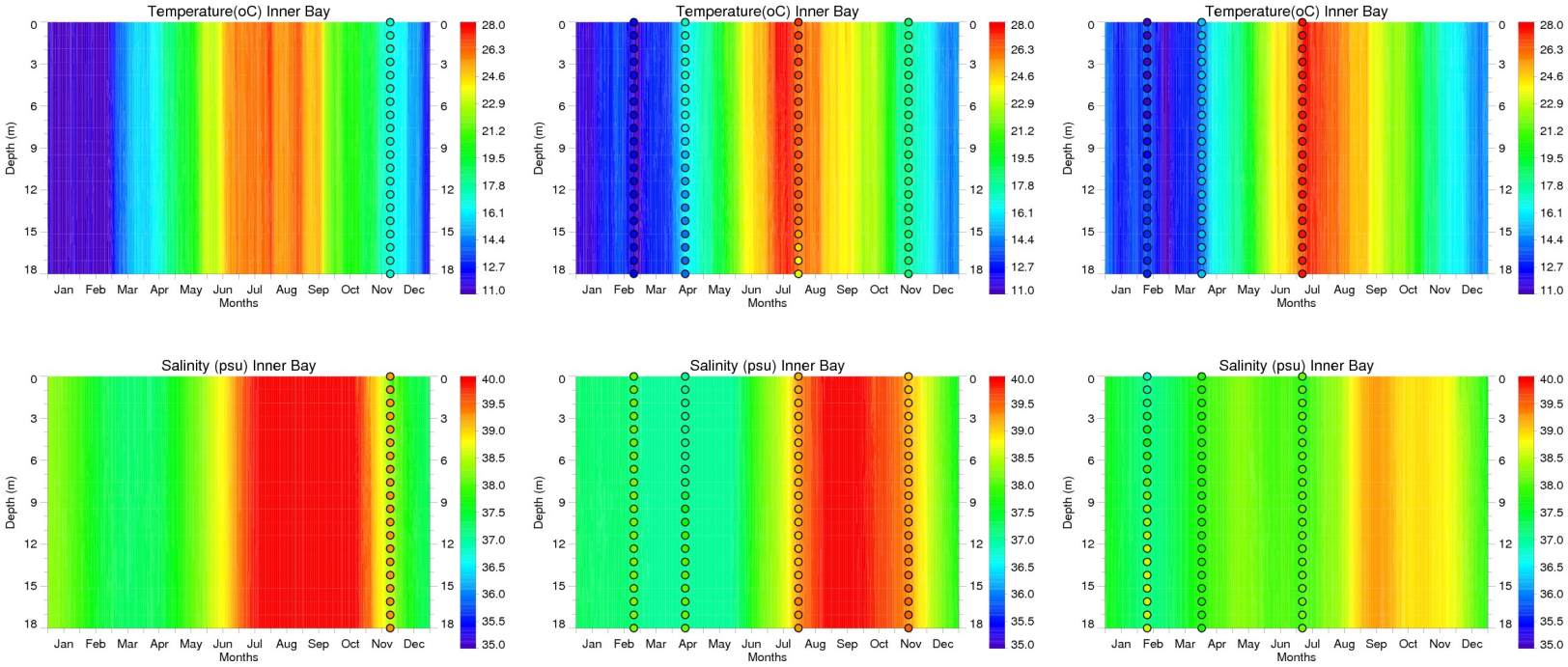

Figure 3.10: Time-depth distribution of temperature (top) and salinity (bottom) model results (background) in comparison to measurements (colored dots) from 2008 (left), 2009 (middle), and 2010 (right) at the Inner Bay station.

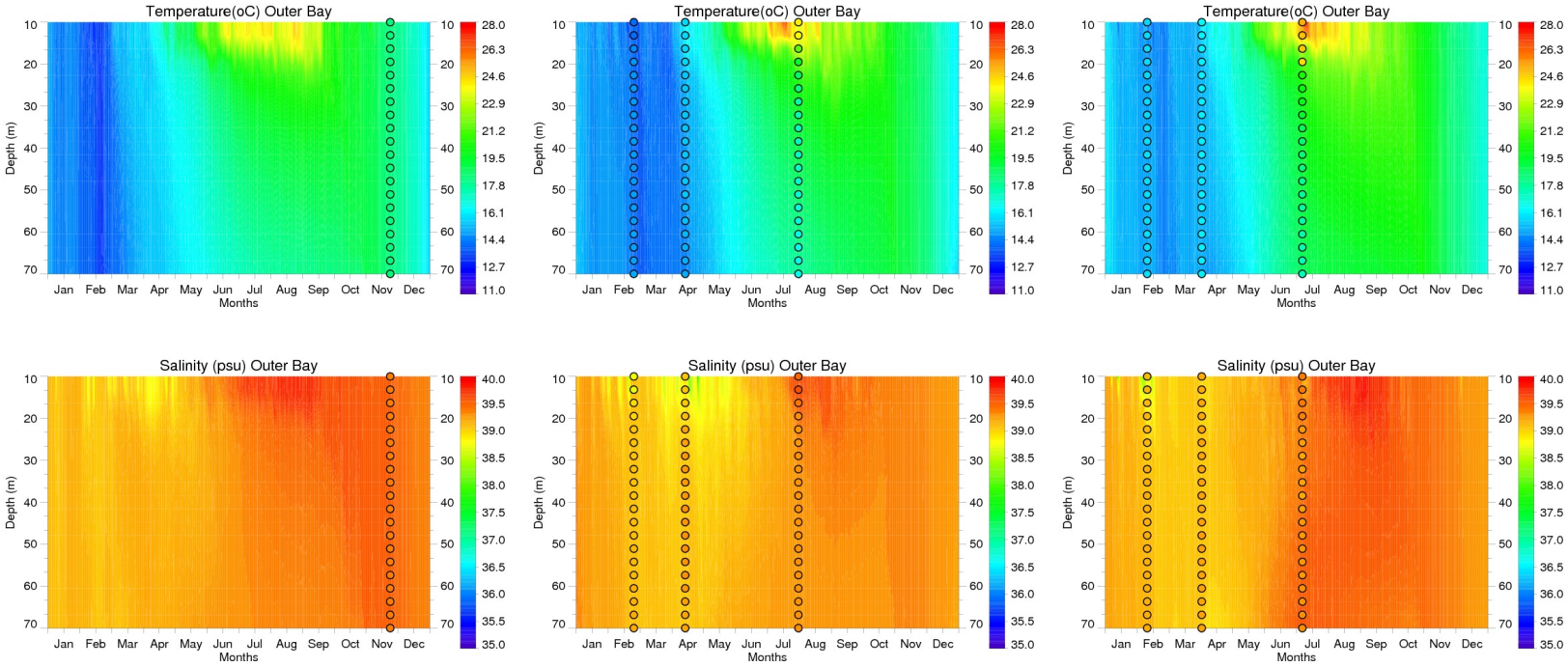

Figure 3.11: Time-depth distribution of temperature (top) and salinity (bottom) model results (background) in comparison to measurements (colored dots) from 2008 (left), 2009 (middle), and 2010 (right) at the Outer Bay station.

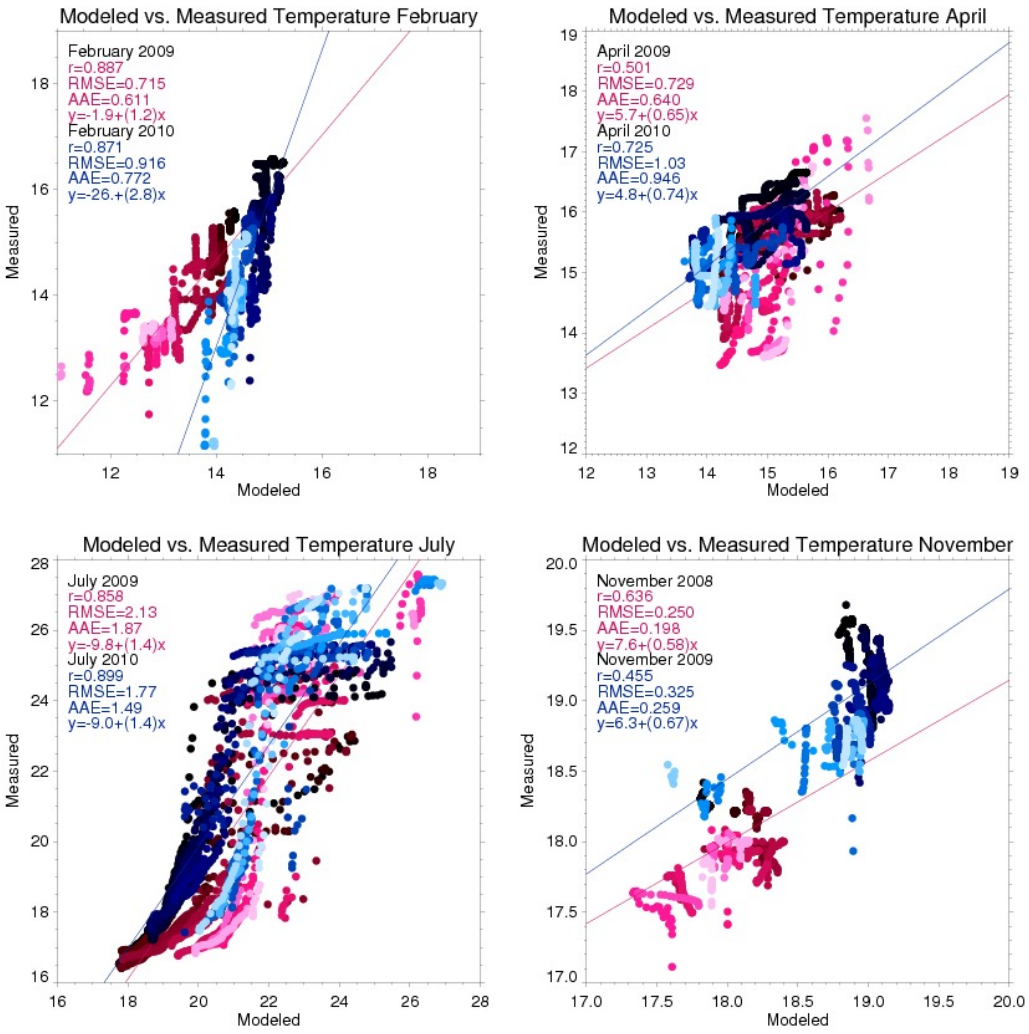

Figure 3.12: Comparison of temperature model results with measurements.

Table 3.1: Summary statistics for temperature.

	r	RMSE	AAE	y-intercept	Slope
November 2008	0.636	0.25	0.198	7.6	0.58
February 2009	0.887	0.715	0.611	-1.9	1.2
April 2009	0.501	0.729	0.64	5.7	0.65
July 2009	0.858	2.13	1.87	-9.8	1.4
November 2009	0.455	0.325	0.259	6.3	0.67
February 2010	0.871	0.916	0.772	-26.	2.8
April 2010	0.725	1.03	0.946	4.8	0.74
July 2010	0.899	1.77	1.49	-9.0	1.4

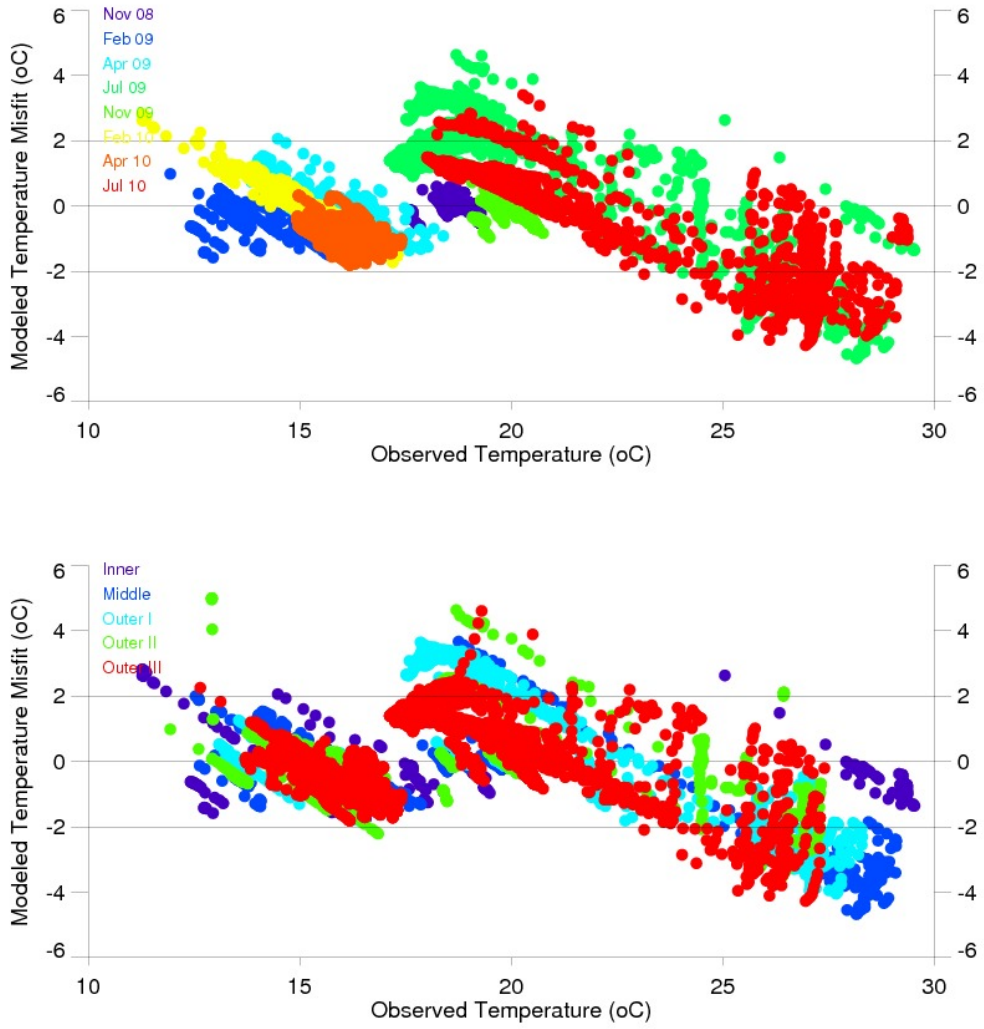

Figure 3.13: Temperature measurements versus model misfit color coded with respect to time (top) and region (bottom).

Comparison of temperature model results with measurements (Figure 3.12 and Table 3.1) show that the model performance is best in autumn and poorest in summer. In February, correlation coefficients (r) are high with values above 0.8 for both years. In year 2009 model shows a reasonable match, but in year 2010 it does poorly estimating the maximum and the minimum, which can also be seen in error statistics with root mean squared error (RMSE) and average absolute error (AAE) higher in February 2010. In April, model correlation is relatively poorer in 2009 than in 2010. Model overestimates the lower temperatures in 2009 and consistently underestimates at every point in 2010. RMSE and AAE values also reveal that the error is greater in April 2010. In July, although r values are high indicating a high

correlation, the biggest mismatch occurs in this season. Model underestimates the high temperatures with great error, and also does poorly producing the minimums. RMSE and AAE are highest with values 2.13 and 1.87 for 2009, and 1.77 and 1.49 for 2010. In November, r values are relatively lower compared to other seasons, but the errors occur to be smallest. Model does very well in 2008 and it is mostly reasonable in 2009 except for underestimating the maximum. The model misfit analyses (Figure 3.13) show that model performance is better in transient seasons, spring and autumn, and in reasonable limits in winter. In summer it fails to produce temperatures above 22 °C and below 18 °C with errors up to 5 °C. Spatially, the majority of the high errors occurs in the Outer I, Outer III and Middle bays, whereas, in shallower Inner and Outer II bays, errors are in acceptable ranges. Overall evaluation of all seasons reveals that model does poorly in maximums and minimums and tends to smooth sharp gradients. This can also be seen in the fact that model does very well in autumn when the bay is under the influence of mixing but poorly in summer when it is strongly stratified. Also, it is clear that model performance declines in deeper regions, indicating discrepancies in vertical dynamics.

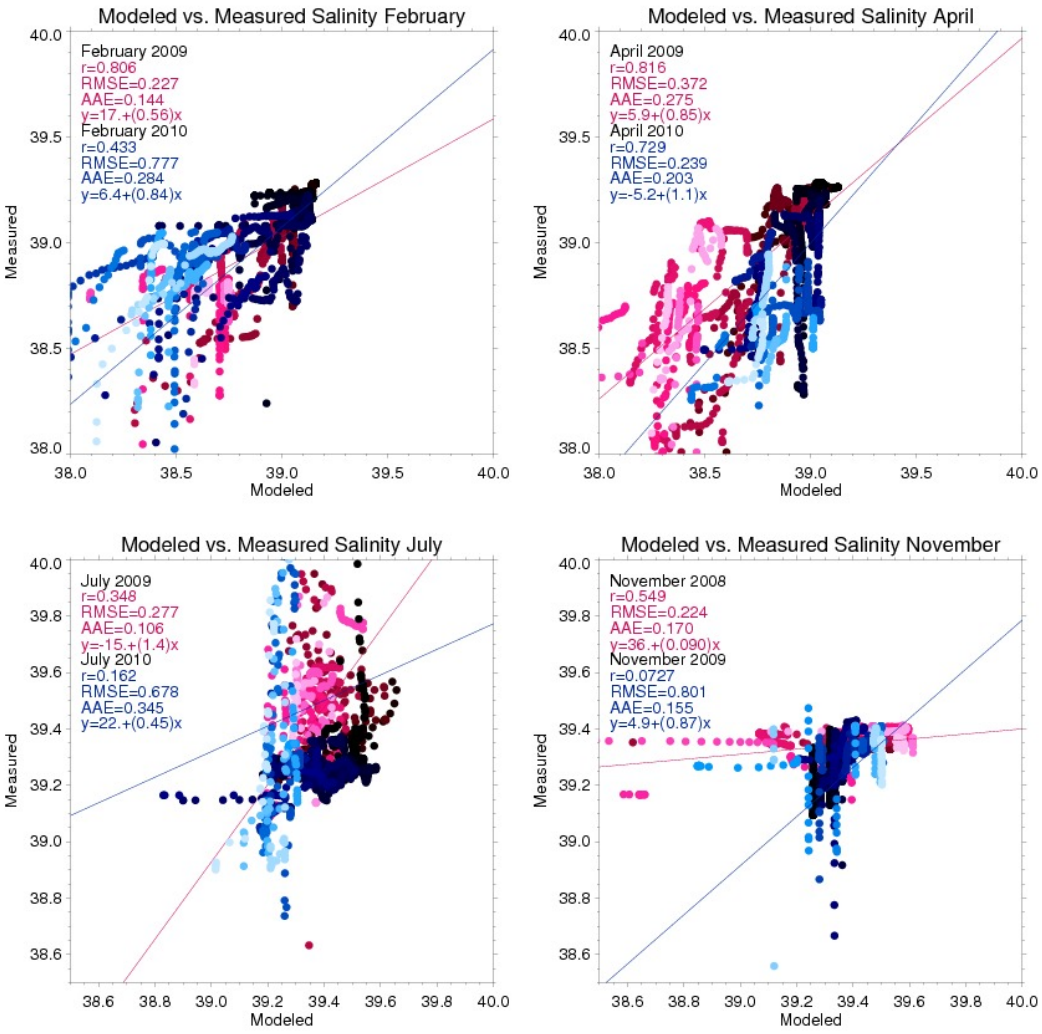

Figure 3.14: Comparison of salinity model results with measurements.

Table 3.2: Summary statistics for salinity.

	r	RMSE	AAE	y-intercept	Slope
November 2008	0.549	0.224	0.17	36.	0.09
February 2009	0.806	0.227	0.144	17.	0.56
April 2009	0.816	0.372	0.275	5.9	0.85
July 2009	0.348	0.277	0.106	-15.	1.4
November 2009	0.0727	0.801	0.155	4.9	0.87
February 2010	0.433	0.777	0.284	6.4	0.84
April 2010	0.729	0.239	0.203	-5.2	1.1
July 2010	0.162	0.678	0.345	22.	0.45

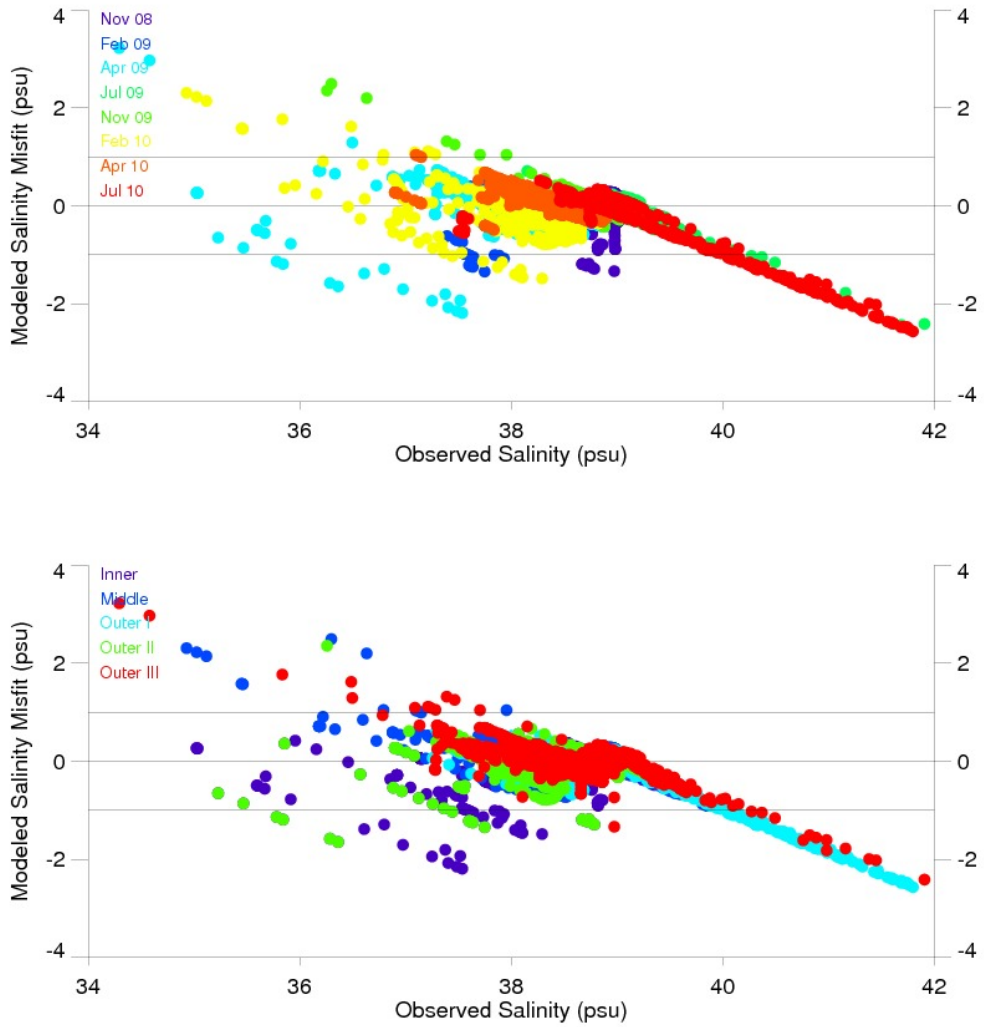

Figure 3.15: Salinity measurements versus model misfit color coded with respect to time (top) and region (bottom).

In terms of salinity, model results versus measurements comparison (Figure 3.14 and Table 3.2) shows that model performance is relatively better in first four seasons than it is in the last four. In February, model does better towards maximum observed salinities but mostly underestimates lower salinities. Error terms are in acceptable limits in 2009, and greater in 2010. In April, r values higher than 0.7 together with reasonably smaller error terms in both years indicate good correlation. Model predictions are slightly lower than the observed maximum salinity, and at lower salinities model mostly underestimates in 2009 whereas it mainly overestimates in 2010. In July, model shows a reasonable performance at majority of lower salinities but does very poorly producing the maximums observed in this season with very

large discrepancies. Model error is greater in July 2010 than in any other season. In November, although *r* values are, on average, lower than other seasons, smaller error terms indicate to a relatively better model performance. The streaks of outliers in the scatter plot show that the major discrepancies occur due to underestimation in 2008, and due to overestimation in 2009. Misfit analyses (Figure 3.15) show that model performance peaks at salinities around 39 psu. Below this value, model misfit becomes larger especially in winter and spring when the influence of fresh water inputs are most significant. These mismatches mainly occur in shallow regions, Inner, Middle and Outer II bays that are the direct receivers of fresh water from small outlets, and in a few points with very large errors in Outer III bay, probably in vicinity of Gediz River plume. In summer, model does very poorly producing the observed salinity over 40 psu, and this discrepancy presents itself more prominently in July 2010. Majority of these errors are in Outer I bay where there exist salt flats at the coast and at a few points in Outer III bay. As in temperature, model fails to predict minimums and maximums, and performs reasonably at and around the average salinity values. It can be deduced that, in terms of salinity the model does better in regions and seasons where external influences such as fresh water inputs or salt intrusions are minimal, hence the model performance is highly dependent on proper prescription of these influences.

3.2 COUPLED ECOSYSTEM MODEL RESULTS AND SKILL ASSESSMENT

As a result of the ecosystem modelling effort, a three-dimensional representation of the biogeochemical processes and time-dependent distributions of related parameters are obtained for İzmir Bay. It is the first study an ecosystem model is applied to the region at such an extent and detail, and used as a tool for further understanding the biological and chemical properties of the region. In this section, surface and time-depth distributions of Chlorophyll-*a* (Chl-*a*), Dissolved Oxygen (DO), Dissolved Inorganic Nitrogen (DIN), Phosphate (PO_4), Particulate Organic Carbon (POC), and Particulate Organic Nitrogen (PON) model results are given in comparison to available measurements. At the end of the section, model skill assessment analyses in terms of the selected parameters are presented.

In November 2008 (Figure 3.16), surface model results show that Chl-*a* ranges between 0 - 0.3 mg m^{-3} in majority of the Outer bays. Around Gediz River mouth, and towards Middle and Inner bays it increases up to 4 mg m^{-3}. In Outer I and II bays measurements are higher with values around 3 mg m^{-3} and in Middle and Inner bays they reach a maximum of about 6 mg m^{-3}. Surface DO model results is homogeneous around 7.5 mg l^{-1} in Outer bays in comparable limits to measurements. In Inner bay they slightly increase up to 8 mg l^{-1} in regions with increased Chl-*a*. Modelled DIN shows little variation throughout the bay with an average of about 0.5 μM and model results fail to match the extremely high values observed in Inner and Middle bays. Surface PO_4 model results ranges between 0 - 0.1 μM in all Outer bays and increases to a maximum around 3 μM towards Inner bay, in very good agreement with measured PO_4. Modelled POC ranges between 0 - 10 μM in Outer bays with an increase to about 40 μM around Gediz River. Towards Inner bay it increases to an average of about 50 μM, which is not observed in measurements. Modelled PON is at lower values of, on average, 0.5 μM in Outer bays with a slight increase around Gediz River mouth. Towards Inner bay it increases up to 4 μM, comparable to measurements in this region.

In February 2009 (Figure 3.17), surface model results of almost every parameter shows a prominent influence originating from Gediz River in Outer III bay, resulting in obvious discrepancies with measurements. Surface Chl-*a* model results reach a maximum of about 5 mg m^{-3} in Inner and Middle bays and, except for the extreme high around Gediz River, it ranges between 0 - 0.5 mg m^{-3} in Outer bays. Modelled DO is around a minimum of 8 mg l^{-1} in the northeast of Outer III bay and increases steadily to around 10 mg l^{-1} towards inner parts

and Gediz River. These values are distinguishably higher than measurements in these regions. Surface DIN model results show the effect of Gediz River input with a sharp increase in that region exceeding 10 μM. In the rest of the bay it is around 0.5 μM with little variation. In Inner and Middle bays measured DIN is quite higher than model results with a maximum of around 6 μM. The model discrepancy around Gediz River is not pronounced in surface PO_4. It varies between 0 - 0.1 μM in Outer bays and increases to around 3 μM in Inner bay. Measured PO_4 also has the same increasing pattern but with a lower maximum of around 1 μM in the Inner bay. POC ranges between 0 - 20 μM in northern parts of Outer III and increases towards Inner bay up to 90 μM where measurements show a lower maximum of around 45 μM. Around the Gediz River mouth an extensive area shows the mentioned discrepancy. Modelled PON, mimicking POC, ranges between 0 - 1 μM in Outer bays and increase to around 10 μM in Inner and Middle bays, in agreement with the measurements in this regions. Similarly, an area of extremely high PON around Gediz River is observed in model results.

In April 2009 (Figure 3.18), model results show that surface Chl-*a* is at a minimum of around 0.3 mg m^{-3} in Outer bays and increase to around 3 mg m^{-3} towards Inner bay, and to around 20 mg m^{-3} in a small region at the Gediz River mouth. Chl-*a* measurements show a steady increase from Outer III to Inner bay, reaching a maximum of 23.7 mg m^{-3}. Modelled DO is around 7.5 mg l^{-1} in Outer III and increase to around 8 mg l^{-1} towards south. Measured DO is lower than model results in Outer I and II bays but quite higher in Inner and Middle bays with a maximum of 10.7 mg l^{-1}. Surface DIN shows little variation in the bay with values ranging between 0.5 - 0.7 μM, except for the Gediz River mouth where it exceeds 10 μM. Surface PO_4 model results range between 0 - 0.1 μM in Outer bays and increase to around 2 μM in Inner and Middle bays, in agreement with the measurements. Modelled POC and PON have a similar distribution to surface Chl-*a* with minimum values in majority of the Outer bays and increases towards Inner bay and Gediz river. In Inner and Middle bays, model results of POC and PON with values around 50 μM and 3 μM, respectively, fail to match the strong increase in measured POC and PON with values of 371 μM and 47 μM.

In July 2009 (Figure 3.19), surface Chl-*a* model results show little variation throughout the bay ranging between 0 - 0.3 mg m^{-3}, whereas, measurements are quite higher in Inner and Middle bays with a maximum of 7 mg m^{-3}. Modelled DO is homogeneous with an average value of 6.5 mg l^{-1}. Surface DIN model results, also uniform in all regions, is around 0.5 μM. Surface PO_4 model results ranges between 0 - 0.1 μM in the entire Outer bays and increases

to a maximum of 3 μM towards Inner bay, which is seen in measurements as well. Modelled POC ranges between 0 - 10 μM in all regions with an increase to around 30 μM towards Gediz River. POC measurements show a sharp increase in Inner and Middle bays with a maximum of around 90 μM. Modelled PON ranges between 0 - 0.5 μM in all regions. Measured PON shows a similar increase as POC in Inner and Middle bays reaching up to 10 μM.

In November 2009 (Figure 3.20), model results show that surface Chl-*a* ranges between 0 - 0.3 mg m^{-3} in majority of the Outer bays. In regions under the influence of Gediz River input, it ranges between 4 - 6 mg m^{-3}, and in direct vicinity of the river mouth it shows a sharp increase which is not seen in measurements. Towards Inner and Middle bays, on average, it increases to around 4 mg m^{-3}. Measured Chl-*a* also increases in this region to a higher maximum of around 10 mg m^{-3}. Surface DO model results show a very similar distribution to Chl-*a* with average values of about 7 mg l^{-1} in the majority of the bay, increasing in the region of Gediz River input. Towards Inner bay it increases to around 8 mg l^{-1}. Modelled DIN is at an average value of around 0.5 μM throughout the bay with little variation, except for a sharp increase seen directly at the Gediz River mouth where an increasing trend is also seen in measurements. Towards Middle and Inner bays, model results fail to match the steady increase observed in measurements with a maximum of around 10 μM. Surface PO_4 model results ranges between 0 - 0.1 μM in Outer bays and increase to around 3 μM in Inner bay, in agreement with the measurements. Modelled POC, with a similar pattern to Chl-*a*, ranges between 0 - 20 μM in majority of the Outer bays, except for the increase seen towards Gediz River. In Inner and Middle bays it increases to an average of around 40 μM while measurements reach a maximum of around 50 μM. surface PON model results range between 0 - 1 μM in Outer bays and show a sharp increase around Gediz River mouth. Towards Middle and Inner bays they increase to about 5 μM, in agreement with measurements.

In February 2010 (Figure 3.21), surface Chl-*a* model results show prominent increases in regions heavily influenced by fresh water inputs. They range between 0 - 2 mg m^{-3} in north-western parts of Outer bays. In most of Outer I and the large area around Gediz River mouth it reaches to a maximum. Inner bays it is on average about 6 mg m^{-3} in agreement with the measurements. In Middle bay a sharp increase is seen. Modelled DO is significantly higher than measured DO in all regions. In northwestern Outer III bay it is at a minimum of around 7.5 mg l^{-1} and towards inner bay it increases to a maximum of about 11 mg l^{-1}, whereas measurements range between 6.5 - 8.5 mg l^{-1}. Surface DIN model results range between 0 -

0.5 μM throughout the bay, except for the increases around Gediz River mouth and south of Outer II bay. Measurements confirm the increase around Gediz River, but in Inner and Middle bays they are considerably higher than model results with a maximum of around 8 μM. Modelled PO_4 ranges between 0 - 0.1 μM in Outer bays and increase to about 3 μM in Inner and Middle bays. This increased values fail to match measurements in this region which are homogeneously at the minimum in all regions. Surface POC model results range between 0 - 20 μM in northwestern parts of Outer III and II bays, in agreement with measured POC. In the rest of the bay they steadily increase towards Gediz River and Inner bay reaching values of around 180 μM, where as measurements reach a maximum of only about 40 μM. Modelled PON ranges between 0 - 2 μM in majority of Outer III and II bays and between 0 - 6 μM in Outer I bay. It increases to an average of around 4 μM towards Middle and Inner bays, which is not seen in measured PON. Around the fresh water influences, as in POC, it shows sharp increases.

In April 2010 (Figure 3.22), surface Chl-*a* model results range between 0 - 0.5 mg m^{-3} in the majority of Outer bays with an increase in vicinity of the Gediz River input. Towards Middle and Inner bays they increase to about 3 mg m^{-3}, while measurements have a similar increase with a higher maximum of about 7 mg m^{-3}. Modelled DO ranges between 8 - 10 mg l^{-1} with higher values seen in regions with increased Chl-*a*. Measured DO, however, is quite low compared to model results ranging between 7 - 8 mg l^{-1}. Surface DIN model results are about an average of 0.5 μM in all regions with very little variation except for the gradual increase south of Outer II and a sharp increase directly at the Gediz River mouth. Measured DIN is in good agreement with model results in Outer and Middle bays, whereas in Inner bay it is higher with a maximum of around 2 μM. Modelled PO_4 ranges between 0 - 0.1 μM in Outer and Middle bays and increase to about 3 μM in Inner bay. Measured PO_4 also increase towards Inner bay in a similar pattern but reaches a lower maximum of about 1 μM. Surface POC model results range between 0 - 20 μM in western parts of Outer III and Outer II bays. In vicinity of the Gediz River input, in southeast of Outer III and north of Outer I, it increases to an average of about 30 μM with a sharp maximum observed around the river mouth. Towards Middle and Inner bays, it increases steadily up to around 50 μM. Measured POC is in agreement with the model results except for in the area around the Gediz River. Modelled PON has a similar distribution to POC. It ranges between 0 - 1 μM in majority of Outer bays and increase towards Gediz River, in agreement with the measurements. In Middle

and Inner bays, it increases up to around 4 μM where measured PON is higher with values around 9 μM.

In July 2010 (Figure 3.23), model results show that surface Chl-*a* ranges between 0 - 0.5 mg m^{-3} in majority of the bay. Towards Gediz River mouth, an increase is observed. In Inner and Middle bays measurements are significantly higher than model results with a maximum of around 5 mg m^{-3}. Surface DO model results are at an average of around 7.5 mg l^{-1} in north of Outer III, Outer II, Middle, and Inner bays. Starting from Outer I towards Gediz River they increase to around 11 mg l^{-1}. Measured DO is, on average, about 6.5 mg l^{-1} in all regions with very little variation. Modelled DIN is homogeneous throughout the bay at around 0.5 μM except for the sharp increase in the small area at the Gediz River mouth. Measured DIN shows an increase towards Inner and Middle bays with values up to 2 μM. Surface PO_4 model results range between 0 - 0.1 μM in Outer bays. In Inner and Outer bays they are at an average of around 4 μM with a gradual increase towards the east. A similar increasing trend is also observed in measured PO_4 in this region. Modelled POC ranges between 0 - 20 μM in Outer III and II bays, as observed in *in-situ* POC. Starting from Outer I bay with an average of around 40 μM it increases gradually towards Gediz River, whereas, measured POC remains between 0 - 20 μM. In Inner and Middle bays it increases to an average of 30 μM, failing to match the higher measured POC of a maximum of about 70 μM. Surface PON model results range between 0 - 1 μM throughout the bay except for the increase in vicinity of the Gediz River input. Measurements are in agreement with model results in Outer bays but show an increase in Inner and Middle bays up to values of around 9 μM.

Surface distribution of DIN/PO_4 ratio model results (Figure 3.24) reveal that Inner and Outer bays show contrasting N-limited and P-limited characteristics, respectively. There is a distinct horizontal gradient in all seasons with values around 20 in Outer bay and ≤ 1 in Inner bay. In winter and spring the influence of DIN input is highly prominent with enhanced P-limitation around Gediz River input in 2009 and in Outer II bay in 2010. In summer and autumn, however, both the decrease in Gediz River flux, thus the decrease in DIN input and increase in PO_4 loads from the WWTP, cause the low DIN/PO_4 ratio to extend further north, enhancing the N-limitation. Although the model has certain discrepancies described in the above paragraphs in terms of both DIN and PO_4, it is able to capture the spatial and temporal distribution of DIN/PO_4 ratio, hence the contrasting natures of the Inner and Outer bays.

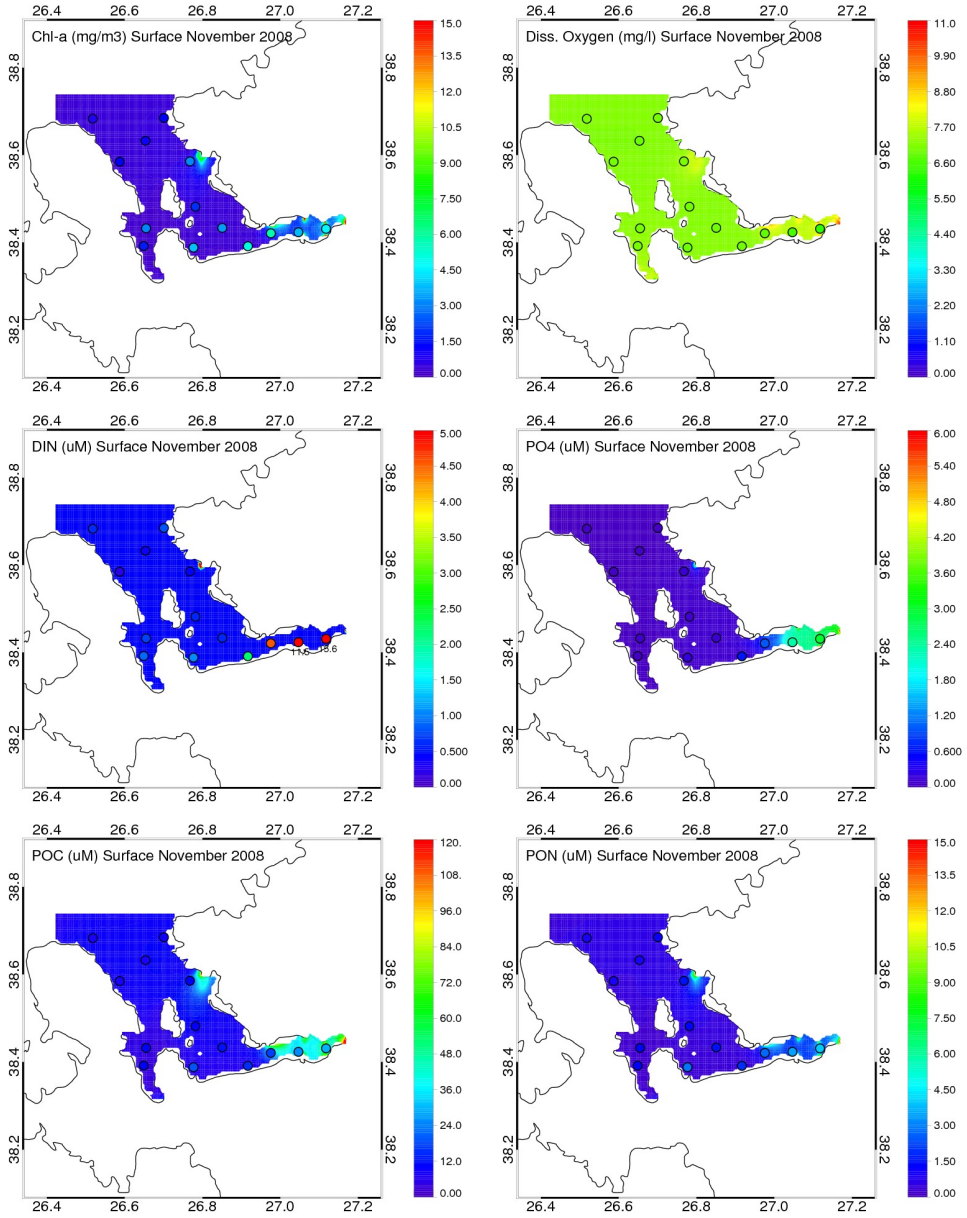

Figure 3.16: Surface Chl-*a*, DO, DIN, PO_4, POC, and PON model results (background) in comparison to measurements (colored dots) from November 2008.

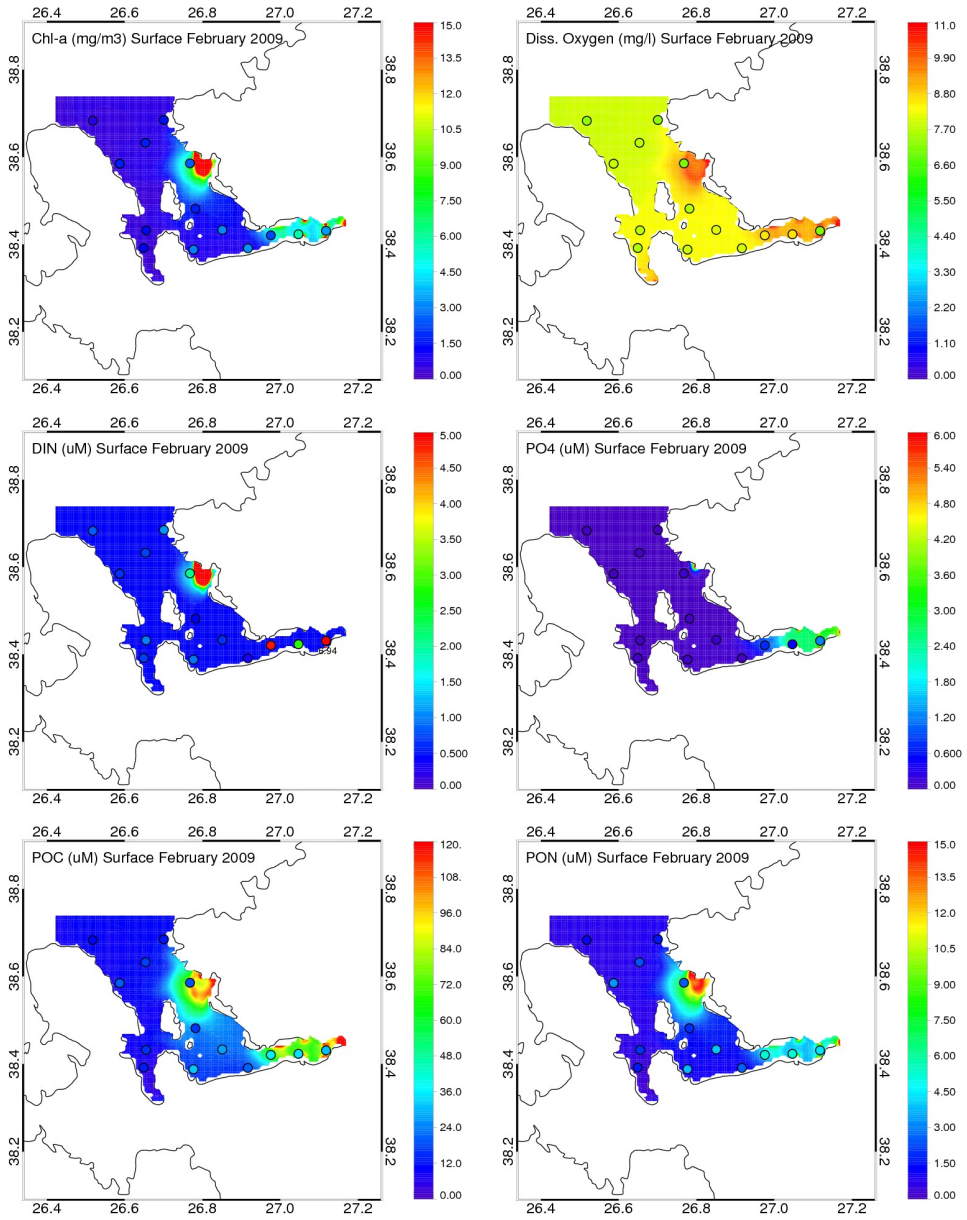

Figure 3.17: Surface Chl-*a*, DO, DIN, PO_4, POC, and PON model results (background) in comparison to measurements (colored dots) from February 2009.

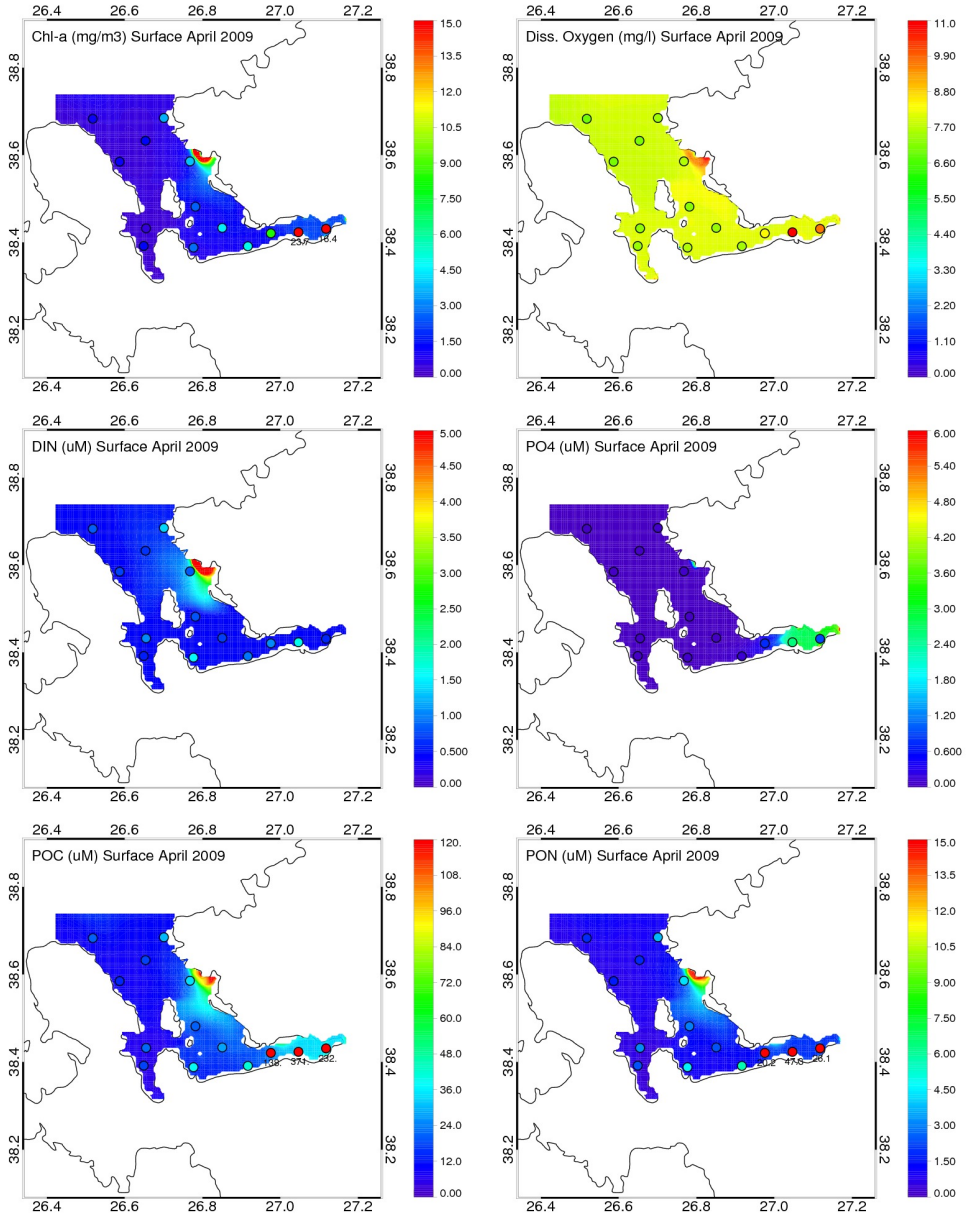

Figure 3.18: Surface CChl-*a*, DO, DIN, PO_4, POC, and PON model results (background) in comparison to measurements (colored dots) from April 2009.

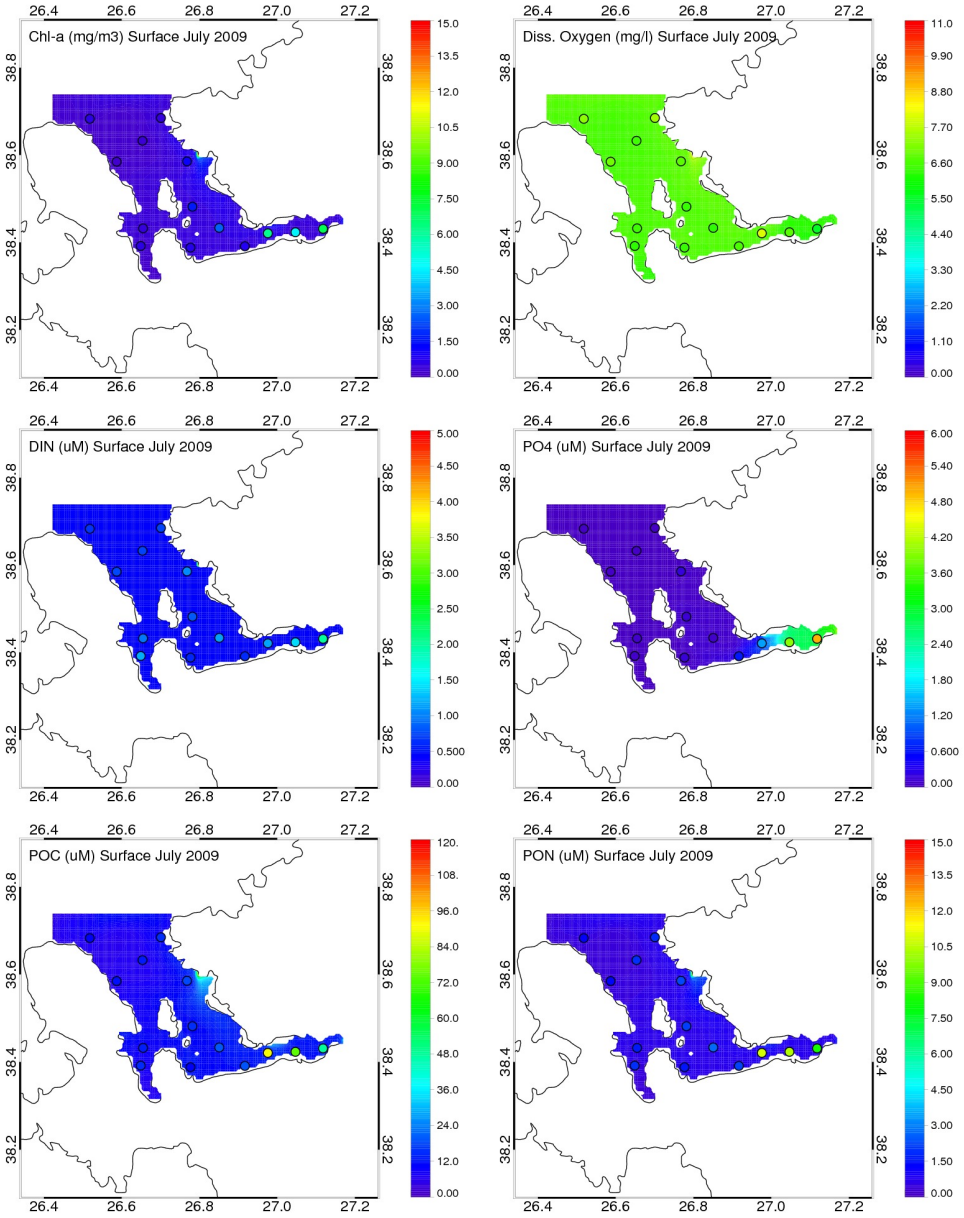

Figure 3.19: Surface Chl-*a*, DO, DIN, PO_4, POC, and PON model results (background) in comparison to measurements (colored dots) from July 2009.

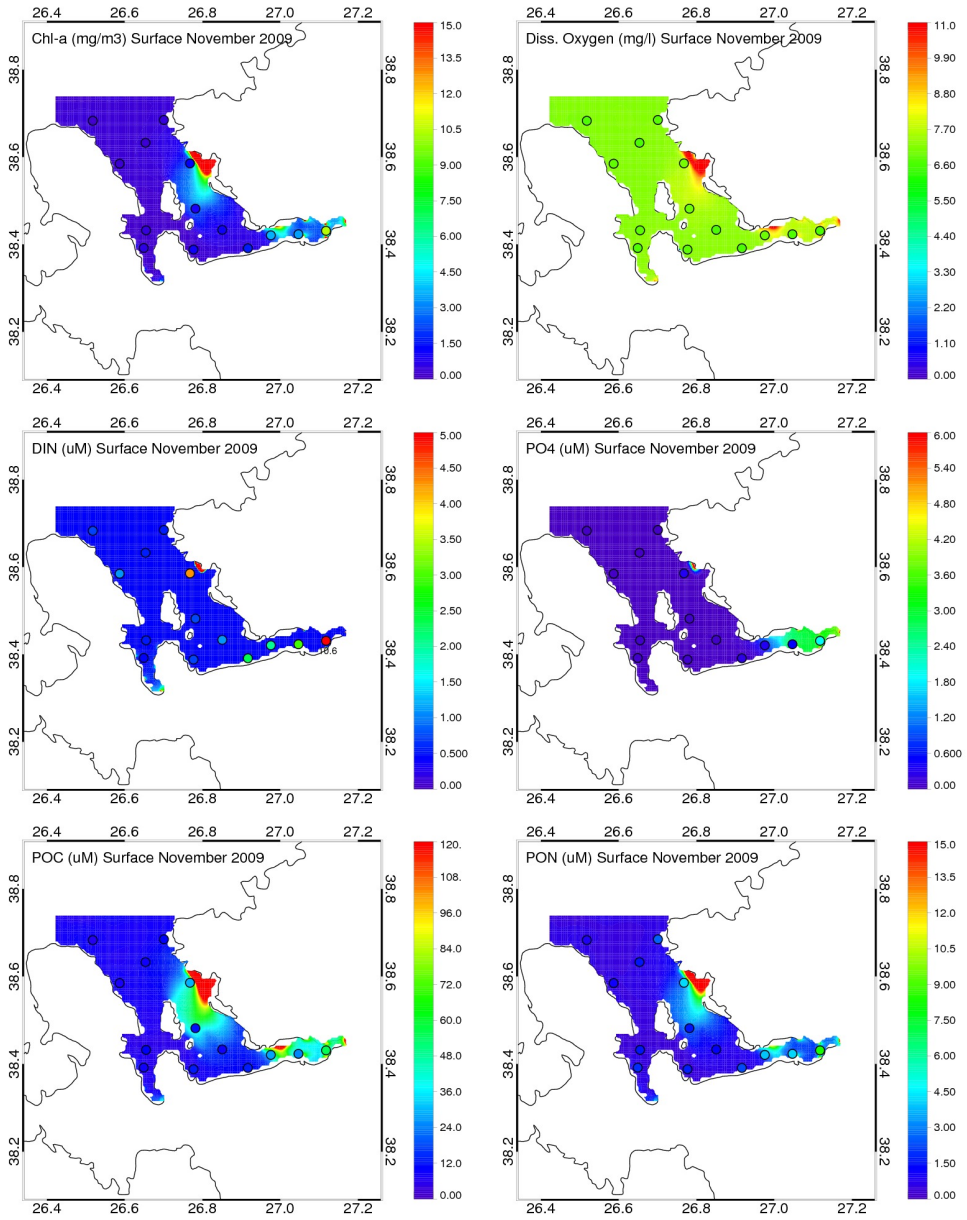

Figure 3.20: Surface Chl-*a*, DO, DIN, PO_4, POC, and PON model results (background) in comparison to measurements (colored dots) from November 2009.

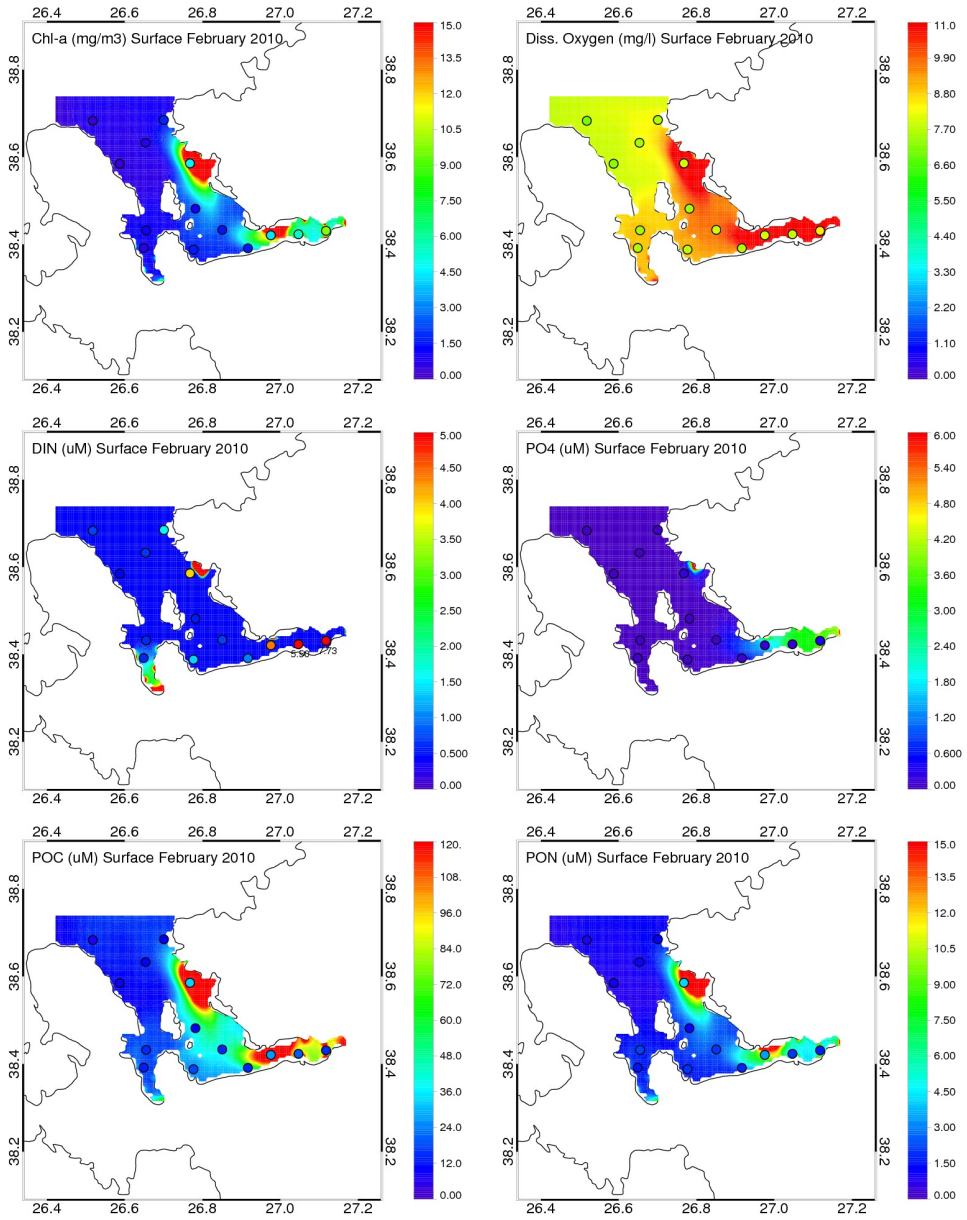

Figure 3.21: Surface Chl-*a*, DO, DIN, PO_4, POC, and PON model results (background) in comparison to measurements (colored dots) from February 2010.

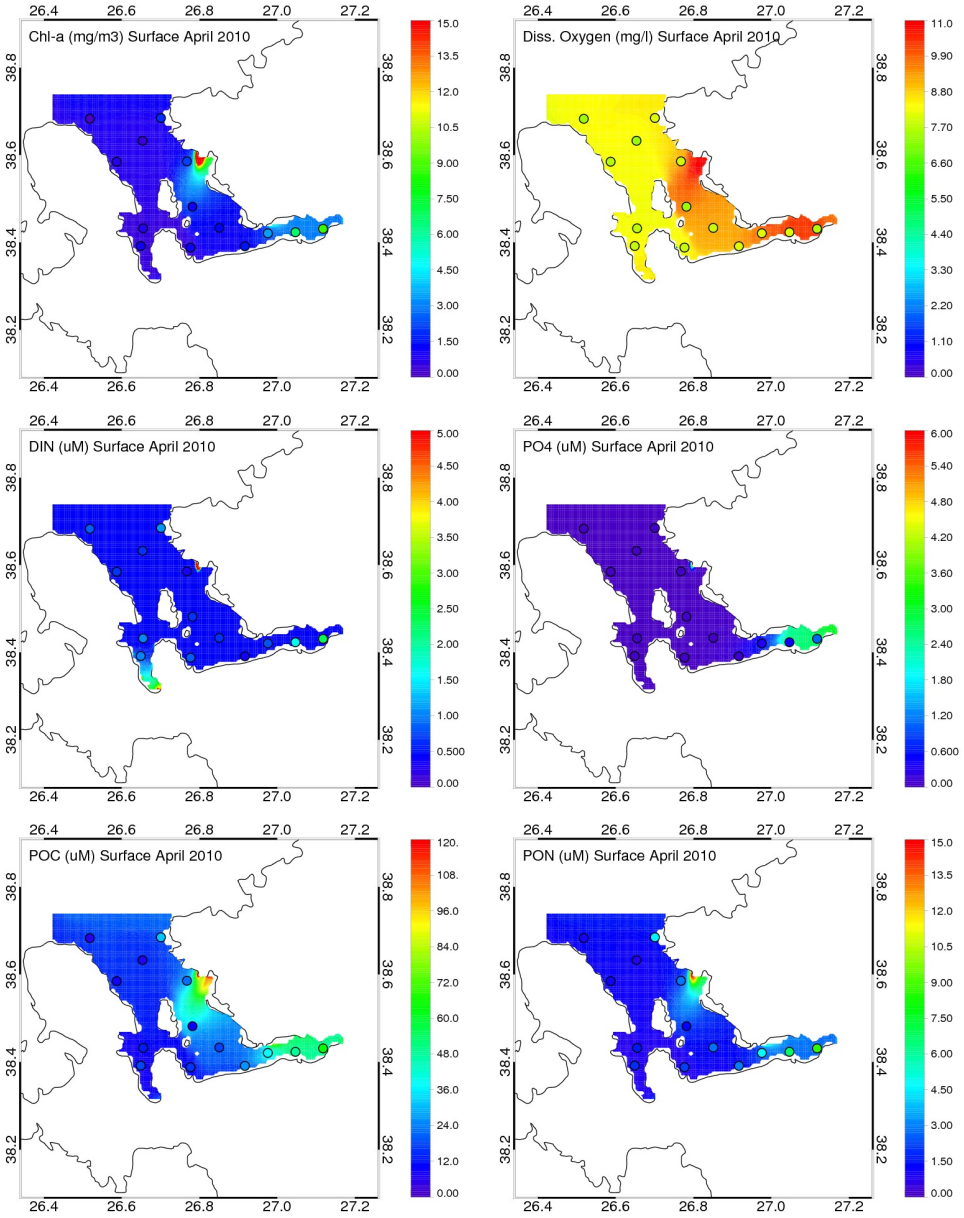

Figure 3.22: Surface Chl-*a*, DO, DIN, PO_4, POC, and PON model results (background) in comparison to measurements (colored dots) from April 2010.

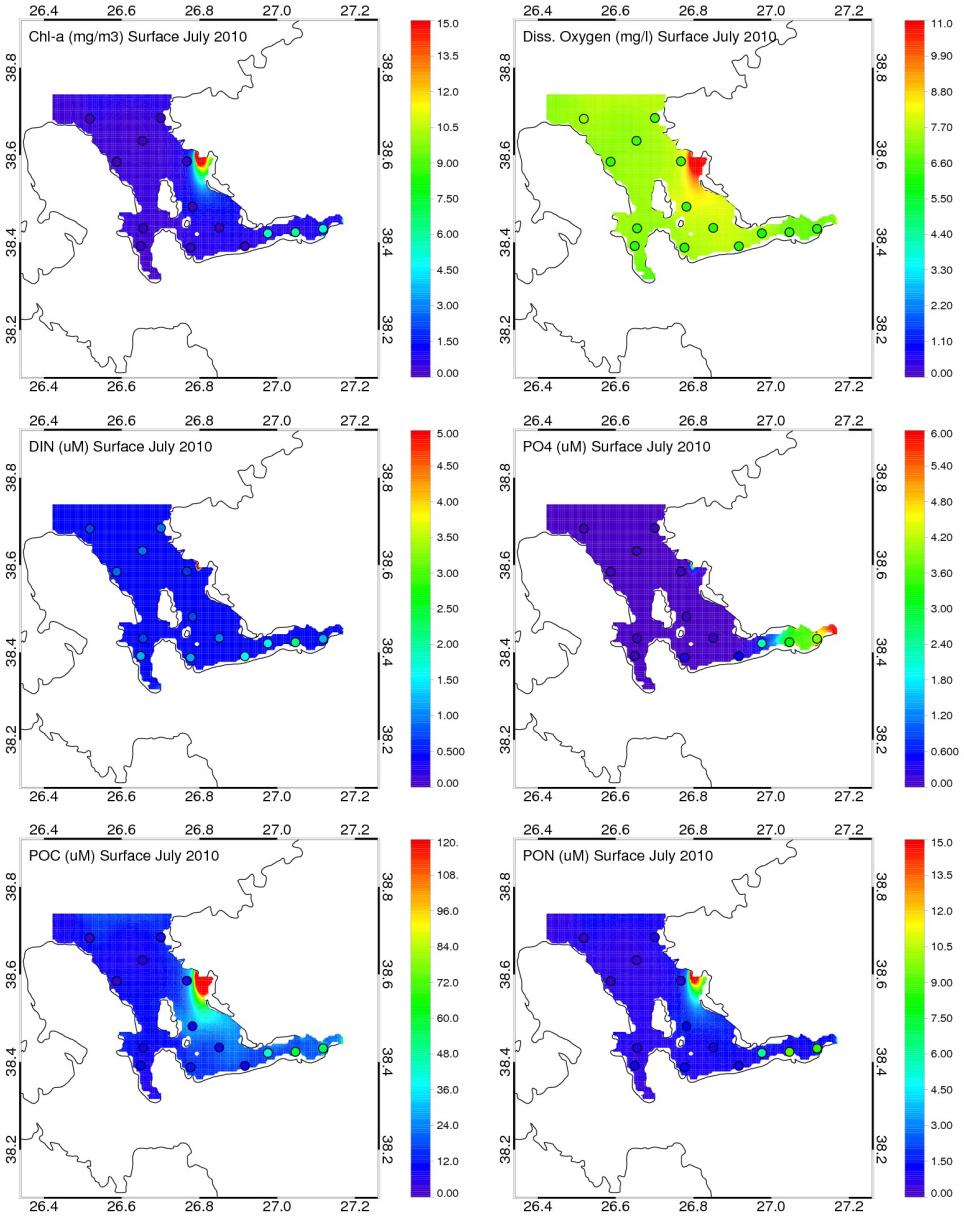

Figure 3.23: Surface Chl-*a*, DO, DIN, PO_4, POC, and PON model results (background) in comparison to measurements (colored dots) from July 2010.

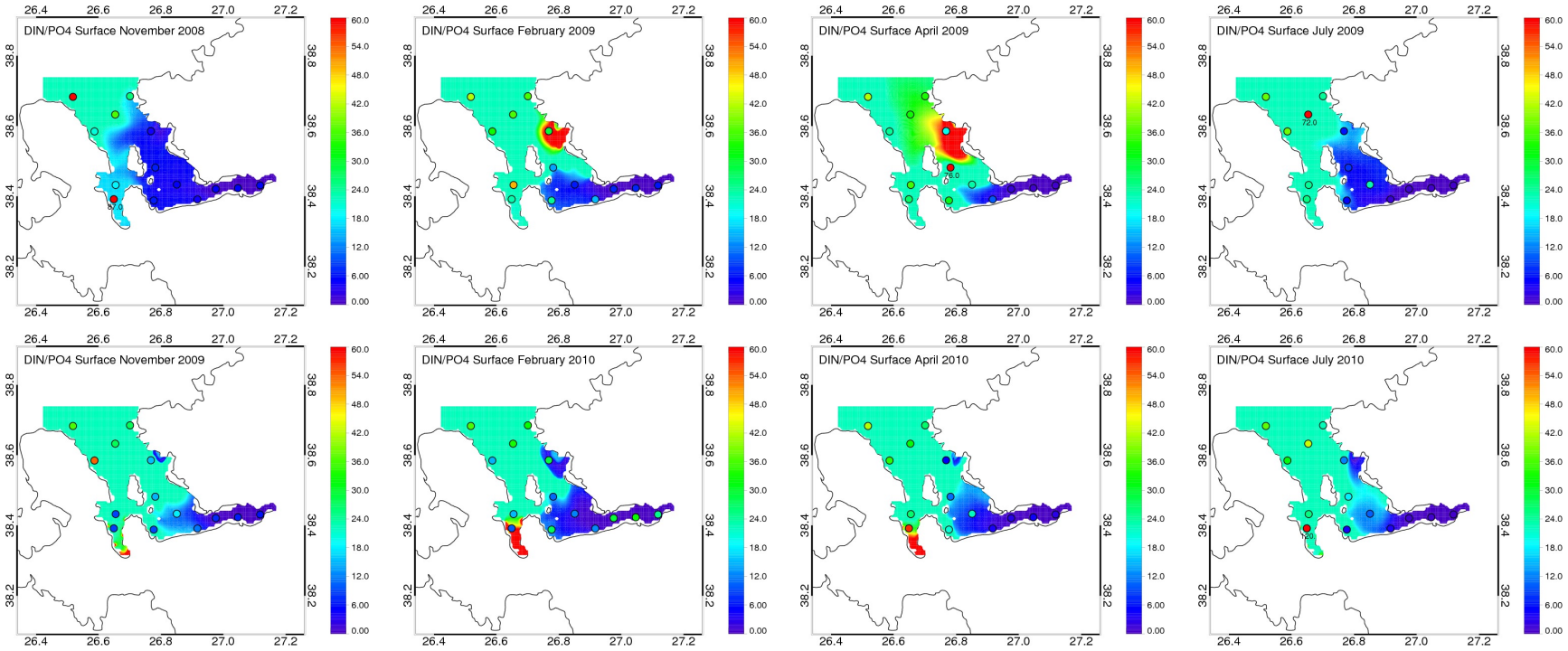

Figure 3.24: Surface DIN/PO_4 model results (background) in comparison to measurements (colored dots).

Time-depth distributions of model results from the Inner bay (Figure 3.25 and 3.26) show that Chl-*a* is increased in the entire water column in early winter and it shows a maximum in surface mixed layer in late winter and towards early spring. In late spring and early summer it has a subsurface maximum which deepens and gradually diminishes towards late summer. With the onset of mixing, it starts to increase in all depths in autumn and continue to increase again in winter. These results are in acceptable ranges compared to measurements, except for the extremely high surface Chl-*a* measured in April 2009. DO model results reflect a similar pattern as seen in Chl-*a*. In winter, it is increased in all depths and towards spring it is more pronounced in upper layers. From late spring until mid autumn it is homogeneously at a minimum. With increasing Chl-*a* it again increases gradually in colder seasons. Modelled DO is significantly higher than measured DO in all seasons with an especially higher difference in 2010. Modelled DIN is at a minimum in surface layers in all seasons. In winter, it increases with depth up to a maximum of around 3 μM due to mixing. This vertical pattern weakens with warming and is no longer significant until autumn. In autumn and towards early winter it again starts to increase in deeper parts. Measured DIN is higher than model results in all seasons except for April 2009. Especially in autumn model results have quite large discrepancies compared to the extremely high measured DIN with values exceeding 15 μM. PO_4 model results are vertically homogeneous in all seasons with no significant seasonal cycle. In winter and spring, model results are significantly higher than measured PO_4 in all depths, whereas they are in good agreement in summer and autumn. Modelled POC has a similar seasonal cycle as Chl-*a*, but with a pronounced vertical stratification. It is increased in winter and early summer in all depths with a pronounced maximum in surface layers. It gradually decreases towards late spring and completely diminishes through summer until autumn. Towards late autumn it starts to increase again starting from surface layers and continue to increase in the entire water column in early winter. PON model results show an increase in all depths in late winter and early spring. From late spring until early autumn it is homogeneously at a minimum in the entire water column and gradually starts to increase in late autumn towards winter.

In Outer III bay, time-depth distributions (Figure 3.27 and 3.28) show that in winter and early spring Chl-*a* model results are increased in the entire water column with a pronounced maximum in surface layers. In late spring and summer a sub-surface maximum is observed at around 20 m, and below this depth Chl-*a* is close to zero. Towards autumn it again starts

to increase at the surface layers. In year 2009 Chl-*a* is lower in all seasons compared to other years. Measurements are significantly higher than the model results at all depths in autumn of 2008 and in winter and spring of 2009 and below 40 m in summer of 2009 but they are in comparable limits in 2010. Modelled DO is highest in winter and early spring at the surface layers in correlation with increased Chl-*a*. In summer a sub-surface maximum is observed and it decreases to a minimum towards bottom. In autumn it starts to increase at all depths. DIN model results are close to zero in the surface layers above 20 m in all seasons. Below this depth it consistently increases with depth all year round, with a prominent seasonal cycle. Starting from late winter until late summer, bottom DIN increases up to 3.5 μM and declines towards autumn. Modelled PO_4 has a very similar vertical pattern as seen in DIN. It is almost completely depleted above 20 m in all seasons and shows an increase with depth which gradually becomes more pronounced towards summer and declines towards autumn. This seasonality in vertical distributions of nutrients is due to increased uptake at all depths from late autumn to early spring and decomposition of sinking organic material during summer. For both DIN and PO_4, measurements show a significantly less pronounced increase with depth. POC and PON model results are identical in terms of vertical and seasonal distributions. They both show an increase at all depths starting from mid winter until mid spring. Maximums are observed in surface layers. In the year 2009, this pattern is weaker than other two years. During summer, a sub-surface maximum is seen around 20 m deep and below this depth POC and PON decrease to a minimum. With the onset of mixing towards autumn, they start to increase in the entire water column. In the autumn of the year 2010, more pronounced increases in both are seen. Measured POC and PON also show a similar increase in winter and spring with higher values at the surface in agreement with the model results, but in summer of 2009 they show increases with depth which do not exist in model results.

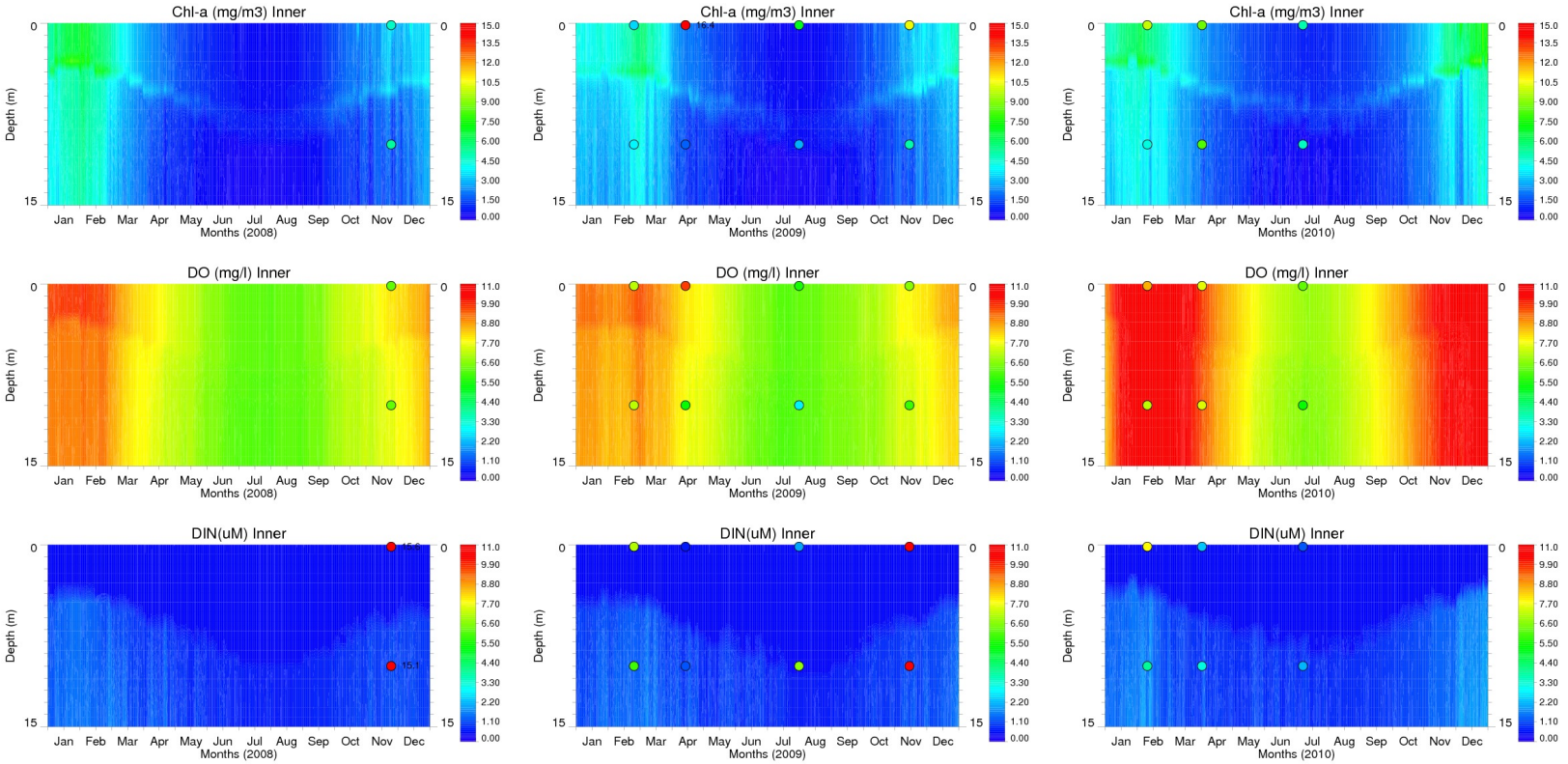

Figure 3.25: Time-depth distribution of Chl-*a*, DO, and DIN model results (background) in comparison to measurements (colored dots) from 2008 (left), 2009 (middle), and 2010 (right) at the Inner Bay station.

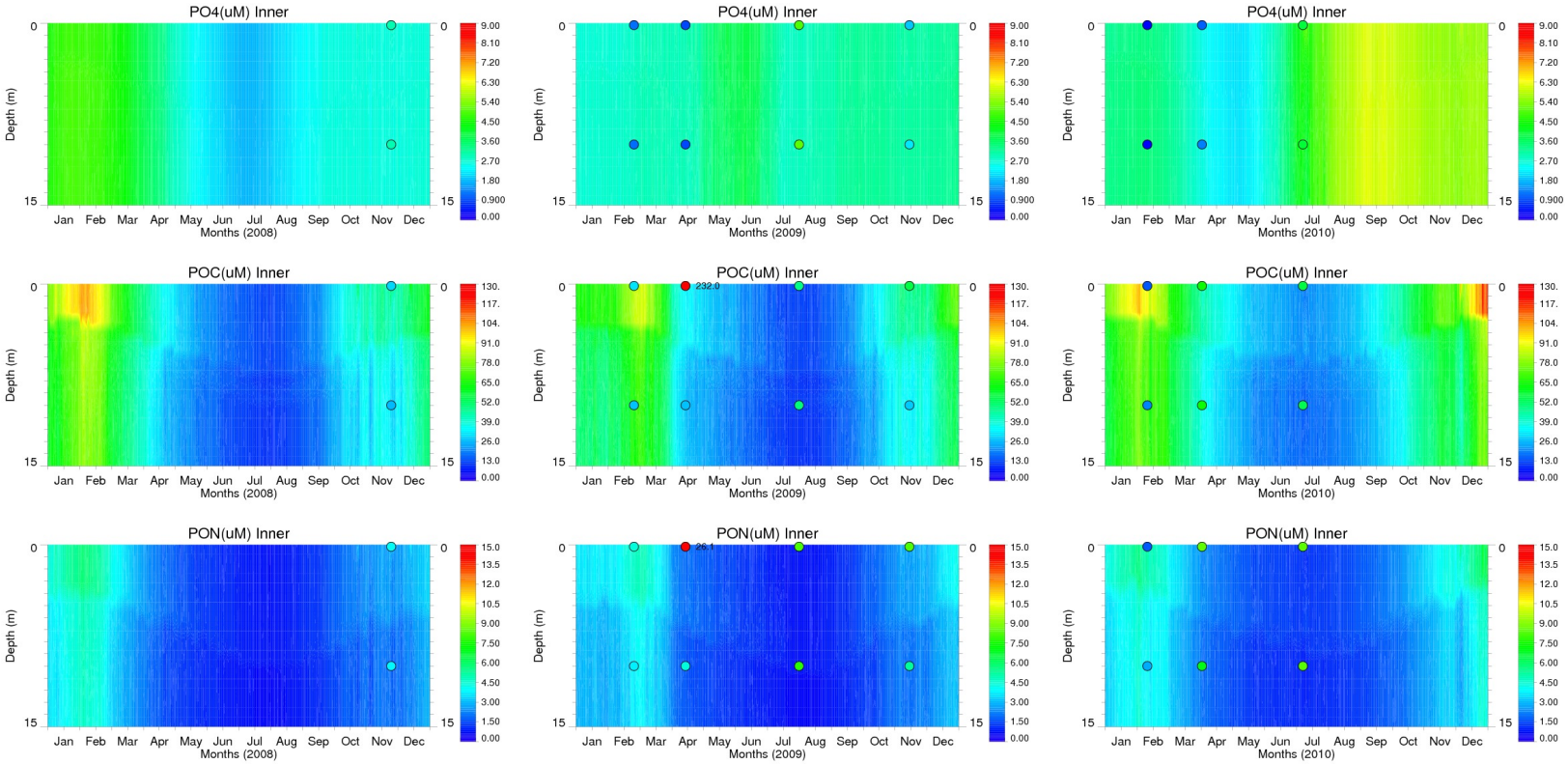

Figure 3.26: Time-depth distribution of PO_4, POC, and PON model results (background) in comparison to measurements (colored dots) from 2008 (left), 2009 (middle), and 2010 (right) at the Inner Bay station.

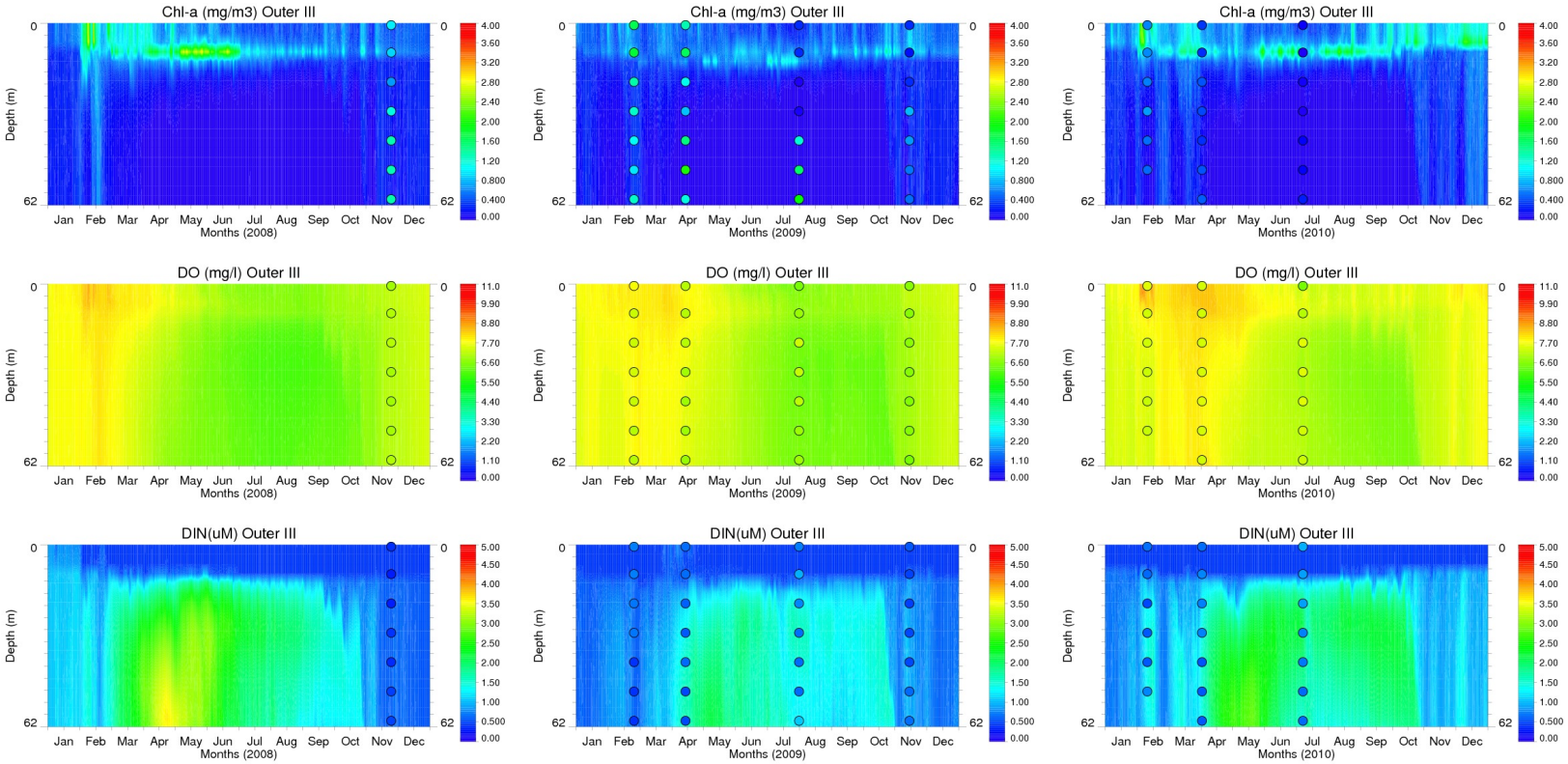

Figure 3.27: Time-depth distribution of Chl-*a*, DO, and DIN model results (background) in comparison to measurements (colored dots) from 2008 (left), 2009 (middle), and 2010 (right) at the Outer Bay III station.

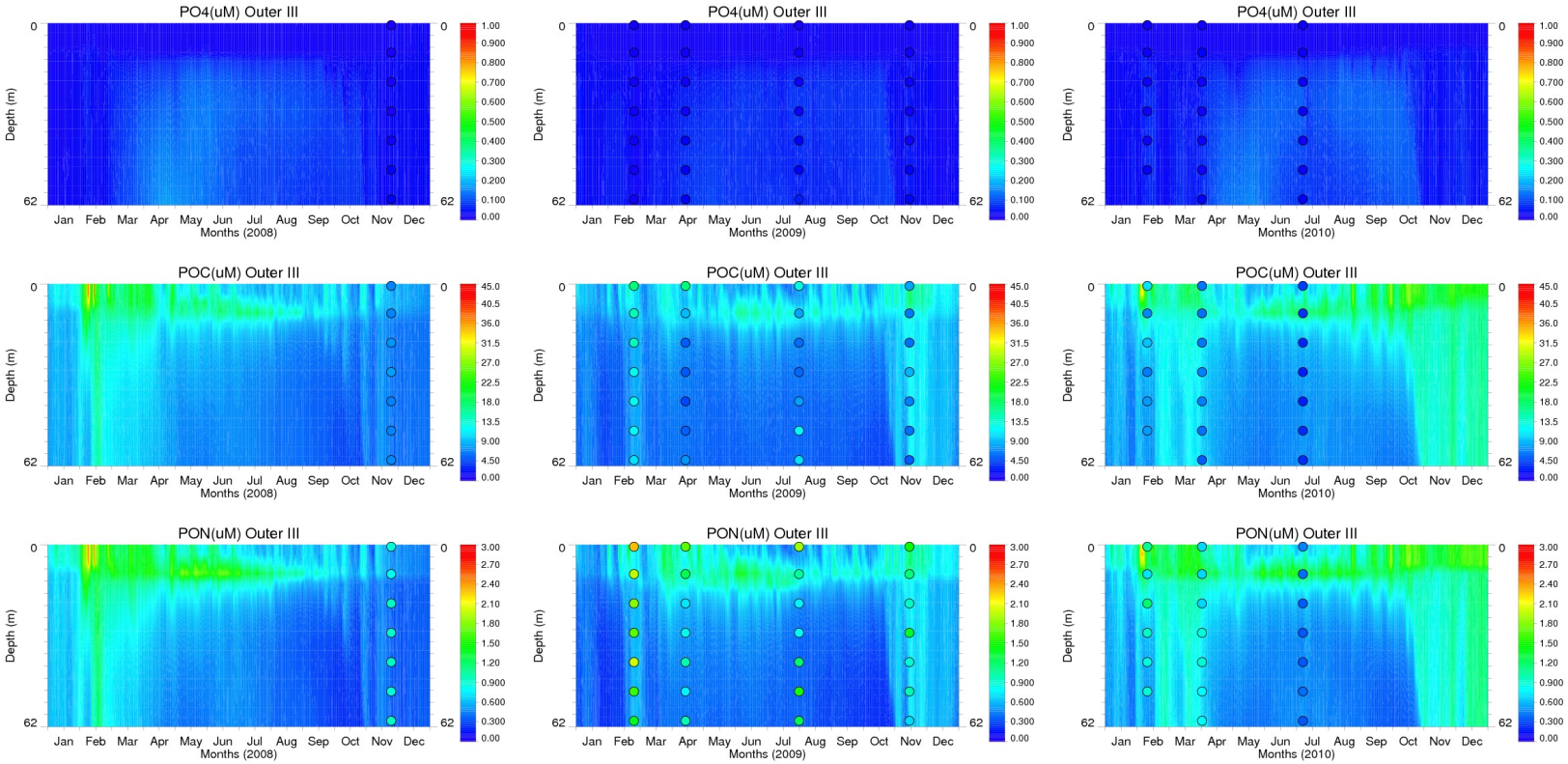

Figure 3.28: Time-depth distribution of PO_4, POC, and PON model results (background) in comparison to measurements (colored dots) from 2008 (left), 2009 (middle), and 2010 (right) at the Outer Bay III station.

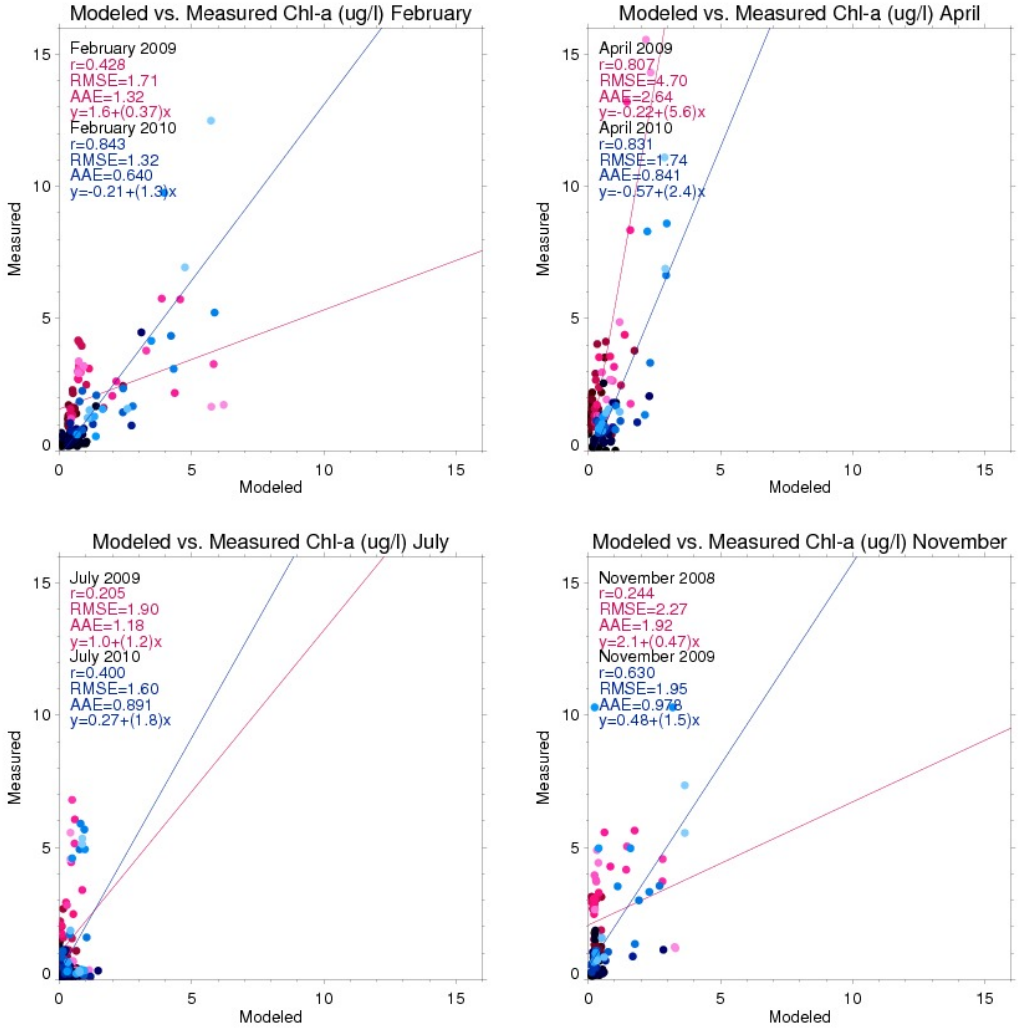

Figure 3.29: Comparison of Chl-*a* model results with measurements.

Table 3.3: Summary statistics for Chl-*a*.

	r	RMSE	AAE	y-intercept	Slope
November 2008	0.244	2.27	1.97	2.1	0.47
February 2009	0.428	1.71	1.32	1.6	0.37
April 2009	0.807	4.7	2.64	-0.22	5.6
July 2009	0.205	1.9	1.18	1.0	1.2
November 2009	0.63	1.95	0.978	0.48	1.5
February 2010	0.843	1.32	0.64	-0.21	1.3
April 2010	0.831	1.74	0.841	-0.57	2.4
July 2010	0.4	1.6	0.891	0.27	1.8

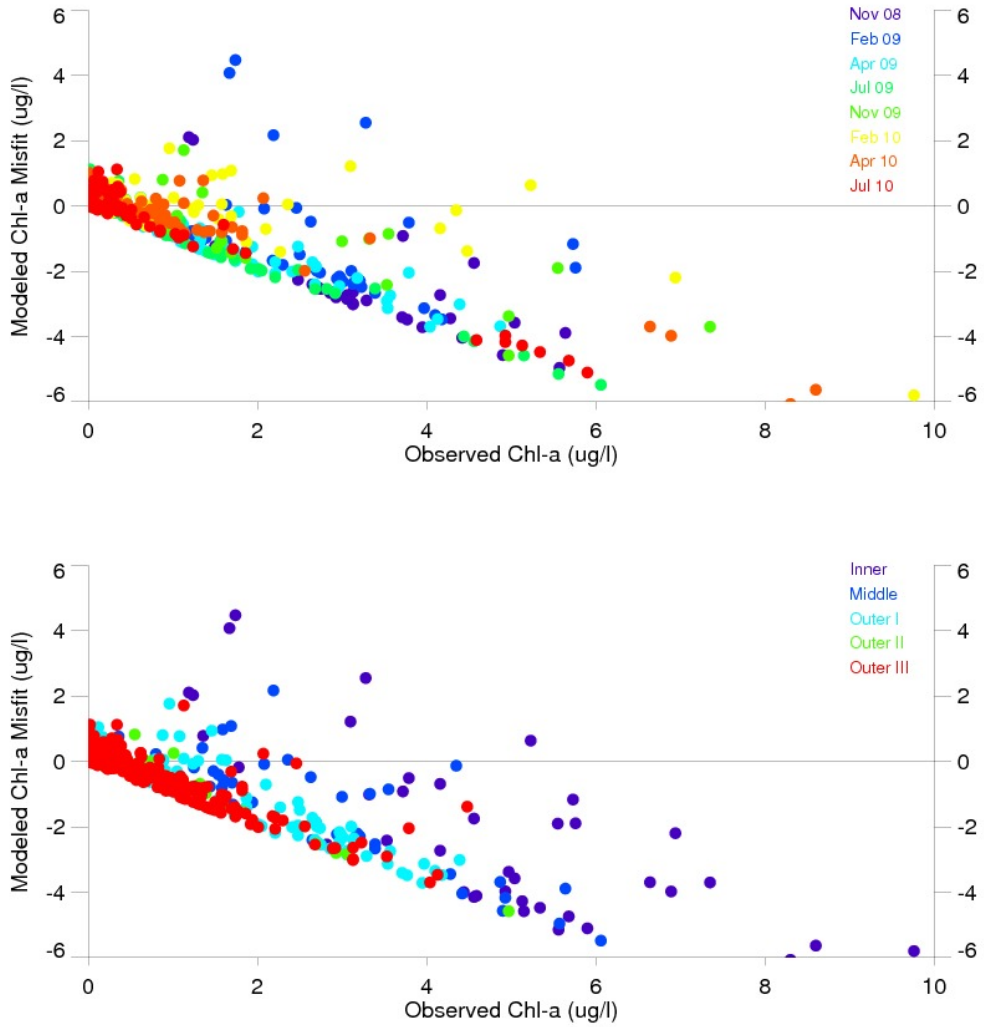

Figure 3.30: Chl-*a* measurements versus model misfit color coded with respect to time (top) and region (bottom).

Comparison of Chl-*a* model results with measurements (Figure 3.29 and Table 3.3) suggests that model does relatively better at lower values but tends to underestimate with increasing Chl-*a*. In February, majority of the model results are comparable to observations towards the minimum. In 2009, model fails to predict the increased values between 1 - 4 mg m^3, whereas, in 2010 it does better in the same range of values, hence the higher correlation and lower error terms. In April, average *r* value is the highest in all seasons, higher than 0.8 in both years, but accompanied by the highest average error terms which indicates that predictions vary in correlation to observations but with a consistent error. Model tends to underestimate almost all of the observed values and completely fails to produce the very high Chl-*a* observed

in this season, more prominently in 2009 than in 2010. In July, since observed Chl-*a* itself varies over a small range and is mainly lower than other seasons, model performance is within acceptable limits. Model fails to predict at a few outlying high observations in both years. In November, model consistently underestimates observations except for a few points. In 2008, since observed Chl-*a* is higher than in 2009 the mismatch is greater. Misfit analyses (Figure 3.30) reveal that majority of the misfit is negative. Model performance is better in summer compared to winter and spring. Error increases towards shallower regions, especially the largest mismatch is in Inner bay.

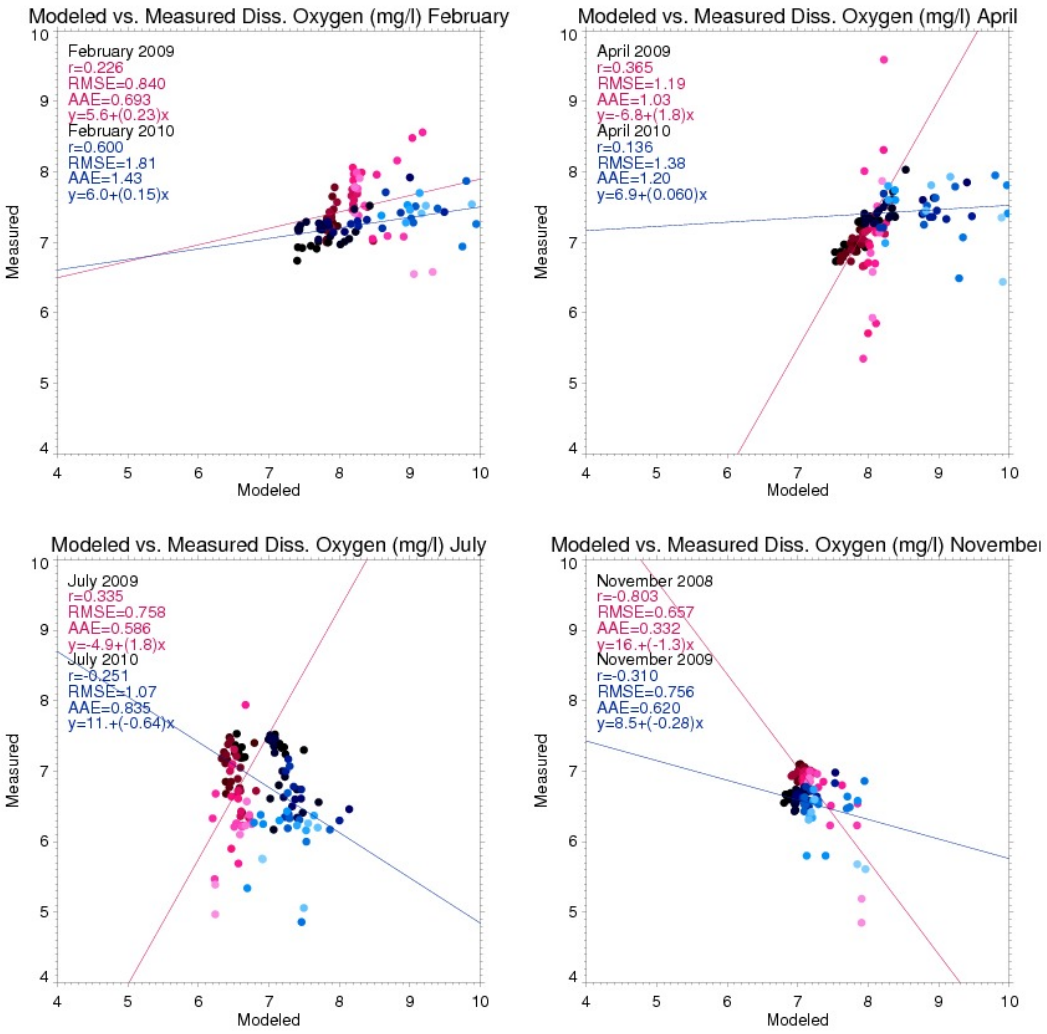

Figure 3.31: Comparison of DO model results with measurements.

Table 3.4: Summary statistics for DO.

	r	RMSE	AAE	y-intercept	Slope
November 2008	-0.803	0.657	0.332	16.	-1.3
February 2009	0.224	0.84	0.693	5.6	0.23
April 2009	0.365	1.19	1.03	-6.8	1.8
July 2009	0.335	0.758	0.586	-4.9	1.8
November 2009	-0.31	0.756	0.62	8.5	-0.28
February 2010	0.6	1.81	1.43	6.0	0.15
April 2010	0.136	1.38	1.2	6.9	0.06
July 2010	-0.251	1.07	0.835	11.	-0.64

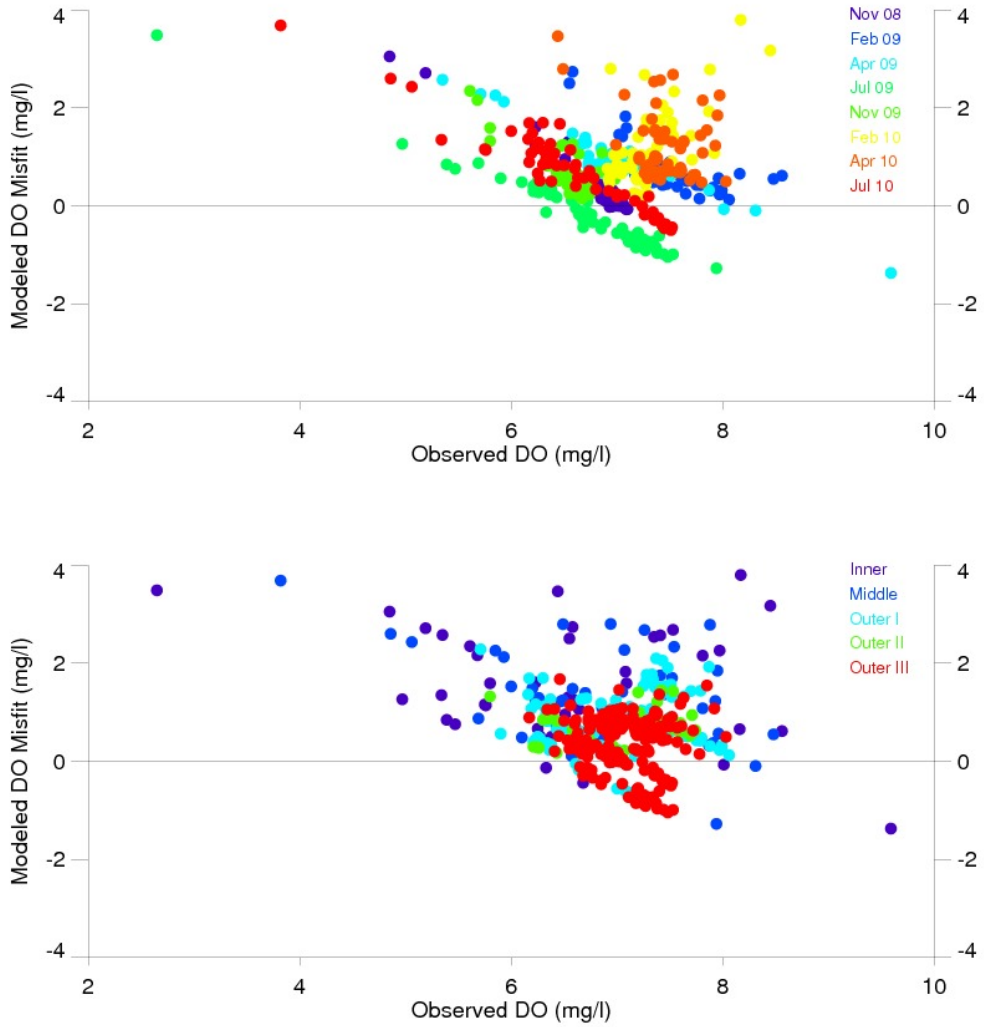

Figure 3.32: DO measurements versus model misfit color coded with respect to time (top) and region (bottom).

Comparison of modelled DO with *in situ* measurements (Figure 3.31 and Table 3.4) show that generally model does better predicting the average values of observed DO but tends to overestimate towards higher values. In February, average error terms are highest in all seasons. Model over-predicts all of measurements but there exists a weak correlation between the two. In April, again all of the model results are higher than observed values. In 2010 model produces artificially high DO values resulting in a significant mismatch. In July, model over estimates the exceptionally low DO values observed in this season but underestimate the maximums. There is a prominent difference between the two predicted years that can be seen in the scatter plot and also indicated by the negative correlation in the year 2010. In November, *r*

values for both years are negative but this fact does not indicate much in this season since both observations and predictions show very little variation. A better indicator in this case, error statistics, on average are lowest in this season. It can be seen in misfit plots (Figure 3.32) that the most of the error lies between the range -/+1, so the model performance can be considered reasonable. Except for the higher values in July and the maximum of April 2009, model overestimates majority of the time. There are two significant error patterns; one is where the model fails to produce DO below 6 mg l^{-1} and the other is over-prediction of increased DO values, both of which result in positive misfits. Model does better in deeper regions especially in Outer III bay and its performance declines towards shallower inner regions.

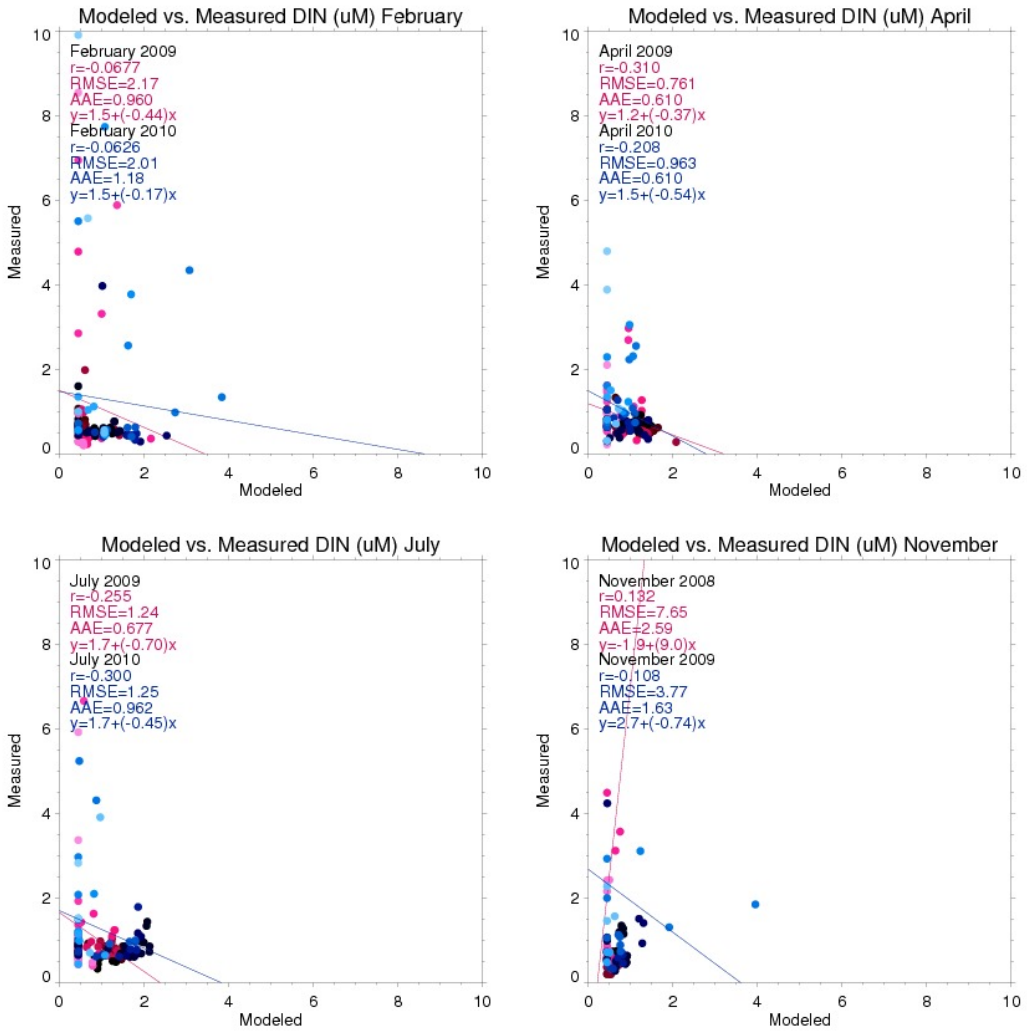

Figure 3.33: Comparison of DIN model results with measurements.

Table 3.5: Summary statistics for DIN.

	r	RMSE	AAE	y-intercept	Slope
November 2008	0.132	7.65	2.59	-1.9	9.0
February 2009	-0.0677	2.17	0.96	1.5	-0.44
April 2009	-0.31	0.761	0.61	1.2	-0.37
July 2009	-0.255	1.24	0.677	1.7	-0.7
November 2009	-0.108	3.77	1.63	2.7	-0.74
February 2010	-0.0626	2.01	1.18	1.5	-0.17
April 2010	-0.208	0.963	0.61	1.5	-0.54
July 2010	-0.3	1.25	0.962	1.7	-0.45

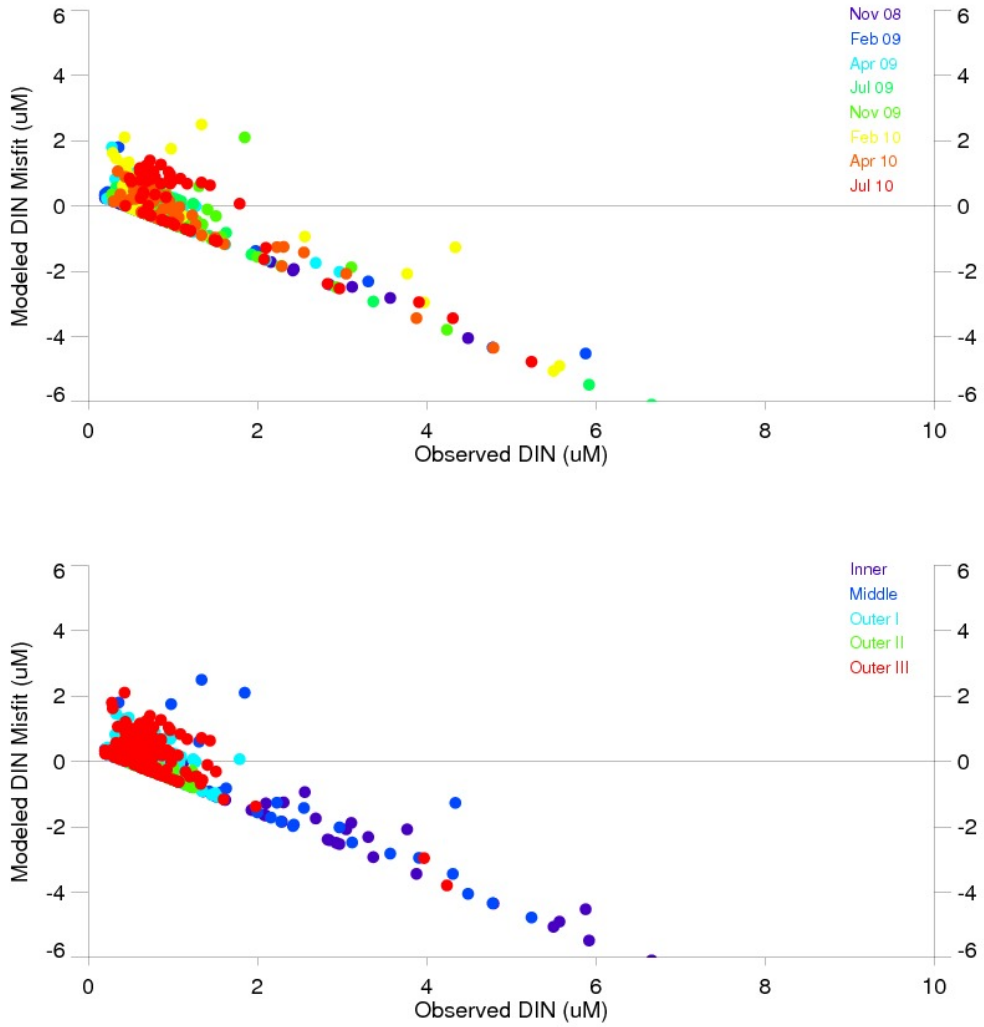

Figure 3.34: DIN measurements versus model misfit color coded with respect to time (top) and region (bottom).

In terms of DIN (Figure 3.33 and Table 3.5) model performs very poorly. The correlation between predictions and observations is negative and error terms exceed reasonable limits most of the time. Error terms indicate that model does very poorly in November when observed DIN is highest and does relatively better in April when it is lowest. Independent of season there can be seen two major patterns in scatter plots; the streak of points parallel to y-axis where model underestimates the increased DIN and the cluster parallel to x-axis where model overestimates the lower DIN, hence the negative correlations. The misfit analyses (Figure 3.34) reveal that the origin of this negative correlation is not a lagged cycle in time but rather the differences in spatial distributions. Outer bays and Inner and Middle bays have completely

distinct characteristics in terms of DIN such that majority of observed DIN in Outer bays is below 2 μM and relatively smaller positive misfit occurs there and almost all of observed DIN above 2 μM is in Inner and Middle bays, where the misfit is negative and becomes greater with increasing DIN.

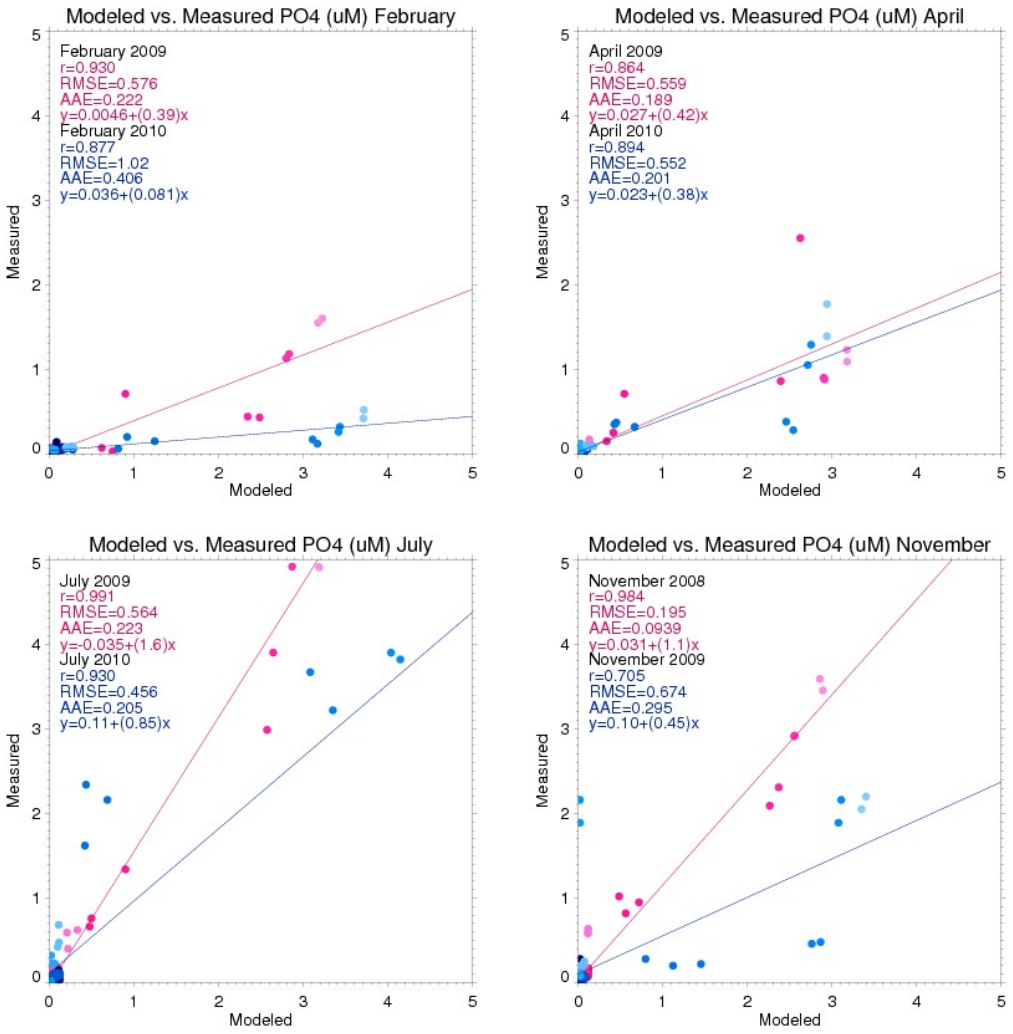

Figure 3.35: Comparison of PO_4 model results with measurements.

Table 3.6: Summary statistics for PO_4.

	r	RMSE	AAE	y-intercept	Slope
November 2008	0.984	0.195	0.0939	0.0031	1.1
February 2009	0.93	0.576	0.222	0.0046	0.39
April 2009	0.864	0.559	0.189	0.027	0.42
July 2009	0.991	0.564	0.223	-0.035	1.6
November 2009	0.705	0.674	0.295	0.1	0.45
February 2010	0.877	1.02	0.406	0.036	0.081
April 2010	0.894	0.552	0.201	0.023	0.38
July 2010	0.93	0.456	0.205	0.11	0.85

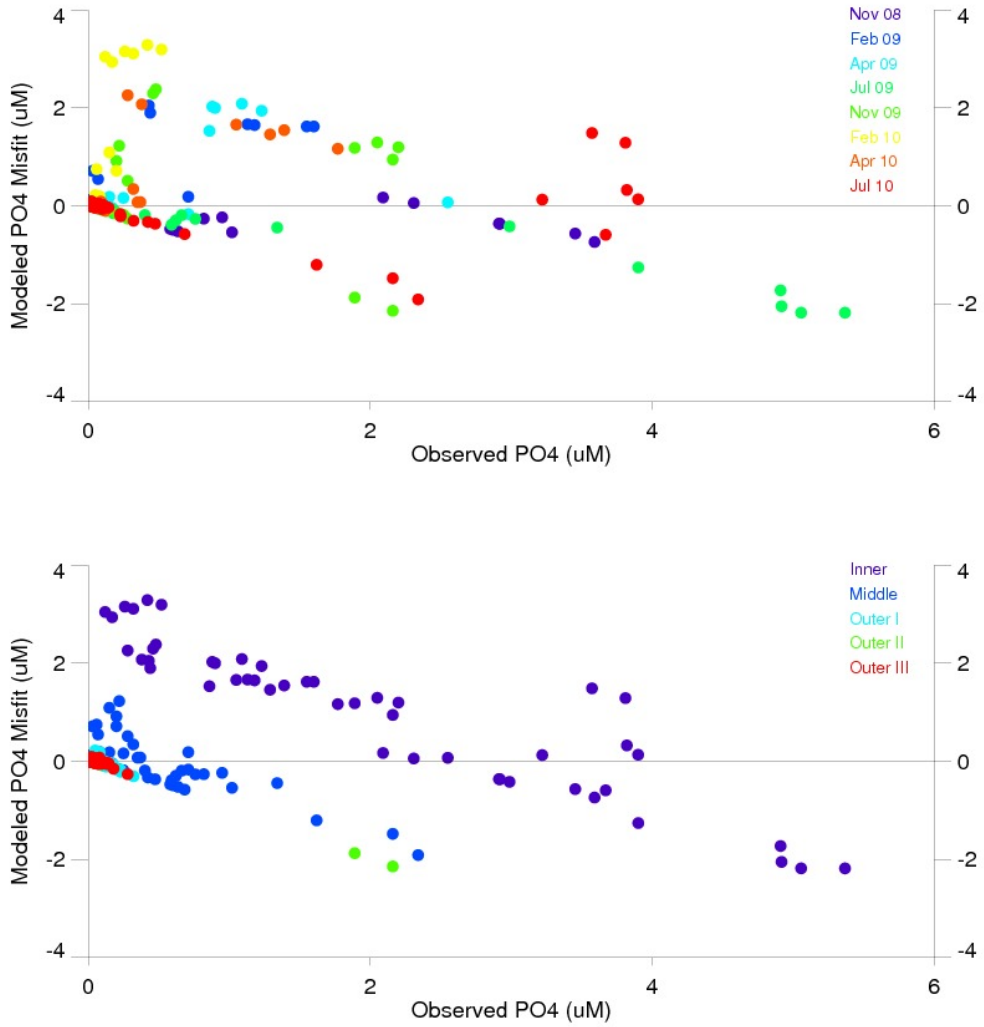

Figure 3.36: PO_4 measurements versus model misfit color coded with respect to time (top) and region (bottom).

Comparison of PO_4 model results with measurements (Figure 3.35 and Table 3.6) show that tough there exist errors, model does very well in terms of correlation. In February, model predicts the lower PO_4 within reasonable limits but overestimates towards increasing values. Error is greatest in February 2010 in all seasons. In April, majority of both predictions and observations except for outliers vary over a very small range and the error is minimal but at higher values model again overestimates. In July, model does very well as indicated by r values higher than 0.9 in both years and reasonably low error terms. Majority of the large error is at the points where model fails to produce the extremely high observed PO_4. In November, model performance is very good in the year 2008 with a very high correlation and smallest

error in all seasons, but poorest in the year 2009 with the lowest correlation and largest error. In the misfit analyses (Figure 3.36) there is no particular pattern in error distribution in terms of seasonality. However, in the lower panel it can be seen that error points in Inner bay form a distinct cluster, indicating that as in DIN, observed PO_4 shows different properties in these regions. Misfit is quite small in deeper regions and increase towards shallow parts, which means model performance is better in oligotrophic environments than eutrophic ones.

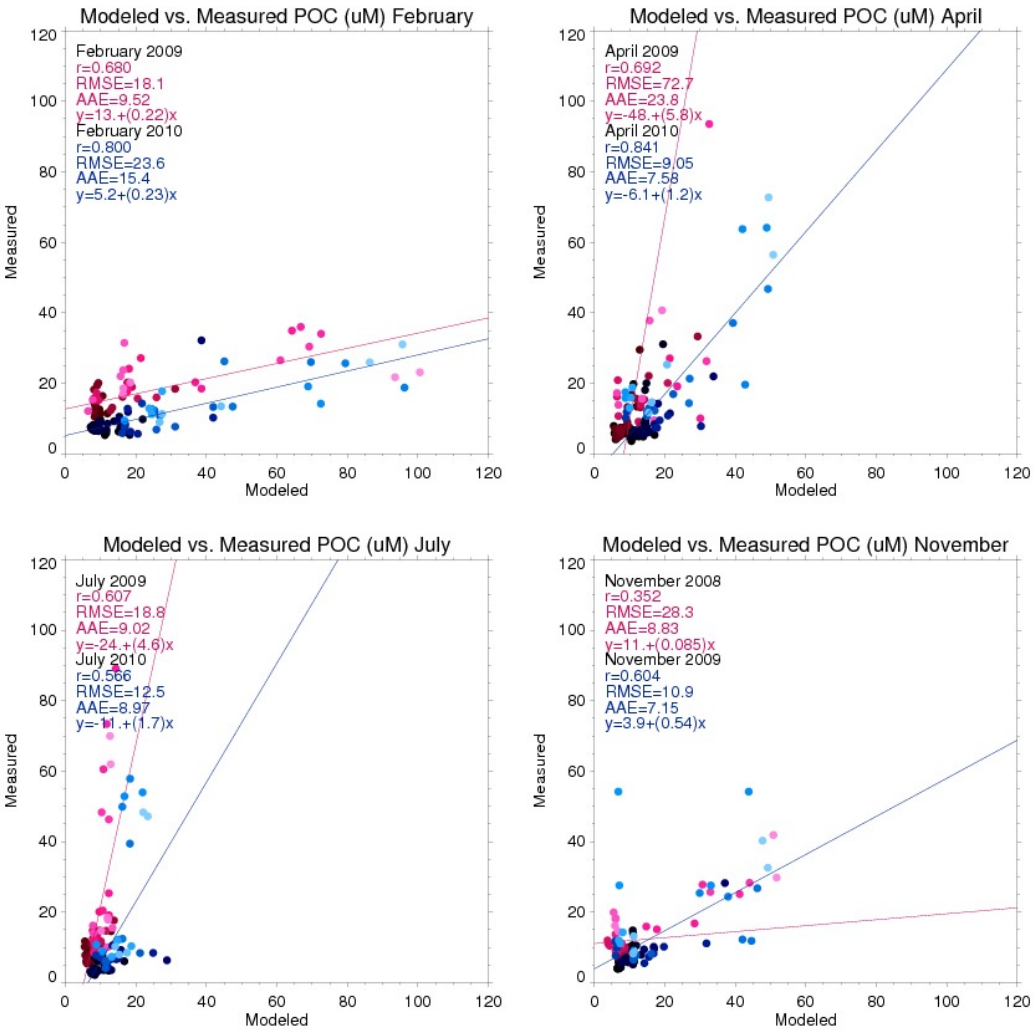

Figure 3.37: Comparison of POC model results with measurements.

Table 3.7: Summary statistics for POC.

	r	RMSE	AAE	y-intercept	Slope
November 2008	0.352	28.3	8.83	11.	0.085
February 2009	0.68	18.1	9.52	13.	0.22
April 2009	0.692	72.7	23.8	-48.	5.8
July 2009	0.607	18.8	9.2	-24.	4.6
November 2009	0.604	10.9	7.15	3.9	0.54
February 2010	0.8	23.6	15.4	5.2	0.23
April 2010	0.841	9.05	7.58	-6.1	1.2
July 2010	0.566	12.5	8.97	-11.	1.7

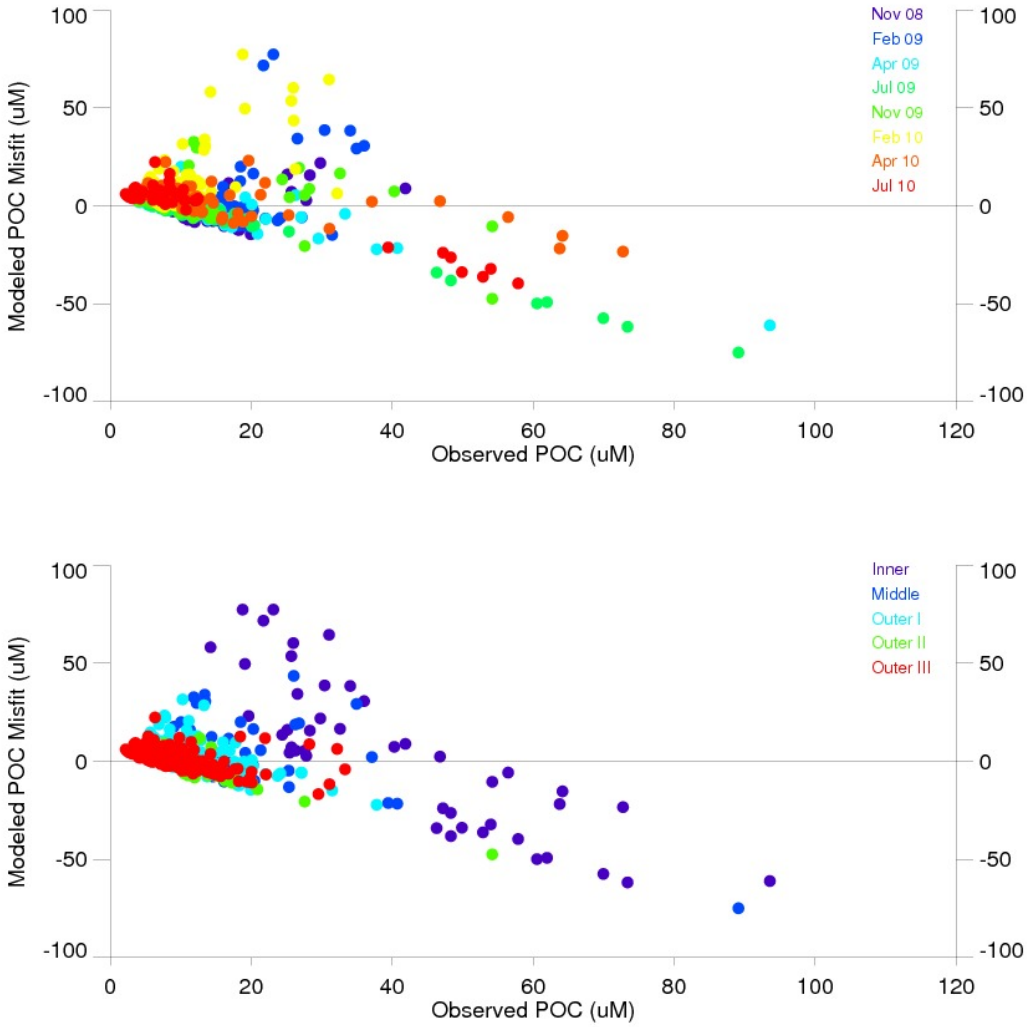

Figure 3.38: POC measurements versus model misfit color coded with respect to time (top) and region (bottom).

Modelled versus measured POC comparisons (Figure 3.37 and Table 3.7) show that model performs reasonably well at lower POC values but fails to predict the higher POC values observed. In February, model does well in terms of correlation but there exist errors due to overestimation of higher POC. In April, model performance is the best in all seasons with the highest r value and the smallest error terms in 2010. In 2009, though the model mismatch is relatively small at and around the minimum POC, model fails to produce the maximum observed in this season resulting in very high errors terms. In July, except for at a few outlying points where model underestimates the observed POC, majority of both the predictions and observations vary over a small range where model performs well. In November, correlation

between model results and observations is weaker compared to other seasons. Model does well in the majority of the lower values but overestimates towards increased POC and fails to predict at a few points with high observed POC. Misfit analyses (Figure 3.38) reveal that positive misfit is greater mostly in February and negative misfit is greater mostly in April and July. Model does relatively better at values below 20 μM, but tends to overestimate values between 20 - 40 μM and underestimate values above 40 μM. Error is minimal in deeper regions, especially in Outer III bay, and increases towards shallower regions. Almost all of the greater errors occur in Inner and Middle bays, forming the distinct cloud of points as seen in the lower panel.

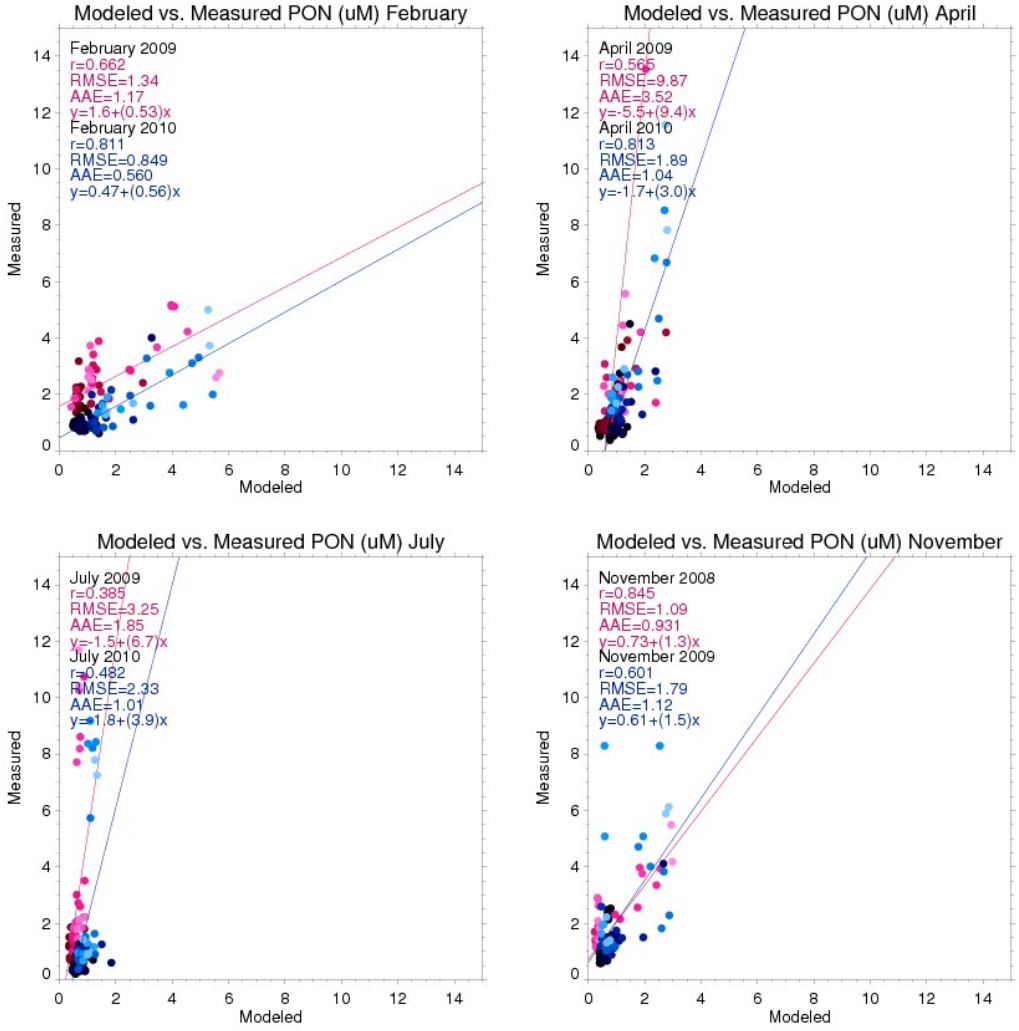

Figure 3.39: Comparison of PON model results with measurements.

Table 3.8: Summary statistics for PON.

	r	RMSE	AAE	y-intercept	Slope
November 2008	0.845	1.09	0.931	0.73	1.3
February 2009	0.662	1.34	1.17	1.6	0.53
April 2009	0.565	9.87	3.52	-5.5	9.4
July 2009	0.385	3.25	1.85	-1.5	6.7
November 2009	0.601	1.79	1.12	0.61	1.5
February 2010	0.811	0.849	0.56	0.47	0.56
April 2010	0.813	1.89	1.04	-1.7	3.0
July 2010	0.482	2.33	1.01	-1.8	3.9

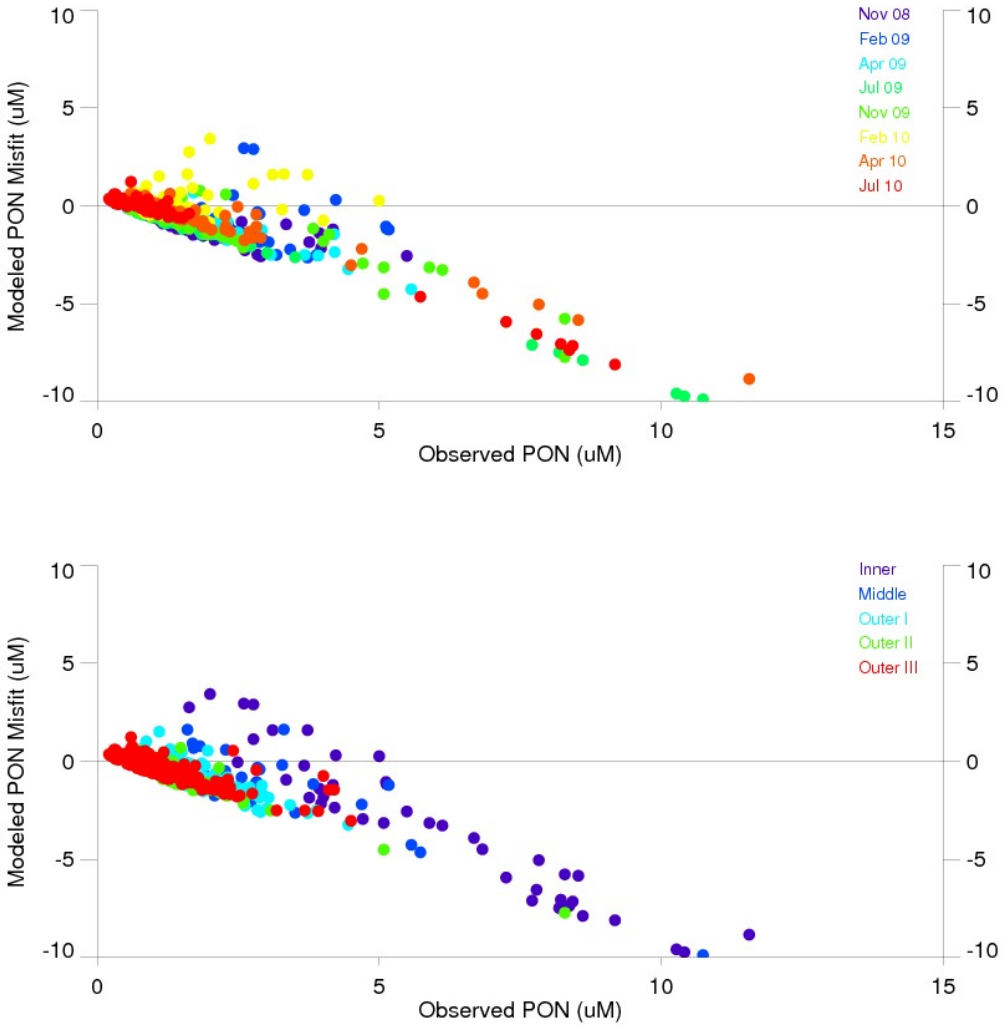

Figure 3.40: PON measurements versus model misfit color coded with respect to time (top) and region (bottom).

In terms of PON (Figure 3.39 and Table 3.8) model performance is very similar to that of POC such that it generally performs well at and around the minimum values and the mismatch increases with increasing PON. In February, model tends to underestimate the lower values and does relatively better at higher values in 2009 whereas in 2010, error is minimal at lower values but increases towards higher PON. In April, model fails to predict the maximums observed in this season in both years, especially in 2009 with the highest error terms, but error becomes minimal towards the minimum values. In July, except for the few outliers where model underestimates, model mainly does well predicting the low PON observed in this season. In November, model performance is very good with high r values and low error

terms. Mismatch is mostly in reasonable limits except for a couple of points in the year 2009 where model underestimates. In the misfit analyses (Figure 3.40) it can be seen that, as in POC, most of the positive misfit occurs in winter and negative misfit occurs in spring and summer. Model does well in Outer bays and the error increases towards Middle and Inner bays such that almost all of the negative misfit at values greater than 5 μM occurs in Inner Bay.

3.3 RESULTS OF THE NUTRIENT ENRICHMENT/REDUCTION SCENARIOS

Table 3.9: List of scenario runs.

Run	PO_4	DIN
Reference	-	-
A	-	+10%
B	-	-10%
C	+10%	-
D	+10%	+10%
E	+10%	-10%

In this section results of the test runs (Table 3.9) are given in terms of the selected parameters. Results are averaged vertically over all depths, horizontally over each subregion, and temporally over each year, then the percent differences are calculated with respect to the reference run.

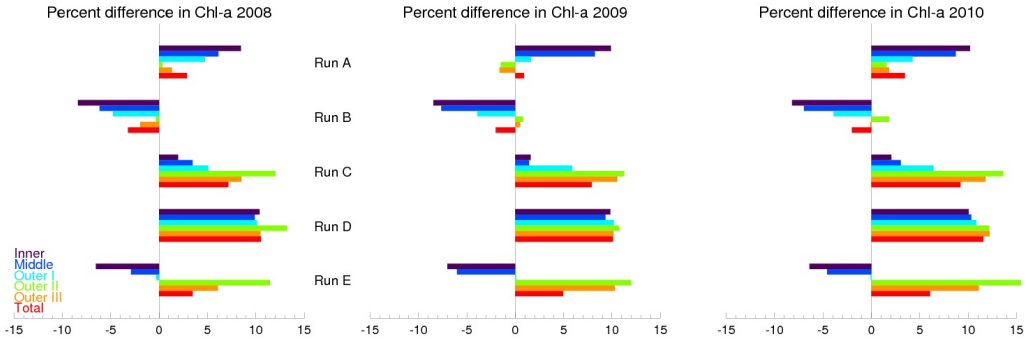

Figure 3.41: Comparison of scenarios in terms of percent differences in Chl-*a*.

Chl-*a* (Figure 3.41), in runs A and B, is positively correlated to DIN input in general except for in Outer II and III bays in 2009 and only Outer II bay in 2010. In total, it increases by 3% in 2008, 1% in 2009, and 3.5% in 2010 in run A, and decrease by 3% in 2008, 2% in 2009, and 2% in 2010 in run B. In runs C and D, Chl-*a* increases with increasing PO_4 consistently in all regions. In run C, increase in Inner and Middle bays are smaller than it is in Outer bays and the smallest in this region compared to other runs, but since spatially Inner and Middle bays occupy a minor fraction of the whole domain, the total increase is still significant such

that it is 7% in 2008, 8% in 2009, and 9% in 2010. In run D, the highest increase occurs in all regions and the total increase is 10.5% in 2008, 10% in 2009, and 11.5% in 2010. In run E, Chl-*a* decreases in Inner and Middle bays but increases in Outer II and Outer III bays, and shows an insignificant change in the transitional Outer I bay. In total, still the change is positive and the increase is by 3.5% in 2008, 5% in 2009, and 6% in 2010.

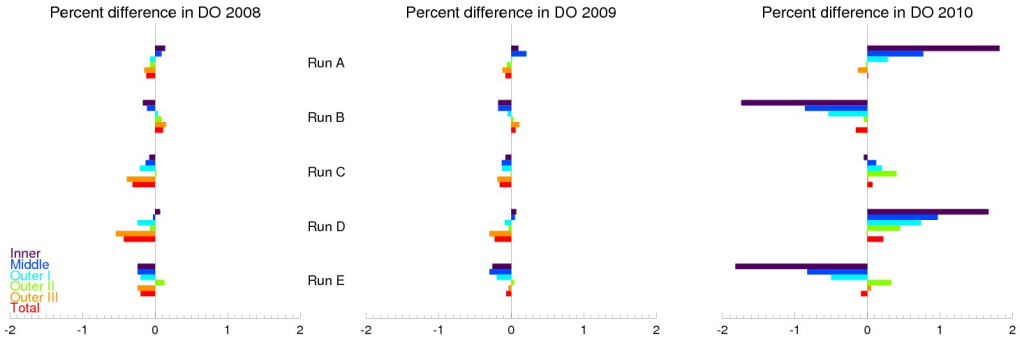

Figure 3.42: Comparison of scenarios in terms of percent differences in DO.

In runs A and B, DO (Figure 3.42) and DIN input is positively correlated in Inner and Middle bays, but negatively correlated in Outer II and Outer III in all years. In Outer I, it decreases in 2008 and increases in 2009 and 2010 in run A, and vice-versa in run B. The change in inner regions in 2010 is very pronounced but there is no significant difference in total change. In run A, percent difference in total is -0.2% in 2008, -0.08% in 2009, and 0.01% in 2010, and in run B, 0.11% in 2008, 0.06% in 2009, and -0.16% in 2010. In run C, DO decreases with increased PO_4 input in all regions but Outer I in 2008 and in all regions in 2009, but increases in all regions but Inner bay in 2010. In total, DO decreases by 0.31% in 2008 and 0.16% in 2009, and increases by 0.07% in 2010. In run D, DO increases only in Inner bay in 2008, in Inner and Middle bays in 2009, and in all regions in 2010. The decrease in 2008 in Outer III bay is highest in this region in all runs. Total change is -0.43% in 2008, -0.23% in 2009, and 0.22% in 2010. In run E, DO decrease in all regions except for Outer I in all years and Outer III in 2010. Total decrease is by 0.2% in 2008, 0.07% in 2009, and 0.09 % in 2010.

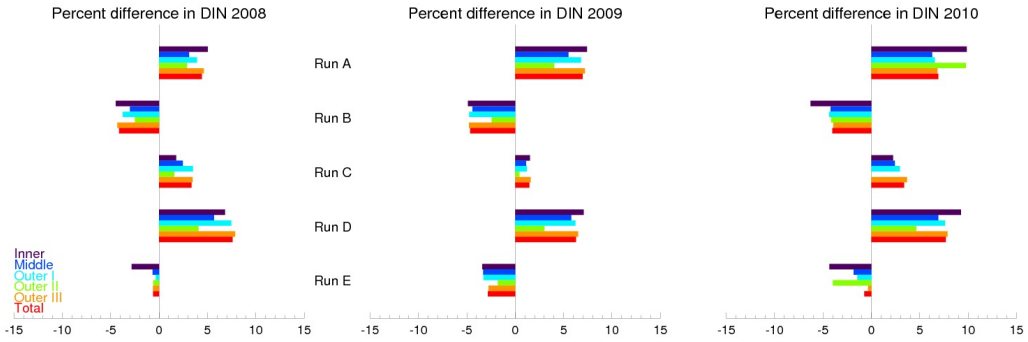

Figure 3.43: Comparison of scenarios in terms of percent differences in DIN.

Percent differences in DIN (Figure 3.43) in runs A and B are in correlation to increase and decrease in DIN input in all regions and years. In run A, total increase is by 4.5% in 2008, 7% in 2009, and 7% in 2010, and in run B, total decrease is by 4% in 2008, 4.5% in 2009, and 4% in 2010. In run C, though DIN input is not changed, DIN increases in all regions in correlation to PO_4 input. Total change is 3.5% in 2008, 1.5% in 2009, and 3.5% in 2010. In runs D and E, again DIN changes according to the change in DIN input, but in this case increase is more and decrease is less pronounced. Total increase in run D is by 7.5% in 2008, 6% in 2009, and 7.5% in 2010, and the total decrease in run E is by 0.6% in 2008, 3% in 2009, and 0.7% in 2010.

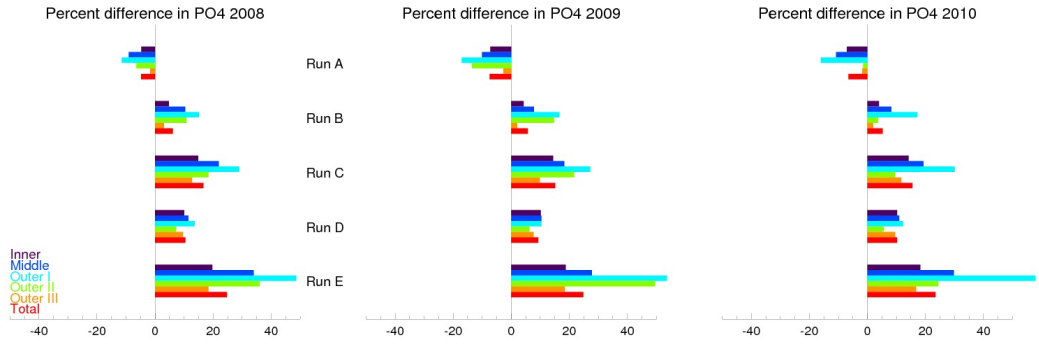

Figure 3.44: Comparison of scenarios in terms of percent differences in PO_4.

In runs A and B, PO_4 (Figure 3.44) is inversely correlated to DIN input in all years and regions, especially in Inner, Middle, and Outer bays. In total it decreases by 5% in 2008, 7.5% in 2009, and 6.5% in 2010, and increases by 6.5% in 2008, 6% in 2009, and 5% in 2010. In runs C, D, and E, PO_4 increases in all regions and years with increased PO_4 input. The change is most prominent in Outer I bay and highest in run E in all regions. Total increase

in run C is by 16.5% in 2008, 15% in 2009, and 15.5% in 2010, in run D by 10.5% in 2008, 9% in 2009, and 10% in 2010, and in run E by 25% in 2008, 25% in 2009, and 23.5% in 2010.

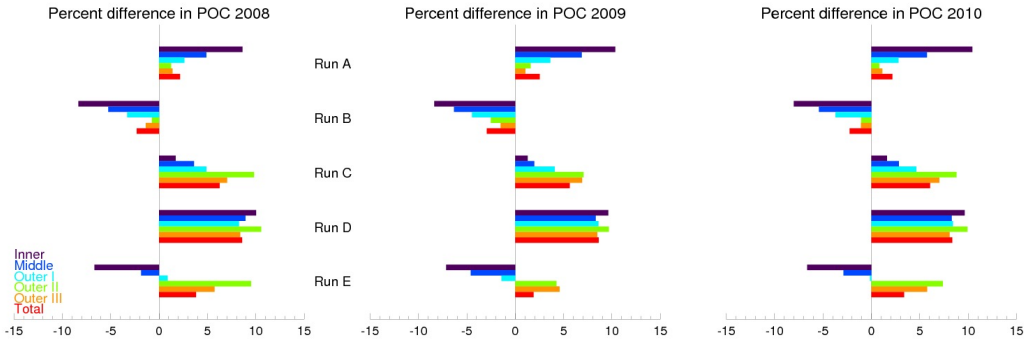

Figure 3.45: Comparison of scenarios in terms of percent differences in POC.

The change in POC (Figure 3.45) is positively correlated to DIN input in runs A and B in all regions and years. Total change is 2% in 2008, 2.5% in 2009, and 2% in 2010 in run A, and -2% in 2008, -3% in 2009, and -2% in 2010 in run B. In run C, POC increases in all years and regions, most prominently in Outer II and Outer III. In total, increase is by 6.5% in 2008, 5.5% in 2009, and 6% in 2010. In run D, POC increases in all regions simultaneously in all years. Total increase is maximum of all runs with 8.5% in 2008, 9% in 2009, and 8.5% in 2010. Similar to Chl-*a*, in run E, in Inner and Middle bays POC decreases in all years and increases in Outer bays in all years except for Outer I in 2009 and 2010. In total, it increases by 4% in 2008, 2% in 2009, and 3.5% in 2010.

CHAPTER 4

DISCUSSION

STUDY AREA: İZMİR BAY

In the light of both observed and modelled parameters, this study presents an overall picture of the current state of İzmir Bay. The major characteristic of the bay is that both physical and biogeochemical properties of the bay show strong horizontal gradients between outer and inner regions in which both natural and anthropogenic influences play important roles. The bay opens to the Aegean Sea at one end and becomes shallower and subject to increasing amounts of effluents at the other. Outer regions are mostly dominated by relatively milder and oligotrophic waters entering the bay from the Aegean Sea, while inner regions, on the other hand, are mainly controlled by local influences such as fresh water inputs. The geography of the region also enhances these differences such that the depth of the Inner bay is quite shallow making it react more drastically to warming/cooling and increased fresh water input/evaporation or increased pollutants. There is a very shallow sill separating Inner bay from the rest of the bay and limiting the exchange of water, hence horizontal gradients occur. Another important characteristic is the very prominent Gediz River input at the eastern coastline. Gediz River is the largest fresh water source of the bay, and is very effective in lowering the salinity and increasing nutrient concentrations, thus Chl-*a* and particulate organics, in the vicinity of its plume.

In terms of modelled physical properties, outer parts show Aegean Sea characteristics with temperature ranging between 14 - 27 °C and salinity ranging between 37 - 39 psu, whereas, in Inner bay temperature ranges between 11 - 29 °C and salinity ranges between 35 - 40 psu. Inner bay is distinct from the rest of the bay such that it is warmest in summer and coldest in winter, and fresher than the rest in all seasons. In winter, mixing is very effective

and temperature and salinity in the entire bay is vertically homogeneous, and fresh water fluxes are highest thus lowering the salinity especially in inner regions. In summer, the bay is strongly stratified with a thermo/halocline at around 20 m deep. These findings are confirmed with measurements and agree with the previous research by Sayın et al. (2006). In this study, time-dependent modelled circulation fields are presented for the first time for this region (see Appendix A for monthly averaged surface horizontal velocity fields model results). The most prominent feature of circulation in the bay is the inflow/outflow in the north. According to model results, in winter and spring, at the surface, inflow occurs off the northwestern coast, and outflow occurs off the northeastern coast. During summer and early autumn, inflow occurs off both coasts, more strongly at the east, and no prominent outflow occurs at the surface. Another feature is the anticyclonic Middle Gyre that forms in Outer I bay during summer and early autumn, when inflow occurs off the northeastern coast, which is also mentioned by Sayın (2003).

The biogeochemical properties of the bay, described by measurements, show that the northern parts are occupied by relatively oligotrophic Aegean Sea water with Chl-*a* ranging between 0 - 2 mg m^{-3}, DIN between 0 - 1 μM, PO_4 between 0 - 0.3 μM, and POC between 0 - 20 μM, whereas, Inner bay is highly eutrophicated with Chl-*a* ranging between 0 - 16 mg m^{-3}, DIN between 0 - 15 μM, PO_4 between 0 - 5 μM, and POC between 0 - 230 μM. These are largely captured by ecosystem model as well. A very important difference between the two regions, that can be seen in the results of this modelling study, is that Outer bay is P-limited but Inner and Middle bays are N-limited with DIN/PO_4 ratios around 20 and ≤ 1, respectively, which is in agreement with earlier studies (Büyükışık and Erbil, 1987; Büyükışık, 1986; Bizsel and Uslu, 2000). This difference can be explained by the facts that the majority of Gediz River's drainage basin consists of agricultural land, thus pollutants it carries into the bay are rich in nitrogen enhancing the P-limited nature of the Outer bays and the excessive amount of domestic waste rich in phosphorus discharging into Middle bay switches the system to N-limited towards inner regions.

MODELLING İZMİR BAY

The modelling study presented in this thesis consists of two parts: the hydrodynamic model that forms the basis, and the ecosystem model that is coupled to the hydrodynamics and which

is the main focus.

The main aim of the hydrodynamic modelling effort is to produce time-dependent three-dimensional fields of all physical properties of the bay within reasonable ranges of the observed variation of these parameters to elucidate the spatial and temporal variation of the physical environment of İzmir Bay.

During the hydrodynamics modeling study it became clear that the quality of data that is available for external forcings has a strong effect on model performance. Lack of sufficient observations that can be used to force the model has been a major problem in this study, such as the observations of current velocity to force the open boundaries and the measurements of fresh water fluxes or temperature to force the discharge points. Aside from external forcings, a number of model coefficients are tuned for the study region. The most suitable set of values are chosen through numerous trials so that the model is able to resolve the horizontal and vertical dynamics. Trials are tested against measured temperature and salinity in terms of model's ability to produce horizontal fields, vertical stratification and mixed layer depth.

Overall performance of the hydrodynamics model is analyzed through model skill assessment measures in terms of temperature and salinity. Model performance can be considered good and the majority of the error can be attributed to the deficiencies mentioned above. In general, the model is successful in producing important features such as the inflow/outflow in the north, distinct characteristics of the shallow regions and distinguishable Gediz River input in Outer III bay. Temporally, the seasonality of the model results matches with that of the observations very well. In terms of temperature, the model does well in seasons when mixing is effective but performance declines when stratification is most prominent, indicating that vertical dynamics of the model may need further improvement. In terms of salinity, model produces the prominent horizontal gradients but has certain discrepancies only in regions heavily influenced by fresh water inputs or where there exist salt production flats, thus it is possible to eliminate these errors by improving the quality of the above described forcing inputs.

The reference ecosystem model simulation has two main purposes: giving a three-dimensional and time-dependent representation of biogeochemical properties in the bay to help understand the ecosystem dynamics that so far has not been fully explained before with observations alone and serving as a reference for applying a series of scenarios to provide information on

the reaction of the bay to changes in nutrient inputs that it may undergo in the future.

The most important challenge in fulfillment of these purposes was to properly prescribe the nutrient loading into the bay. Information on nutrient loads are not always readily available; they might not be continuously measured, made public, or measured at all as in the case of rain drainage outlets. Details of available data and methods used to cover for unavailable data are explained in Chapter 2. The aspect to be discussed here is the fact that a considerable part of this crucial external input has to be based on approximations and hence is a source for uncertainties that reflect in model performance. Another challenge was to decide on which processes to include in the set-up of the model to make it as realistic as possible. The bay has very distinct characteristics in which several different processes such as resuspension or decomposition in the sediment are important at the same time, and most of these processes are not yet fully understood. Model constants and rates related to this multitude of processes had to be tuned for the region through many trials since no similar study has been performed before in this region and literature is very scarce. As much as the external loads, it is essential to include processes, as well as to tune the rates which govern these processes together with the general water quality and primary production processes simultaneously. Trials are tested against measurements in terms of models ability to produce seasonality and spatial distributions that possess the distinctive features.

Given the limited amount of information and expertise, instead of aiming for a good performance in terms of all biological and chemical parameters, it is considered adequate for the reference ecosystem model results to be in comparable ranges to observations in general. Model performance in terms of all parameters is good in the majority of Outer bays, and gradually declines towards Gediz River and inner regions, where fresh water influence and nutrient input is increased. This is significant proof that one major deficit of the model originates from the uncertainty in the external inputs carried by fresh waters and can be improved if adequate measurements are available. In terms of Chl-*a* the model does well in producing the spatial patterns and the discrepancies mostly occur in areas where observed Chl-*a* is very high. This shows that performance can be improved by further tuning of the primary production parameters. Although the model has certain errors producing nutrient concentrations, it is able to produce the observed DIN to PO_4 ratios in all seasons within reasonable ranges indicating that model actually captures the contrasting natures of N-limited and P-limited regions in the bay.

The series of nutrient enrichment/reduction scenarios applied gives profound insight on how the bay responds to the possible changes in nutrient loads it receives. The results of these scenario runs, analyzed in terms of percent differences to the reference ecosystem run, are given in yearly sub-region averages to avoid differences due to the seasonality and spatial variability of selected parameters.

In runs A and B, when only DIN input is changed, the Inner and Middle bays respond to the increase/decrease in DIN input more pronouncedly than Outer bays, in terms of Chl-*a* and POC. The N-limited nature of Inner and Middle bays makes them more sensitive to changes in DIN, therefore an increase/decrease in DIN input directly results in an increased/decreased production. DIN levels in all subregions respond similarly to the increase/decrease in DIN input positively. PO_4, in all subregions, more pronouncedly in Inner, Middle and Outer I bays, is negatively correlated to DIN input. The accumulated PO_4 as a consequence of this N-limitation gets utilized and decreases when there is more DIN available but gets accumulated more when DIN is less available.

In run C, when only PO_4 is increased, Chl-*a* and POC increase more in the Outer bays than in the Inner and Middle bays, since Outer bays are more sensitive to PO_4 due to their P-limitation. DIN increases in all regions even though PO_4 is increased. This can be explained such that, since a larger volume of the bay, especially the deeper Outer bays, is P-limited rather than N-limited, an increase in PO_4 input increases production more than the increase in DIN input does in total, and remineralization of organic matter before it sinks starts to act as a source of nutrients. This can be also supported by the fact that the increase in PO_4 input is only 10 % but the increase in PO_4 level in total is around 20 %. This outcome is not observed when only DIN input is increased because it increases the production in the rather shallow inner regions and organic matter sinks before it can act as a source. In other words, when production increases in deeper regions, remineralization in the water column increases the availability of inorganic nutrients.

In run D, when inputs of both nutrients are increased, Chl-*a*, POC, DIN, and PO_4 increase in all subregions simultaneously. This response shows that increasing both nutrients results in the reaction that is the sum of the reactions to increasing them individually but not in an

increased one. The reaction of one region is mainly dependent on the changes in the nutrient it is limited by, than the reaction it gives to the other nutrient. So even all subregions react similarly, the nutrient they are reacting to is different.

In run E, when PO_4 input increases and DIN input decreases, the response of the bay is again the sum of the responses it gives to individual changes in these nutrients. Chl-*a* and POC decrease in Inner and Middle bays but increase in Outer bays. In total, production increases since the volume of Outer the bays is much larger than of the Inner and Middle bays and more determining of the total. The decrease in DIN level is less pronounced than the decrease seen when only DIN input is decreased because of the above mentioned effect of PO_4 on DIN availability. Also, the increase in PO_4 level is the sum of the increase due to accumulation of unutilized PO_4 caused by decreased DIN input, and increased availability. This run shows that even if a reduction occurs in DIN inputs, it can not be fully effective if PO_4 input is not prevented from increasing, because PO_4 affects a larger volume of the bay and it increases the availability of both nutrients.

Overall analysis of these runs shows that the N-limited Inner and Middle bays and the P-limited Outer bays, give contrasting reactions to changes in inputs of DIN and PO_4 such that the former is more sensitive to DIN input where as the latter is more sensitive to PO_4 input. DIN input negatively affects the availability of PO_4 because it increases its uptake/accumulation in N-limited regions. Increase of PO_4 pronouncedly increases production in P-limited regions, that are larger and deeper, therefore has a greater impact on the bay in total. Also, this increased production in deeper regions increase the availability of nutrients by increasing the amount of remineralized organic matter. It is revealed that if PO_4 input increases, the bay gets more eutrophicated even DIN input decreases. In light of this analysis, run B, when PO_4 input is kept in today's level and DIN input is decreased, is the best possible scenario towards a reduced eutrophication in the bay.

CHAPTER 5

CONCLUSION

In this study, a three-dimensional time-dependent coupled ecosystem model is applied to İzmir Bay for the first time to help understand the current physical and biogeochemical state of the bay and the processes contributing to its eutrophication. Delft3D modelling suite's FLOW and ECO modules are adapted and tuned for the region. A reference model covering three years is produced whose results, together with measurements collected during SINHA cruises, provide a detailed description of the physical and biogeochemical dynamics of the area, their seasonal cycle and spatial variability. Model skill assessment methods are used as a measure of model performance and to address the shortcomings of it. The hydrodynamics model is able to produce physical features in terms of seasonality and spatial distribution, whereas the ecosystem model has certain discrepancies which can be reduced with improved quality of model inputs such as open boundary conditions, and fresh water and nutrient fluxes. Then the model is used as a tool with predictive capacity to assess the ecosystem response of the bay to possible changes that it may undergo in the future. Five nutrient enrichment/reduction scenarios are constructed on the basic assumptions that it is unrealistic that a reduction in external PO_4 inputs will occur as urbanization continues to grow and it is not treated effectively, and external DIN input is subject to any possible change.

Results suggest that both physical and biogeochemical properties of the bay show strong horizontal gradients between outer and inner regions in which both natural and anthropogenic influences are effective. It is revealed that Outer bays are mostly occupied by waters originating from the Aegean Sea, with temperature and salinity ranging between 14 - 27 °C and 37 - 39 psu, that are relatively oligotrophic with Chl-*a* ranging between 0 - 2 mg m^{-3}, DIN between 0 - 1 μM, PO_4 between 0 - 0.3 μM, and POC between 0 - 20 μM. Inner and Middle bay waters, on the other hand, have their unique characteristics resulting from their sensitivity

to local influences, with temperature and salinity ranging between 11 - 29 °C and 35 - 40 psu, that are highly eutrophicated with Chl-*a* ranging between 0 - 16 mg m^{-3}, DIN between 0 - 15 μM, PO_4 between 0 - 5 μM, and POC between 0 - 230 μM. There exist contrasting P-limited and N-limited environments simultaneously in the bay, due to the facts that the majority of Gediz River's drainage basin consists of agricultural land, thus pollutants it carries into the bay are rich in nitrogen enhancing the P-limited nature of the Outer bays and the excessive amount of domestic waste rich in phosphorus discharging into Middle bay switches the system to N-limited towards inner regions. Results of the nutrient enrichment/reduction scenarios reveal that:

- Two contrasting environments, the N-limited Inner and Middle bays and the P-limited Outer bays, give contrasting reactions to changes in inputs of DIN and PO_4,
- Availability of one nutrient is dependent on the availability of the other, and treatment of both should be considered in parallel,
- Among the tested scenarios, the best possible option to reduce eutrophication in İzmir Bay is preventing the increase of PO_4 input together with reducing the DIN input

These outcomes are aimed to provide an insight for coastal policy makers and environmental managers to understand and forecast how changes in anthropogenic influences (increase/decrease of urbanization, and agricultural or industrial activities) can impact the marine ecosystem of the bay.

Bibliography

A. Acara and U. Nalbantoglu. Preliminary report on the red-tide outbreak in the gulf of Izmir. *Rapp. Comm. Int. Mer. Medit*, 15(3):33–38, 1960.

N. Bizsel and K.C. Bizsel. The occurrence and behaviour of phosphate fractions in İzmir Bay, Aegean Sea. *Hydrobiologia*, 450(1):5–18, 2001.

N. Bizsel and O. Uslu. Phosphate, nitrogen and iron enrichment in the polluted İzmir Bay, Aegean Sea. *Marine environmental research*, 49(2):101–122, 2000.

N. Bizsel, H.A. Benli, K.C. Bizsel, G. Metin, and İ.T. Bornova. A synoptic study on the phosphate and phytoplankton relationship in the hypereutrophicated İzmir Bay (Aegean Sea). *Turkish Journal of Engineering and Environ. Sciences*, 25:89–99, 2001.

A.N. Blauw, H.F.J. Los, M. Bokhorst, and P.L.A. Erftemeijer. GEM: a generic ecological model for estuaries and coastal waters. *Hydrobiologia*, 618(1):175–198, 2009.

B. Büyükışık. *İzmir İç Körfezi ve Gülbahçe Körfezi'nde Karşılaştırmalı olarak Nutrient Dinamikleri Üzerine Araştırmalar*. PhD thesis, Ege Üniversitesi, İzmir, 1986.

B. Büyükışık and Ö. Erbil. İzmir iç körfezâde nutrient dinamikleri üzerine araştırmalar. *Doğa, Müh. ve Çev. DC*, 11:379–395, 1987.

R. Geldiay, A. Kocataş, and Z. Ergen. İzmir Körfezinin genel hidrografisi üzerine ilk görüşler. *TBTAKV Bilim Kongresi*, pages 315–326, 1975.

H.A. Gençay and B. Büyükışık. Effects of sewage outfall on phytoplankton community structure in İzmir Bay (Aegean Sea). *J. Fisheries and Aq. Sciences*, 21(1-2):107–111, 2004.

V. A. Ivanov, A. I. Kubryakov, E. N. Mikhailova, and N. B. Shapiro. Modelling of circulation in the Gulf of Izmir. *Physical Oceanography*, 8(1):47â55, 1997.

V. A. Ivanov, A. I. Kubryakov, and N. B. Shapiro. Thermohaline structure and dynamics of waters in the Izmir Bay. *Physical Oceanography*, 9(4):273â296, 1998.

M. Koçak, N. Kubilay, S. Tugrul, and N. Mihalopoulos. Long-term atmospheric nutrient inputs to the Eastern Mediterranean: sources, solubility and comparison with riverine inputs. *Biogeosciences Discussions*, 7(4):5081–5117, 2010.

A. Kocataş and R. Geldiay. Effects of domestic pollution in İzmir Bay (Turkey). *Helgoland Marine Research*, 33(1):393–400, 1980.

A. Kontas, F. Küçüksezgin, O. Altay, and E. Uluturhan. Monitoring of eutrophication and nutrient limitation in the İzmir Bay (Turkey) before and after Wastewater Treatment Plant. *Environment international*, 29(8):1057–1062, 2004.

M.D. Krom, N. Kress, S. Brenner, and L.I. Gordon. Phosphorus limitation of primary productivity in the eastern Mediterranean Sea. *Limnology and Oceanography*, pages 424–432, 1991.

M.D. Krom, S. Brenner, N. Kress, A. Neori, and L.I. Gordon. Nutrient dynamics and new production in a warm-core eddy from the Eastern Mediterranean Sea. *Deep Sea Research Part A. Oceanographic Research Papers*, 39(3):467–480, 1992.

F. Küçüksezgin, A. Kontas, O. Altay, E. Uluturhan, and E. Darılmaz. İzmir Körfezi'nin Kimyasal Özelliklerine Genel Bakış. *Türk Sucul Yaşam Dergisi*, 2(2):346–355, 2004.

F. Küçüksezgin, A. Kontas, O. Altay, and E. Uluturhan. Elemental composition of particulate matter and nutrient dynamics in the İzmir Bay (Eastern Aegean). *Journal of Marine Systems*, 56(1):67–84, 2005.

F. Küçüksezgin, A. Kontas, O. Altay, E. Uluturhan, and E. Darılmaz. Assessment of marine pollution in İzmir Bay: Nutrient, heavy metal and total hydrocarbon concentrations. *Environment International*, 32(1):41–51, 2006.

H. Los. *Eco-hydrodynamic modelling of primary production in coastal waters and lakes using BLOOM*, volume 1. Ios PressInc, 2009.

METU-IMS and DEU-IMST. 2007 Final Raporu, Kuzeydogu Akdeniz ve Ege Denizi ve Kiyi Alanlarinda Uzun Sureli Biyolojik Izleme, Degisim ve Uyum Izleme. MED POL Phase IV, METU-IMS, DEU-IMST, 2007.

METU-IMS and DEU-IMST. 2008 Final Raporu, Kuzeydogu Akdeniz ve Ege Denizi ve Kiyi

Alanlarinda Uzun Sureli Biyolojik Izleme, Degisim ve Uyum Izleme. MED POL Phase IV, METU-IMS, DEU-IMST, 2008.

METU-IMS and DEU-IMST. 2009 Final Raporu, Kuzeydogu Akdeniz ve Ege Denizi ve Kiyi Alanlarinda Uzun Sureli Biyolojik Izleme, Degisim ve Uyum Izleme. MED POL Phase IV, METU-IMS, DEU-IMST, 2009.

W. Numann. Fish mortalities event in Izmir Bay. *Hidrobiology Mec., A*, 3(2):90–93, 1955.

E.Y. Özkan, A. Kocatas, and B. Büyükışık. Nutrient dynamics between sediment and overlying water in the inner part of İzmir Bay, Eastern Aegean. *Environmental monitoring and assessment*, 143(1):313–325, 2008.

E. Sayın. Physical features of the İzmir Bay. *Continental shelf research*, 23(10):957–970, 2003.

E. Sayın, İ. Pazi, and C. Eronat. Investigation of water masses in İzmir Bay, western Turkey. *Turkish J. Earth Sci*, 15:343–372, 2006.

SINHA. Technical Report Vol. I, TUBITAK, 2010.

C.A. Stow, J. Jolliff, D.J. McGillicuddy, S.C. Doney, J. Allen, M.A.M. Friedrichs, K.A. Rose, and P. Wallhead. Skill assessment for coupled biological/physical models of marine systems. *Journal of Marine Systems*, 76(1):4–15, 2009.

U. Sunlu, M. Aksu, B. Büyükışık, and F.S. Sunlu. Spatio-temporal variations of organic carbon and chlorophyll degradation products in the surficial sediments of Izmir Bay (Aegean Sea/Turkey). *Environmental monitoring and assessment*, 146(1):423–432, 2008.

A. Tselepides, V. Zervakis, T. Polychronaki, R. Danovaro, and G. Chronis. Distribution of nutrients and particulate organic matter in relation to the prevailing hydrographic features of the Cretan Sea (NE Mediterranean). *Progress in oceanography*, 46(2):113–142, 2000.

UNEP. Costs and benefits of measures for the reduction of degradation of the environment from land-based sources of pollution in coastal areas. A - Case study of the Bay of Izmir. B - Case study of the Island or Rhodes. MAP Technical Reports Series 72, UNEP, 1993.

UNEP. Integrated Management Study for the Area of Izmir. MAP Technical Reports Series 84, UNEP, 1994.

WL | Delft Hydraulics. Delft3D-WAQ User Manual. 2009a.

WL | Delft Hydraulics. Delft3D-WAQ SWITCH Technical Reference Manual. 2009b.

WL | Delft Hydraulics. Delft3D-FLOW User Manual. 2009c.

APPENDIX A

APPENDIX A

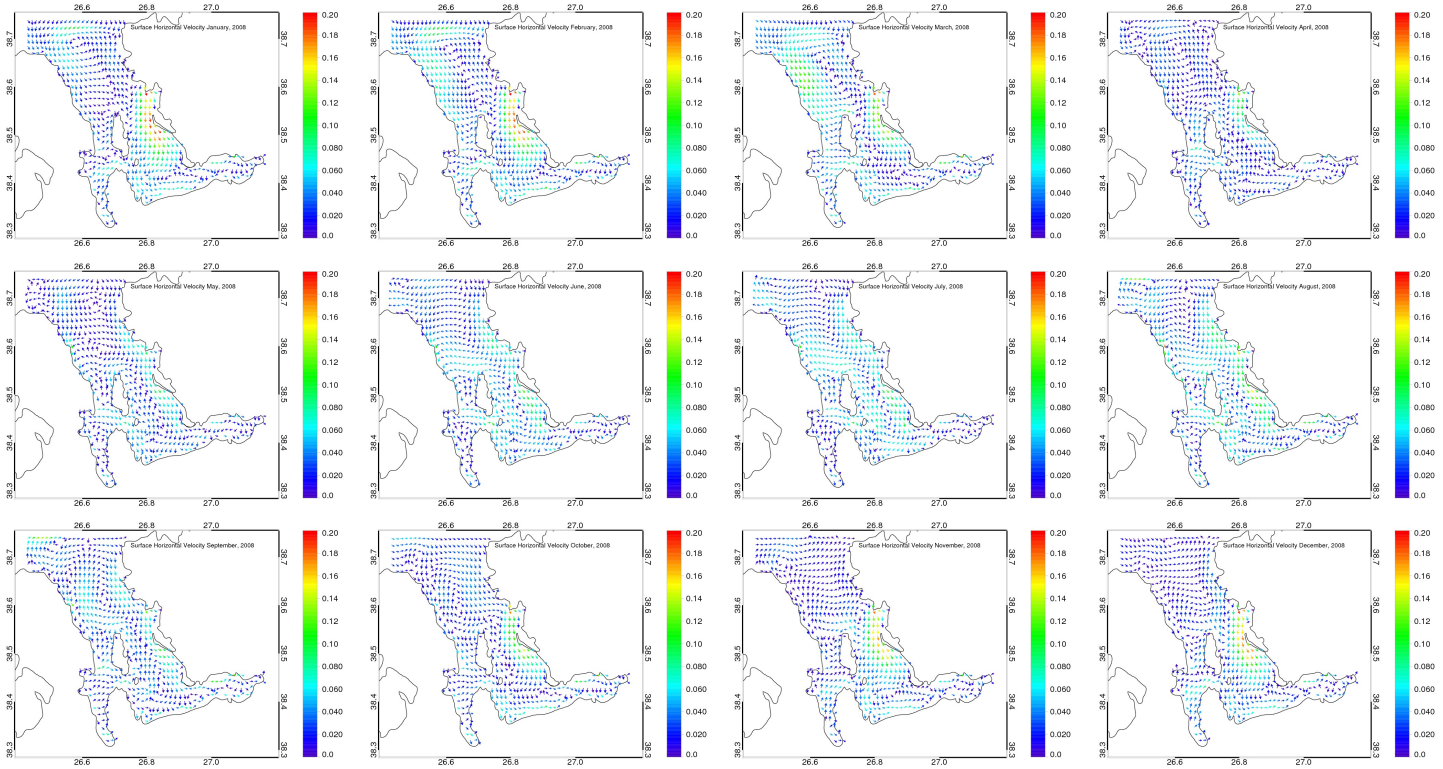

Figure A.1: Monthly averaged surface horizontal current velocity model results from 2008.

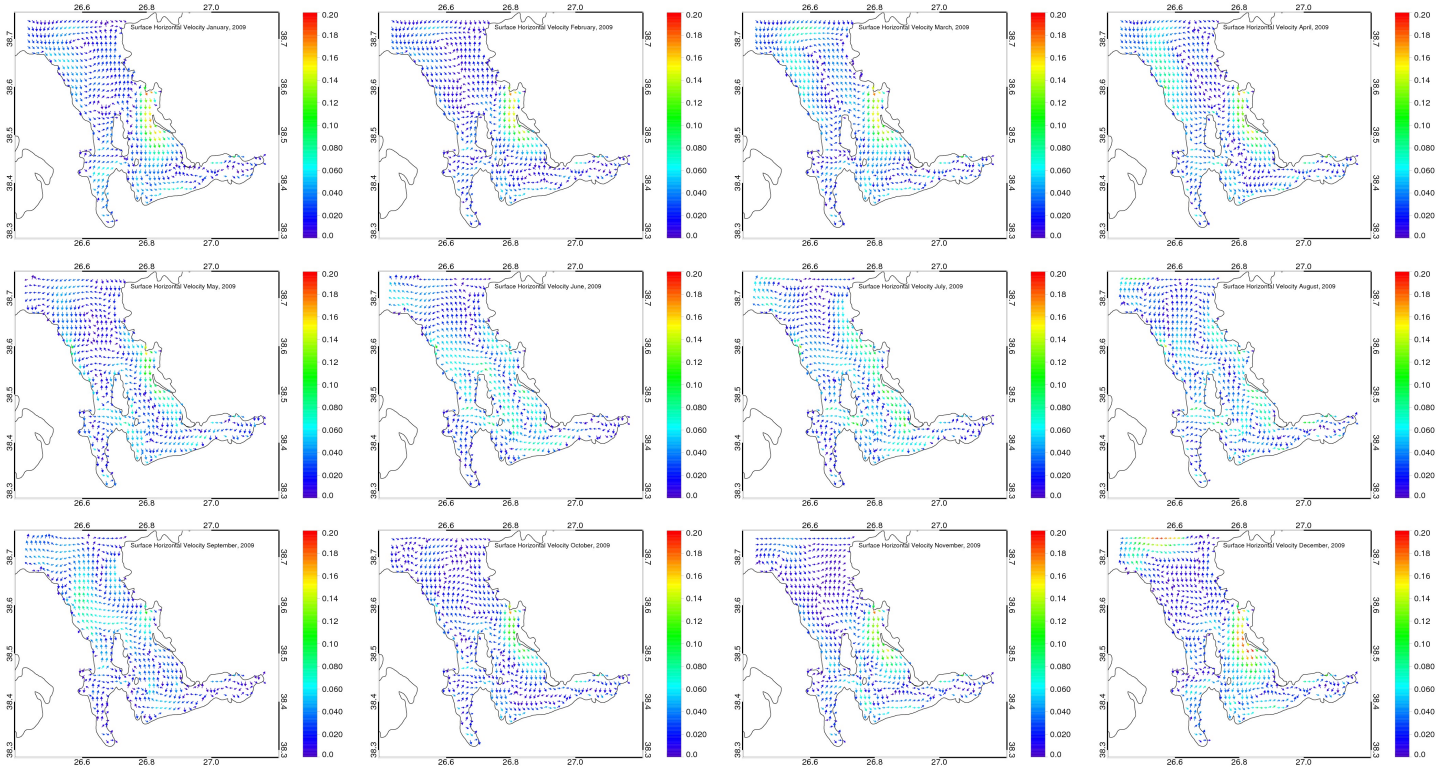

Figure A.2: Monthly averaged surface horizontal current velocity model results from 2009.

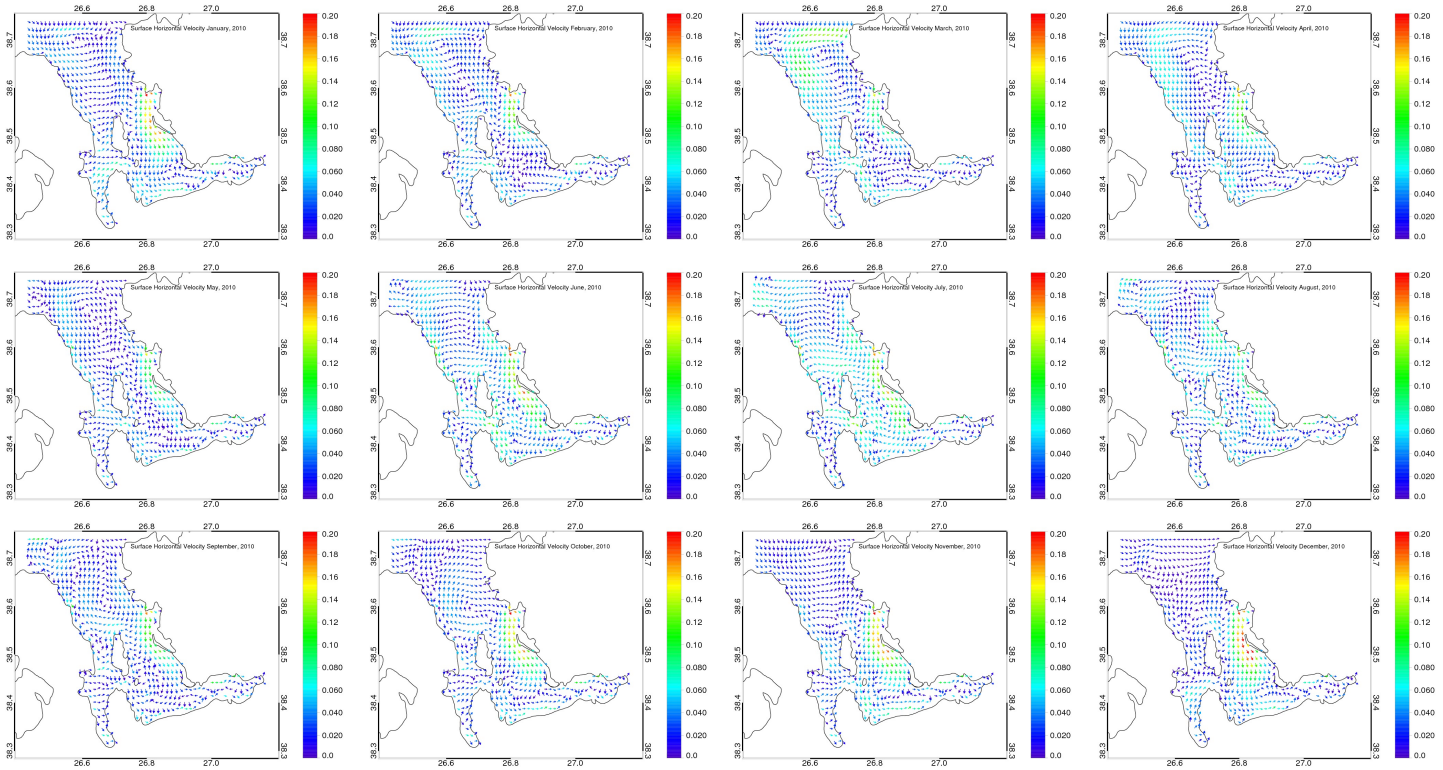

Figure A.3: Monthly averaged surface horizontal current velocity model results from 2010.